Investigating mechanisms of hemodynamic control in the brain

Brenda R. Chen

Submitted in partial fulfillment of the
Requirements for the degree of
Doctor of Philosophy
In the Graduate School of Arts and Sciences

COLUMBIA UNIVERSITY
2013

Abstract

Investigating mechanisms of hemodynamic control in the brain

Brenda R. Chen

Neurovascular coupling is the relationship between neural activity and blood flow that allows the brain to exhibit increases in blood flow to areas of elevated neural activity during sensory stimulation. It is these localized changes in blood flow, collectively known as the hemodynamic response, that are detected by modern neuroimaging techniques such as functional magnetic resonance imaging (fMRI). Intact neurovascular coupling is imperative to neural health as de-coupling of neural activity from blood flow modulations has been implicated in many neurodegenerative diseases such as Alzheimer's disease, dementia, traumatic brain injury, and ischemic stroke. Despite the importance of neurovascular coupling for both fMRI interpretation and neurological disease, the mechanisms underlying the control of blood flow in the brain remain poorly understood. While previous studies have proposed a range of different cellular mechanisms capable of mediating vascular changes in the brain, it remains difficult to reconcile these mechanisms with a unified theory that is also consistent with the complex spatiotemporal features of the hemodynamic response.

The goal of this dissertation is to study the vascular components of the hemodynamic response and the cellular mechanisms that orchestrate them. Using novel high-speed multi-spectral optical imaging of the exposed rodent somatosensory cortex, a detailed characterization of the cortical hemodynamic response is conducted. These observations guide cellular level two-photon microscopy of neural and glial cell activity. The precise spatiotemporal characteristics of the neurovascular response elucidated in these *in vivo* studies are then used to construct and constrain a conceptual framework for the signaling and actuation pathways that orchestrate the hemodynamic response. To test this framework, targeted light-dye treatment and optogenetic stimulation are used to selectively activate or deactivate targeted signaling pathways. The findings of this research strongly suggest that at least two different mechanisms control the sensory-evoked blood flow response, the first of which critically depends on the vascular endothelium.

Table of Contents

List of Figures

List of Tables

Acknowledgements

I would like to express my gratitude to my advisor Elizabeth Hillman, whose support and guidance has forever shaped my professional and personal development. Without her vision and the confidence she placed in me, this research would not have been possible.

I thank the members of my thesis committee, Dr. Aniruddha Das, Dr. Barclay Morrison, Dr. Elizabeth Olson, and Dr. Paul Sajda for sharing their critical insights and advice throughout.

This dissertation would also have not been possible without the help and support of my colleagues and friends in the Laboratory for Functional Optical Imaging. I am grateful to have shared this part of my life with you.

Finally, very special thanks to my family for their continued support and confidence, and to Sol for being there every step of the way, from the very beginning. You are all an endless source of inspiration.

For supporting my research, I thank Columbia University and the National Science Foundation.

Dissertation Committee

Elizabeth M.C. Hillman, Ph.D
Department of Biomedical Engineering
Columbia University

Paul Sajda, Ph.D
Department of Biomedical Engineering
Columbia University

Barclay Morrison, Ph.D
Department of Biomedical Engineering
Columbia University

Elizabeth S. Olson, Ph.D
Department of Biomedical Engineering and Auditory Biophysics
Columbia University

Aniruddha Das, Ph.D
Department of Neuroscience
Columbia University

Chapter 1

Introduction & background

1.1 Neurovascular coupling

The brain exhibits a localized increase in blood flow to regions of elevated neuronal activity. This unique relationship between blood flow and neural activity, known as neurovascular coupling, is not well understood and remains a vital area of research due to its important consequences for both medical diagnostics and neuroscience research.

The hemodynamic response to brain activity forms the basis for clinical imaging modalities such as functional magnetic resonance imaging (fMRI), which utilizes changes in local deoxy-hemoglobin (HbR) as a surrogate measure of neural activity. Although fMRI has had undeniably important impacts on clinical and scientific brain research, interpretation of the blood oxygenation level dependent (BOLD) signal in fMRI remains limited by incomplete knowledge of how underlying neural activity relates to subsequent

vascular changes (Attwell & Iadecola 2002, Iadecola 2004). It is thought that these localized changes in blood flow provide the necessary influx of glucose, oxygen, and other nutrients required by active brain tissues during normal brain function (Iadecola 2004, Villringer & Dirnagl 1995). However, the positive BOLD signal in fMRI corresponds to a decrease in HbR which results from an over-oxygenation of the responding region, a state that is induced by local vasodilation. This blood flow increase begins 200-400 ms after stimulus onset and typically peaks 3-5 seconds after stimulus onset, even for short stimuli lasting less than 2 seconds. Experimentally inducing baseline levels of excessive oxygen or glucose through hyperoxia or hyperglycemia does not alter the hemodynamic response (Lindauer et al 2003, Wolf et al 1997). These features of the blood flow response underscores that the BOLD signal is not directly proportional to the energetic demands of the tissue nor is it simply motivated by neuronal feedback.

Because these blood flow changes overcompensate for metabolic demand, it is difficult to understand the purpose of the hemodynamic response (Lindauer et al 2003); nevertheless, tight coupling between neuronal activity and blood flow appears to be important for normal brain function. Previous studies have suggested that impaired neurovascular coupling could lead to neurodegeneration and underlie pathologies such as stroke, dementia, and Alzheimer's disease (Girouard & Iadecola 2006).

It is therefore critical to understand how the coupling between neuronal activity and blood flow is mediated, both to correctly interpret changes in blood flow observed with fMRI (Logothetis 2008) and to identify therapeutic targets for treating impaired neurovascular coupling (Lindauer et al 2010).

1.2 Approach

Understanding the relationship between cerebral blood flow and neural activity is a complex problem that has inspired a wide array of investigations ranging from the systems level to the molecular level. In general, these studies have focused on various aspects of the following questions: 1) What is the hemodynamic response? – What are the blood volume and tissue oxygenation manifestations of this localized change in blood flow? (Berwick et al 2008, Chen et al 2011, Hillman et al 2007, Sheth et al 2005, Vanzetta et al 2005) 2) How does it occur? - What are the signaling and actuation pathways that translate neural activity into localized changes of blood flow? (Fernández-Klett et al 2010, Lecrux et al 2011, Peppiatt et al 2006, Takano et al 2005, Wang et al 2006) and 3) Why does it occur? - Is there a metabolic motivation or biochemical need for a blood flow change? (Magistretti & Pellerin 1996a, Martindale et al 2005b, Moore & Cao 2008, Pellerin et al 1998, Shibuki et al 2003, Takano et al 2005).

This dissertation focuses on studying the first two questions: What are the characteristics of the hemodynamic response, and What are the cellular mechanisms underlying them? Although recent studies have suggested a range of different cellular mechanisms as having the potential to mediate vascular changes in the brain, it remains difficult to reconcile these mechanisms into a unified theory of blood flow control (Abbott et al 2006, Fernández-Klett et al 2010, Lecrux et al 2011, Wang et al 2006). This difficulty is due in part to differences in imaging techniques, animal models, and stimulus paradigms, but also to the absence of an organized framework for integrating our knowledge of different features of neurovascular coupling into a consistent model. The experiments

presented in this dissertation are therefore designed to seek a unifying framework for blood flow control in the brain.

1.3 Thesis overview

This thesis documents the exploration of neurovascular coupling, beginning with the development of new techniques for observation and the documentation of novel observations, through the testing of specific hypotheses, and ending with a general framework for hemodynamic control in the brain. The chapters of the thesis, presented in sequence, represent the logical progression of our investigations, with each chapter describing a study that was designed based on our previous findings.

Chapters 1 & 2 provide an overview and demonstration of the imaging systems and analysis techniques that were developed in order to study neurovascular coupling *in vivo*. The high spatiotemporal resolution of these imaging techniques made it possible to conduct a detailed characterization of the vascular dynamics that comprise the hemodynamic response (**Chapter 3**). Knowledge of these vascular changes and their properties are then used to guide investigations at the cellular level and studies that manipulate properties of the evoking stimulus. The culmination of evidence from these studies leads to the development of hypotheses concerning candidate mechanisms (**Chapter 4**). To directly test these hypotheses, light-dye treatment and optogenetic stimulation are used to selectively activate or deactivate targeted pathways (**Chapter 5 & 6**). Finally, the findings from each of these studies are summarized and integrated into a general framework of vascular control that can be used to guide future studies of neurovascular coupling (**Chapter 7**).

1.4 Chapter summaries

Chapter 1: Introduction & Background. In the remainder of Chapter 1, I provide an overview of the cellular and vascular components hypothesized to be involved in neurovascular coupling and their roles in mediating blood flow changes, insofar as both are currently understood. The optical imaging techniques used in subsequent chapters and their underlying principles are also discussed in the context of *in vivo* imaging of neurovascular coupling.

Chapter 2: Methods of *in vivo* imaging of neurovascular coupling. In Chapter 2, I describe the protocol that I developed for conducting *in vivo* imaging in an exposed rodent cortex, including animal preparation, stimulus paradigms, and imaging procedures. I developed this protocol in parallel with the development of our high-speed multi-spectral optical intrinsic signal imaging system and two-photon microscope by other members of the Laboratory for Functional Optical Imaging[1]. Using example data sets acquired through this process, I demonstrate the analysis methods that can be used to extract quantitative information from high-resolution multi-spectral data, including oxygenation changes, vasomotor dynamics and intracellular calcium activity.

Chapter 3: High-speed vascular dynamics of the hemodynamic response. Understanding the detailed vascular dynamics that comprise the hemodynamic response to sensory stimulation is a critical first step towards developing a model for neurovascular

[1] System development performed by: Matthew B. Bouchard, Andrew J. Radosevich, Lauren E. Grosberg, and Elizabeth M.C. Hillman.

coupling and its underlying cellular mechanisms. Thus, in Chapter 3, I implement the tools developed in Chapter 2 to conduct a thorough characterization of the spatiotemporal dynamics of surface vessels during functional hyperemia. In observations of particular interest, I find that the earliest hemodynamic change following stimulation is initiated in the capillary bed and rapidly propagates along the vascular tree to surface pial arterioles at speeds up to 1-2 mm/s. I also observe that the response onset and the return to baseline state exhibited different spatiotemporal patterns, suggesting that distinct mechanisms with corresponding properties may underlie their control. The properties of the hemodynamic response discovered during this characterization are used to formulate hypotheses about the underlying cellular mechanisms in Chapters 4 and 5. The work presented in this chapter was published in Neuroimage in 2011 (Chen et al 2011).

Chapter 4: Distinct phases of the hemodynamic response. In Chapter 4, I conduct two-photon microscopy studies of sensory-evoked astrocytic calcium changes in an attempt to correlate astrocyte reactivity with the hemodynamic response. My results fail to implicate astrocytes as the cellular mechanism mediating the onset of the vascular responses, but agree with existing literature that documents a ~2-3 second delay in astrocyte calcium responses relative to stimulus onset (Schummers et al 2008, Wang et al 2006). These findings suggest that the delayed recruitment of astrocytes may correspond to a similarly delayed component of blood flow control. Together with the hypothesis that different mechanisms control the onset and decay of hemodynamic response from Chapter 3, these results led to a series of experiments aimed at characterizing the blood flow response to varying durations of stimulation. In response to prolonged somatosensory stimulation, I

observe what appear to be distinct "hemodynamic phases" which I characterize by differences in their spatiotemporal patterns. The results in Chapter 4 ultimately lead to our hypothesis that multiple mechanisms are responsible for orchestrating the hemodynamic response: an initial phase exhibits "reflex-like" properties while a second phase looks as if it is relatively more dependent on the energetic and metabolic state of the local environment.

Chapter 5: Light-dye injury to cerebral vascular endothelium eliminates propagation of stimulus-evoked vasodilation. In Chapter 5, based on the evidence gathered from previous chapters, I design an experiment to directly test the hypothesis that the vascular endothelium is critically involved in mediating the rapid vasodilation evoked during the initial hemodynamic response. Employing a well-established light-dye injury technique to selectively disrupt the endothelium, while keeping smooth muscle cells and neural activity unaltered, I find that the first phase of the hemodynamic response does indeed depend on endothelial signaling pathways. Furthermore, I find that the second phase of the response is relatively unaffected by light-dye treatment, suggesting that a mechanism independent of the endothelium is recruited to mediate these changes. These findings represent the first empirical evidence that distinct cellular pathways contribute to the blood flow changes evoked by sensory stimulation.

Chapter 6: Resolving the hemodynamic response elicited via optogenetic stimulation. A question that builds upon the findings of Chapter 5 is whether the early component of the hemodynamic response, which is mediated by the endothelium, is driven by pre-synaptic or post-synaptic mechanisms. Specifically, this chapter is motivated by the hypothesis that

direct innervation of the vasculature from the thalamus, rather than post-synaptic processing, plays a role in the first hemodynamic phase. To explore this question, I develop and implement a protocol for integrating optogenetic techniques with the tools that we use to observe neurovascular coupling *in vivo*. Optogenetic stimulation enables us to selectively activate excitatory neurons via direct cortical stimulation with blue light. I describe the procedures involved in performing simultaneous optogenetic stimulation and exposed cortex imaging and present preliminary results documenting the subsequent hemodynamic response. While the response appears strikingly similar to native responses, further optimization of blue light stimulus parameters is required to draw clear conclusions. The establishment of the optogenetic protocol will allow future studies to incorporate the use of selective activation or inhibition of specific sub-populations of cells in order to evaluate the effects on hemodynamic control.

Chapter 7: Implications and future directions. In the final chapter of this thesis, I synthesize the key findings regarding the hemodynamic response that result from the studies in previous chapters. I integrate these findings into a general multi-phase framework for hemodynamic control and discuss the implications that such a framework could have on fMRI data analysis and neurodegenerative disease therapies. Finally, I conclude with recommendations for future research in this field.

1.5 Background

The "neurovascular unit" is comprised of all neuronal and non-neuronal cells that are involved in the relationship between brain cells and their blood supply. Cortical cells

include excitatory and inhibitory neurons, as well as pericytes and astrocytes. The cerebrovascular compartments include arteries, veins, and the capillary bed. This section will provide an overview of the current understanding of these components of the neurovascular unit.

1.5.1 Cortical cell types of the neurovascular unit

Somatosensory organization Sensory information is relayed from the periphery through the spinal cord and brain stem to the thalamus, where feed-forward and feedback signals are integrated and directed to the somatosensory cortex. The sensory cortices are well organized with specific cortical regions corresponding to each sensing organ. In the somatosensory cortex, the somatosensory homunculus reflects the relative density of innervation of each body part.

Within the somatosensory cortex, cortical inputs from the thalamus are received by pyramidal and stellate neurons in layer IV, which is also the layer that receives intra-hemispheric corticocortical afferents. The thalamus has many complex functions that relay information between subcortical areas and the cerebral cortex. Every sensory system, except the olfactory bulb, has an associated thalamic nucleus. Thus, thalamic inputs have been of interest to the study of neurovascular coupling in a variety of sensory stems. Investigations at the systems level have tried to understand the relative contributions of thalamic inputs to the cortex and cortico-cortical signaling to orchestration of the hemodynamic response (Enager et al 2009). Other studies have also extended neurovascular coupling research to understanding the different modes of coupling in non-cortical structures such as thalamus and brainstem (Devonshire et al 2012).

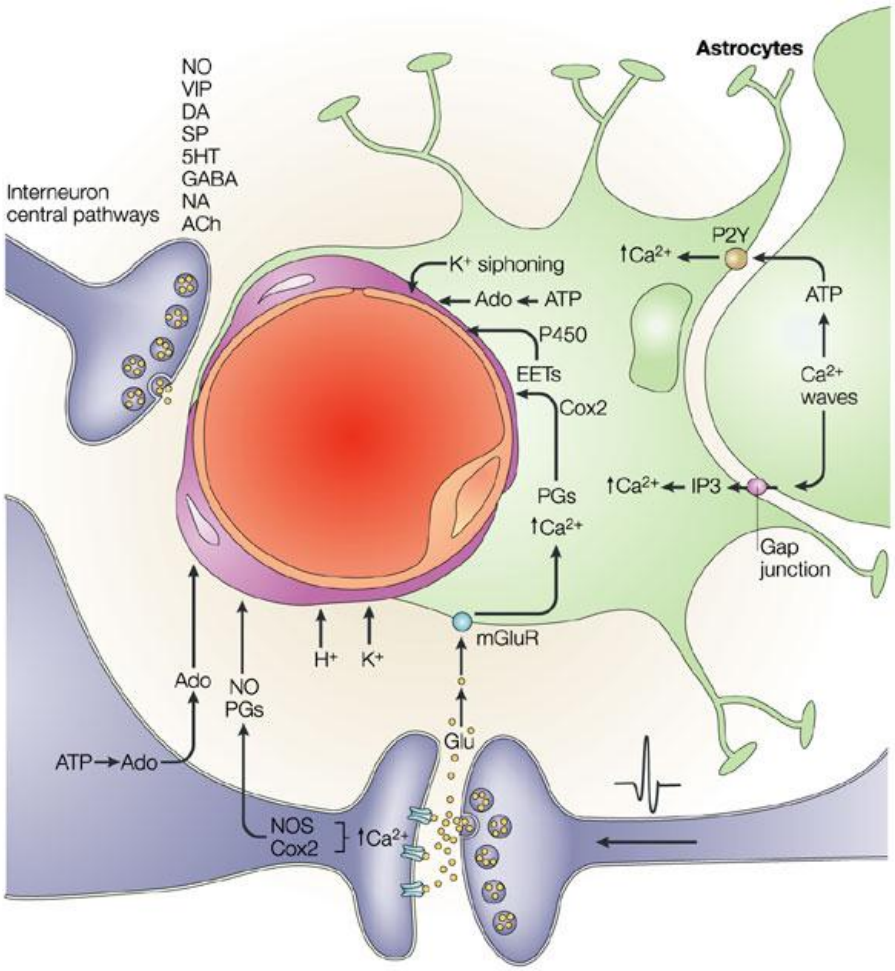

Figure 1.1 Vasoactive mediators released from neurons and astrocytes
Astrocytes are closely associated with the blood brain barrier and form many connections with vascular endothelium, smooth muscle cells, and neurons. Increases in intracellular calcium concentration in astrocytes trigger several pathways that result in the release of vasoactive mediators. Image reproduced from Iadecola 2004.

Glial and perivascular cells Astrocytes used to be considered passive elements in the brain, acting as structural and metabolic supporters of neurons (Figure 1.1). They are the most abundant type of glial cell in the brain and are intimately connected with the both blood vessels and neurons (Haydon & Carmignoto 2006). More recently, however, several studies have proposed that astrocytes play a critical role in facilitating stimulus-evoked

blood flow changes in the brain (Anderson & Nedergaard 2003, Attwell et al 2010, Petzold & Murthy 2011, Schummers et al 2008). The close proximity of astrocytes to the site of both neural activity and nutrient exchange makes them an attractive candidate for mediating the relationship between neural activity and blood flow (McCaslin et al 2011, Zonta et al 2003).

Astrocytes lack the ability to generate action potentials, and thus do not communicate via propagating electrical signals as neurons do. Instead astrocyte signaling is conducted through changes in intracellular calcium concentration, which may be triggered by local neuronal stimulation (Bernardinelli et al 2011, Hirase et al 2004b). The use of calcium sensitive fluorescent indicators has made it possible to use microscopy to study astrocytic calcium activity, both *in vitro* and *in vivo*, in response to a variety of chemical or electrical stimuli. In addition, astrocytes are capable of responding to neuronal activity and neurotransmitters through the activation of metabotropic receptors and can release gliotransmitters ATP, D-serine, and glutamate which can, in turn, affect local neuronal activity (Haydon & Carmignoto 2006).

Astrocytes have also been found to be capable of releasing vasodilators and vasoconstrictors which can influence arteriolar tone. It has been observed that variations in intracellular Ca^{+2} in astrocytes can modulate the cerebral microcirculation, through the release of compounds such as arachidonic acid metabolites prostaglandin E_2 and epoxyeicosatrienoic acid (EETs) that are known to induce arteriolar dilation, and 20-HETE, which induces arteriolar constriction (Haydon & Carmignoto 2006, Koehler et al 2006). *In vitro* work by Gordon et al showed that astrocytes may either elicit vasodilation or constriction depending on the oxygen availability of the surrounding environment,

indicating that astrocytes can potentially act both as sensors of metabolic needs as well as actuators of vessel diameter (Gordon et al 2008). Astrocytes have also been suggested to play a role in metabolism by supplying neurons with lactate for ATP production (Kasischke et al 2004, Magistretti & Pellerin 1996b).

Many of the studies exploring properties of astrocytes have been done in cell cultures or brain slices. Only recently have *in vivo* studies been able to observe astrocytic reactivity in response to stimulation via glutamate application, calcium uncaging, or sensory stimulation (Schummers et al 2008, Takano et al 2005, Wang et al 2006, Zonta et al 2003). In addition, our group conducted a survey of astrocyte morphology and distribution *in vivo* using two photon microscopy (McCaslin et al 2011). We found comprehensive astrocytic sheathing surrounding all penetrating arterioles, capillaries and ascending veins, as well as astrocytes with multiple endfoot processes encircling vessels (McCaslin et al 2011).

A growing body of literature on astrocyte-neuron-vascular associations appears to confirm the notion that astrocytes are indeed involved in mediating stimulus evoked blood flow changes. Nevertheless, observations of astrocyte activity (denoted by intracellular calcium changes) accompanying or preceding vascular changes *in vivo* have been inconsistent across accounts and difficult to interpret. This is partially due to the differences in imaging parameters and stimulus paradigms as well as the difficulties associated with imaging astrocyte activity on a cellular level, when in fact they may be just one component of a larger system that orchestrates blood flow changes to an entire brain region.

Pericytes have also been identified as important contributors to blood flow regulation in the brain, although their dynamics *in vivo* have not been as extensively explored. Pericytes

are a type of vascular mural cell that are found on the outer surface of microvessel endothelium (capillaries, pre-capillary arterioles, and post-capillary venules) where they have been shown to form junctional complexes with underlying endothelial cells (Armulik et al 2005). They are related to vascular smooth muscle cells and also possess contractile abilities, suggesting that may be capable of modulating blood flow (Hirschi & D'Amore 1996). A series of *in vitro* studies demonstrated that pericytes are found at discrete locations along capillary vessels and are capable of causing localized constriction along the vascular network (Peppiatt et al 2005, Peppiatt et al 2006). Despite this ability to induce constrictions, a more recent study using transgenic mice has suggested that the functional role of pericytes *in vivo* may be limited (Fernández-Klett et al 2010).

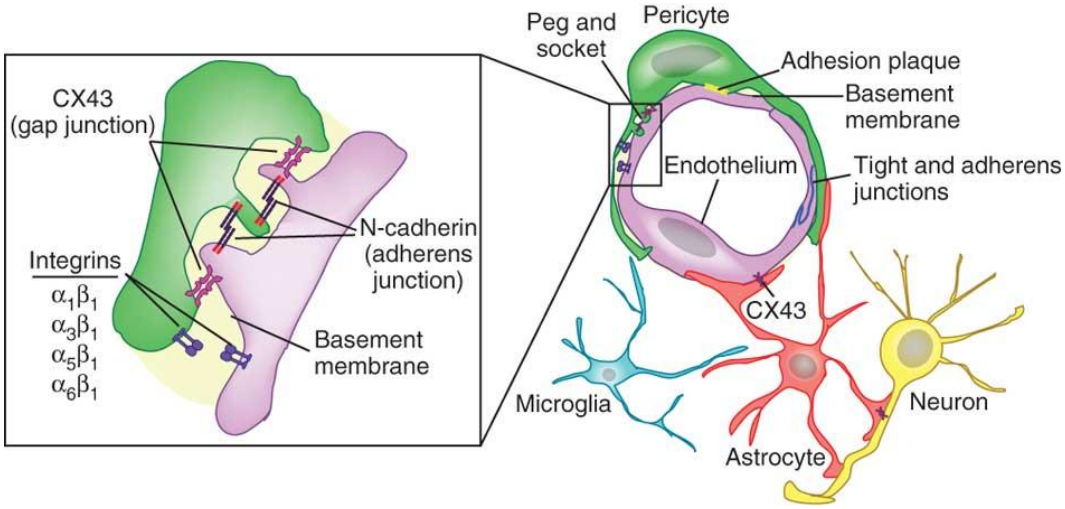

Figure 1.2 Structural and molecular pericytes connections within the neurovascular unit Pericytes and endothelial cells are connected to a common basement membrane by several types of integrin molecules and gap junctions. Pericytes have been hypothesized to play an integral role in coordinating and effecting neurovascular functions, including regulation of blood brain barrier permeability and regulation of cerebral blood flow. Image reproduced from Winkler et al 2011.

Interneurons, which primarily utilize inhibitory neurotransmitters GABA and glycine, have also been shown to elicit vascular changes in nearby vessels (Cauli et al 2004). Their rich innervations to microvessels have led some to suggest that GABA interneurons may be integrators of the local vascular response (Vaucher et al 2000). However, the large number of interneurons subpopulations that have been identified exhibit complex morphology and connectivity, making it difficult to understand their role in functional hyperemia *in vivo* (Cauli et al 2004).

1.5.2 Vascular components of the neurovascular unit

Vascular organization and properties The vascular architecture of the mammalian brain is specialized for maintaining and regulating blood distribution by creating redundancies in blood flow that ensure adequate delivery of blood gases, nutrients, and metabolites. The middle and anterior cerebral arteries arise from the Circle of Willis, at the base of the brain, to supply the primary motor and sensory areas of the cortex, among other regions. These large arteries form a network of vessels at the cortical surface which branch off into penetrating arterioles that dive down beneath the surface of the brain to feed the microvascular capillary bed where most gas, nutrient, and heat transfer occurs (Figure 1.3). The blood flow out of the capillary bed is directed back to the surface of the cortex through penetrating venules that connect to a surface network of larger draining veins.

The vascular compartments of the brain (arteries, capillaries, and veins) each exhibit different properties that make them suited for their role in the circulatory system. Arteries differ from capillaries and veins in that they have a thicker layer of smooth muscle along the vessel walls.

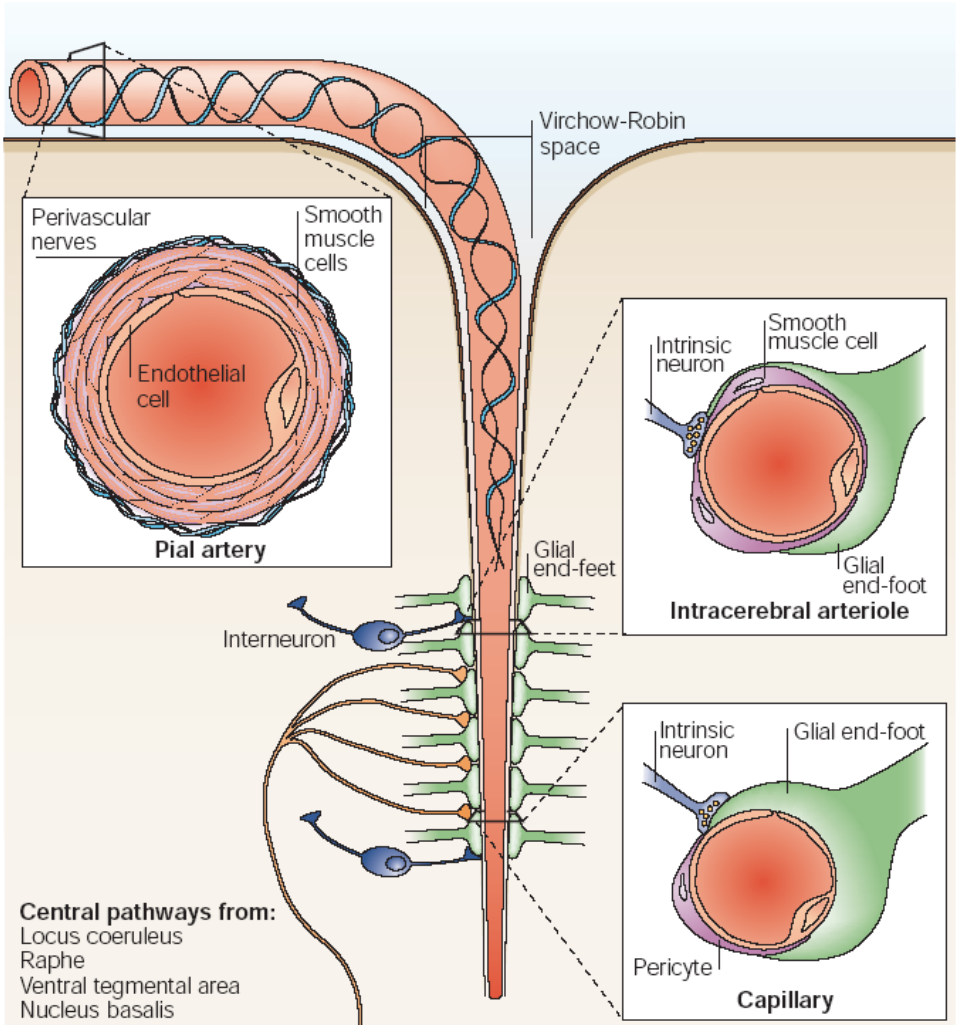

Figure 1.3 Vascular organization and the neurovascular unit
Pial arteries on the brain surface have perivascular nerves that give rise to penetrating arterioles. As penetrating arterioles become parenchymal arterioles within the brain cortex, they become associated with neurons and astrocytes. Image reproduced from Iadecola 2004.

The presence of smooth muscle on arterial vessel walls makes it possible for arteries to maintain vessel tone in the presence of blood pressure fluctuations. Smooth muscle cells wrap around the circumference of the vessel and have the ability to contract and relax, providing a mechanism by which arterioles can exhibit active vasomotion (Attwell et al 2010). In contrast, veins do not possess the same smooth muscle layers and thus exhibit passive changes in vessel tone and diameter that result from changes in blood flow and pressure.

Perhaps the most unique feature of brain vasculature belongs to the tightly packed endothelial cells and astrocytic endfeet, which comprise the protective blood brain barrier (BBB). Capillaries outside of the brain exhibit gaps in their endothelial walls that allow gases and other molecules, such as glucose, to pass between the blood and the surrounding tissue via diffusion or specialized transporters (Figure 1.4).

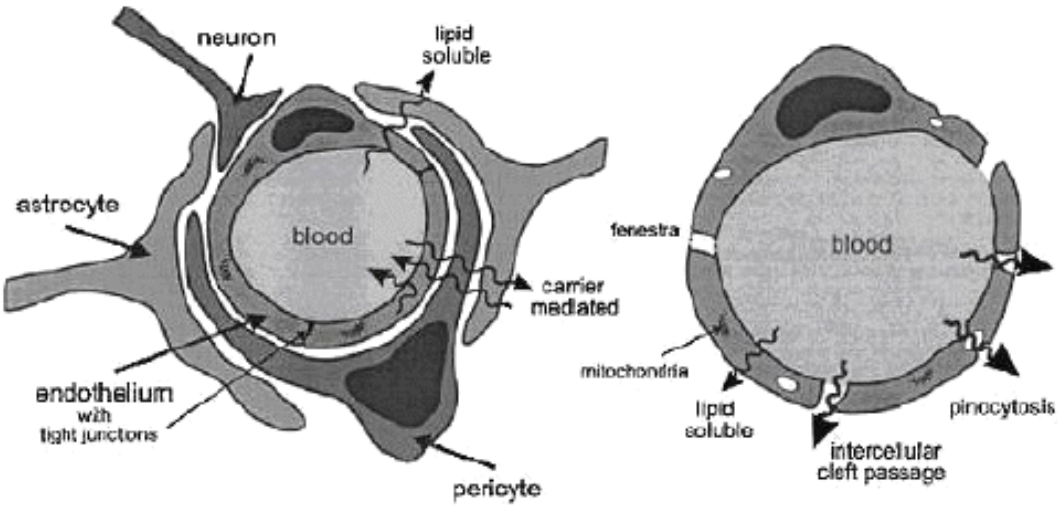

Figure 1.4 Brain capillaries exhibit specialized structures
Diagram showing the differences between brain capillaries (left) and general capillaries (right). Brain capillaries exhibit a tightly sealed barrier between the blood and surrounding brain tissue, whereas general capillaries do not. Image reproduced from Misra et al 2003.

However, in the brain, the BBB's highly impermeable tight junctions of endothelial cells and astrocytic processes control the permeability of capillary walls to certain molecules (Abbott et al 2006). The BBB effectively protects the brain from bacteria, viruses or harmful substances that may be present in the blood circulation.

Vascular signaling pathways and actuation of vasomotion Understanding how blood flow is controlled in the brain requires knowledge of both the signaling pathways associated with triggering a vascular change as well as the mechanism actuating changes in vessel tone and diameter. The proposed signaling pathways that are associated with the brain vasculature itself include cell-to-cell signaling between smooth muscle cells, endothelial cells, and along networks of astrocyte processes encircling vessels. Gap junctions form channels through which these cells can communicate via hyperpolarization or transmission of biochemical substances. Specific gap junctions across cell types also allow communication between smooth muscle cells, endothelial cells, and astrocytes. Myoendothelial gap junctions (MEGJ) specifically refer to gap junctions that couple endothelial cells to the smooth muscle cells that wrap around the outside of the vessel. The tightly packed longitudinal orientation of endothelial cells parallel to the length of the vessel makes them an attractive mode of signal conduction along the length of vessels.

Smooth muscle cells, in contrast, are oriented perpendicularly to the endothelial cells, appear to wrap their cell bodies around the circumference of the vessel, and are capable of actuating changes in vascular diameter by relaxing and contracting (Figure 1.3). The astrocyte sheathing has been shown to encircle most of the vasculature and contains gap

junctions through which astrocytes can communicate between each other as well as to the smooth muscle cells and endothelial cells (Abbott et al 2006). Prior studies have hypothesized that the signaling relay between neurons at the capillary bed may propagate to the surface pial arteries through astrocytic and/or endothelial signaling, which subsequently contact smooth muscle cells that actuate vascular change (Andresen et al 2006, Xu et al 2008).

The modes through which these vascular cells communicate with one another have their own dedicated literature. Endothelial cells are well known to react to a variety of pharmacological substances such as acetylchloline (ACh) and adenosine (Ado), which cause endothelial cells to release the vasodilator nitric oxide (NO) that initiates relaxation of smooth muscle cells [2]. Endothelium independent vasodilator substances such as phenylephrine (PE) or norephinephrine, act on the biochemical pathways in smooth muscle cells instead, triggering a chain of reactions that lead to either relaxation (dilation) or contraction (constriction) (Ignarro et al 1999, Welsh & Segal 1998). It has been hypothesized that vasodilating pathways that are independent of the release of NO exist and have been termed endothelial derived hyperpolarization factors (EDHF). Because the process is not well understood, the term EDHF may refer to either a substance or a pathway that actuates endothelium dependent vasodilation in the absence of NO (Andresen et al 2006).

Potential pathways associated with EDHF-mediated vasodilation include hyperpolarization of endothelial cells following changes in intracellular levels of calcium

[2] Before its discovery, NO was often referred to as the endothelium derived relaxation factor (EDRF).

and potassium that occur through gap junctions and calcium dependent potassium channels. It has also been hypothesized that signaling is conducted via intraluminal pressure sensors or mechanical shear stress receptors found on the inside of endothelial cells (Ngai & Winn 1995).

Prior study of endothelial hyperpolarization and subsequent propagation of vasodilation has been primarily conducted in peripheral vessels of skeletal muscles (Bartlett & Segal 2000, Budel et al 2003, Emerson & Segal 2000, Looft-Wilson et al 2004, Wölfle et al 2011), though some have also be conducted in the brain or in isolated cerebral vessels (Dietrich et al 2009, Dietrich et al 1996, Hannah et al 2011, Rosenblum 1986). It is important to note that characteristics of peripheral vessels may not necessarily be the same as those exhibited in the brain vasculature.

1.6 Imaging Techniques

1.6.1 Rodent model for *in vivo* imaging

A large quantity of neurovascular coupling research has been conducted using *in vitro* preparations. While it is possible to study cellular level interactions in brain slices or cell cultures, it is not possible to replicate the vascular and neural networks that are involved in neurovascular coupling on a systems level in an *ex vivo* preparation. Intact circulation and nervous systems are inevitably linked to complex homeostatic processes that govern normal physiology and metabolism that can influence the relationship between neural activity and blood flow. For this reason, we focus on the use of *in vivo* models of neurovascular coupling.

A major advantage of using animal models for studying brain dynamics is the ability to expose the cortex for high resolution imaging of blood oxygenation and vascular dynamics, making it possible to study functional responses with higher resolution and more information than the fMRI blood oxygenation level dependent (BOLD) signal (Hillman 2007). The ability to introduce cell specific or intravascular fluorescent dyes and to create transgenic animal models that express genetically-targeted fluorophores such as green fluorescent protein (GFP) or other active probes provides additional sources of optical contrast that allow simultaneous studies of vascular and cellular dynamics (Bouchard et al 2009, Feng et al 2000, Fernández-Klett et al 2010, Hirase et al 2004a, Wang et al 2006).

While some recent studies have conducted imaging experiments on awake, un-anesthetized animals (Martin et al 2006), the majority of *in vivo* optical imaging studies of the brain are done with anesthetized animals undergoing some form of sensory stimulation. All of the *in vivo* studies conducted here are performed with exposed cortex in anesthetized rats undergoing electrical paw stimulation, a well-established model for somatosensory activation. The details of the surgical preparation and physiological monitoring systems implemented during these experiments are included in Chapter 2 and Appendix A.

1.6.2 *In vivo* imaging of neurovascular coupling

In response to almost any stimulus, discrete regions of the brain will experience an increase in blood flow. It is this hemodynamic response that provides a quantifiable signal that can be measured via fMRI (Kwong et al 1992). Mapping these changes in blood flow has significantly improved our understanding of the way the brain organizes and processes information (Blood et al 2002, Fox et al 2005, Owen et al 1998, Ts'o et al 1990). In 1986,

Grinvald et al. demonstrated that these changes in blood flow could be detected in mammalian brain by simply imaging the exposed cortex using a photodiode array and optical illumination (Grinvald et al 1986). Since then, improvements in digital camera technology, light sources, and optical filters have led to widespread use of so-called 'optical intrinsic signal imaging' (OISI) for neuroscience research (Attwell & Iadecola 2002, Devor et al 2003, Lu et al 2009, Pouratian et al 2002, Vanzetta et al 2005). Changes in reflected light intensity primarily originate from variations in the concentration of oxy- and deoxyhemoglobin that occur as a result of changes in vessel diameter, oxygen delivery, and oxygen extraction (Hillman et al 2007).

Blood flow changes can be detected using a wide range of optical illumination wavelengths, yet the wavelength chosen can dramatically affect the conclusions that are drawn about the spatial extent and temporal evolution of the hemodynamic response (Hillman et al 2007, Sheth et al 2005, Vanzetta et al 2005). This is because oxy- and deoxyhemoglobin (HbO_2 and HbR) have unique absorption spectra and exhibit different spatiotemporal responses in the vascular compartments within the cortex (arteries, veins, and capillaries) (Figure 1.5, Sirotin et al 2009). A significant advance in recent years has been the use of multiple illumination wavelengths and spectroscopic analysis, allowing direct estimation of the changes occurring in HbO_2 and HbR concentrations (Berwick et al 2005, Bouchard et al 2009, Sheth et al 2005). Adding simultaneous measurements of blood flow to this approach makes it possible to infer oxygen delivery and extraction dynamics. Together, these methods hold the potential to link hemodynamic changes to the metabolic demands of the cortex and are therefore closer measures of the underlying neuronal activity (Devor et al 2003, Dunn et al 2005). To date, blood flow dynamics have been imaged using

speckle-flow imaging (Dunn et al 2001) or evaluated at discrete points using Laser Doppler (Jones et al 2001).

Optical imaging methods have also been used to study cellular function. Even before OISI was demonstrated, voltage sensitive dyes were used for cortical mapping of changes in membrane potential (Orbach et al 1985). More recently, calcium sensitive dyes have provided a means to measure changes in neuronal intracellular calcium concentrations (Hillman 2007, Ohki et al 2005). Simultaneous electrophysiological recordings with OISI are also widely used to measure neural activity underlying the blood flow responses (Devor et al 2003).

1.6.3 Optical intrinsic signal imaging

OISI of the exposed cortex offers a method of exploring wide-field spatial and temporal characteristics of the hemodynamic response within the superficial layers of the cortex (Berwick et al 2005, Bouchard et al 2009, Das & Gilbert 1999, Grinvald et al 1986, Sheth et al 2005). OISI measurements consist of camera images acquired while the cortical surface is illuminated with specific wavelengths of light. Changes in the light intensity measured by the camera predominantly reflect changes in absorption due to changes in the concentrations of oxy- and deoxy-hemoglobin ([HbO] and [HbR] respectively). The resulting OIS images represent a 2D, superficially weighted sum of these hemodynamic signals from the pial vasculature and the deeper microvasculature of the parenchyma.

It is possible to compute changes in hemoglobin concentrations from these signals by utilizing the known absorption spectra of HbO and HbR, and an estimate of the distance the light travels in the tissue before reaching the camera sensor (Figure 1.5, equation 1).

The basis of this conversion from signal intensity to concentrations of hemoglobin is given by the modified Beer-Lambert law, which states:

$$\frac{I}{I_0} = e^{-\mu_a DPFx + G} \quad (1)$$

where I is the detected intensity, I_0 is the incident intensity, DPFx is the mean pathlength traveled by photons in the tissue (wavelength dependent "differential pathlength factor"), G is a geometry-dependent factor, and μa is the absorption coefficient of the tissue.

The absorption coefficient is the linear sum of absorbances of major chromophores in the tissue, in this case, HbO and HbR (equation 2). The contribution of each absorber to μa is computed by multiplying ξ n, the wavelength-dependent specific absorption coefficient with its concentration cn :

$$\mu_a = \sum_n \xi_n c_n \quad (2)$$

Since I_0 and G are both difficult to accurately determine, it is common to consider changes in detected signal and changes in hemoglobin concentration, rather than absolute quantities. For observations at two moments in time, t and t_0, the intensity of observed light can be compared using equation 1, rewritten in equation 3 as:

$$ln\left[\frac{I(t)}{I(t_0)}\right] = -[\mu_a(t) - \mu_a(t_0)]DPFx$$

$$\Delta\, ln(I) = -\Delta\mu_a DPFx \quad (3)$$

In order to distinguish changes in HbO and HbR simultaneously, at least two measurements of Δln(I) must be acquired at two different wavelengths (λ_1 and λ_2). Δ[HbO] and Δ[HbR] are then obtained by solving simultaneous equations:

$$\Delta\, ln(I)_{\lambda_1} = -\left(\xi_{HbO,\lambda_1}\Delta c_{HbO} + \xi_{HbR,\lambda_1}\Delta c_{HbR}\right) DPFx_{\lambda_1}$$
$$\Delta\, ln(I)_{\lambda_2} = -\left(\xi_{HbO,\lambda_2}\Delta c_{HbO} + \xi_{HbR,\lambda_2}\Delta c_{HbR}\right) DPFx_{\lambda_2} \quad (4)$$

DPFx, the mean path traveled by photons, is wavelength dependent and generally estimated using a Monte Carlo model of light propagation in tissue (Berwick et al 2005), which requires an estimate of background absorption and oxygenation level of the brain tissue (Kohl et al 2000).

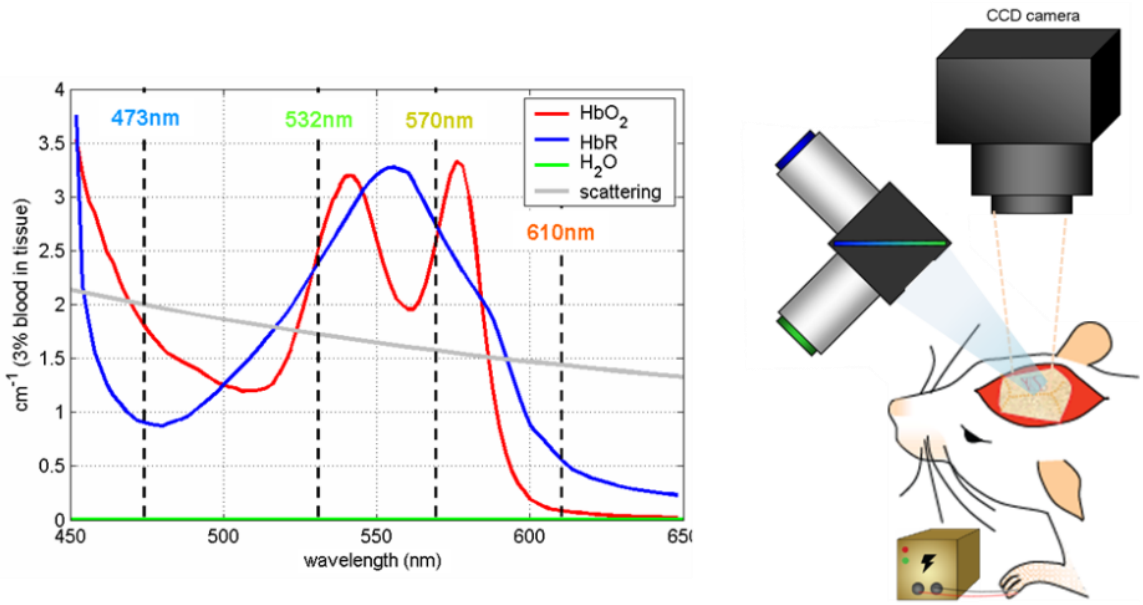

Figure 1.5 Optical intrinsic signal imaging of exposed rodent cortex
(Left) Absorption spectra of HbO and HbR and light scattering. (Right) Setup for exposed cortex imaging using LED illumination and CCD camera. Somatosensory stimulation is delivered in 1mA electrical pulses at 3Hz.

1.6.4 Two-photon microscopy

Two-photon and confocal microscopy are both forms of laser scanning microscopy in which a focused beam of light is raster-scanned across a specimen in order to produce a 2D image. The difference between the two techniques is in the way they accomplish depth discrimination. In confocal microscopy, a pinhole is placed in front of the detector to reject scattered light, thus isolating signals originating from the focus of the scanning beam. Alternatively, two-photon microscopy achieves depth sectioning by only exciting fluorescent molecules at the focus of a high-powered laser (Denk et al 1990). Two-photon microscopy is valuable for studying the living brain because it allows simultaneous imaging of fluorescent vascular tracers, specific cell labels, and active fluorescent dyes with high resolution, significant depth penetration, and less photo-damage to the tissue compared to confocal microscopy.

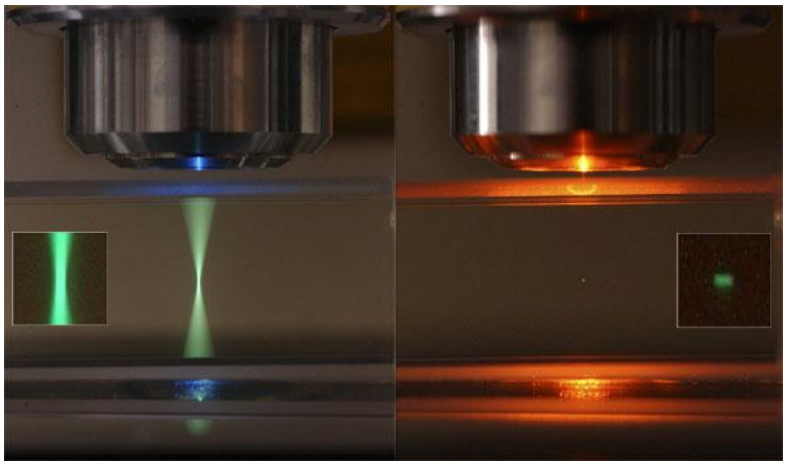

Figure 1.6 Comparison of confocal and 2-photon microscopy
(Left) In fluorescence microscopy, excitation occurs within an entire column of the sample above and below the focal point. (Right) In two-photon microscopy, a small excitation spot is produced at the focal plane. Image by Steve Ruzin and Holly Aaron, UC Berkeley.

In two-photon microscopy, fluorophores are excited by the near simultaneous arrival of two photons of half the energy (twice the wavelength) compared to photons that would excite one-photon fluorescence. This need for two photons to be absorbed virtually at the same time means that femtosecond pulsed lasers with high peak powers are required to generate the highest possible spontaneous photon flux. It also means that two-photon excitation occurs primarily at the focus of the laser beam, and not in areas of lower illumination such as above and below the focus. The long wavelength, lower energy photons used in two-photon microscopy allow deeper tissue penetration, less light scattering, and reduced photo damage and bleaching above and below the focal plane compared to confocal microscopy, making it well suited to in-vivo imaging (Denk et al 1990, Hillman 2007). Tunable lasers make it possible to adjust the excitation wavelengths of the laser to maximize fluorescence emission from a given dye or intrinsic fluorescence source. Dichroic filters can be chosen to distinguish the fluorescent emission signals from multiple fluorescent sources by directing each band of emission wavelengths to a separate detector channel.

Sources of fluorescence contrast The use of two-photon microscopy to study neurovascular coupling *in vivo* is highly dependent on the development of cell-specific fluorescent markers and activity-dependent fluorescent indicators (Table 1.1). Cell specific indicators, such as sulforhodamine 101 (SR101) which is selectively taken up by astrocytes, provide a critical method through which investigations of cellular structure and function can be conducted (Nimmerjahn et al 2004). Transgenic mice with specific cell types tagged with GFP or other fluorescent proteins are also commonly used in conjunction with

exogenous active dyes to identify specific neurons, interneurons, and pericytes in the brain relative to neighboring vasculature (Fernández-Klett et al 2010, Livet et al 2007).

In addition to inert fluorescent cell tags that can be used to identify different cell types, active dyes that can exhibit environment-sensitive changes in spectral properties are also used to study cellular function. In particular, voltage-sensitive dyes (VSDs) and calcium sensitive dyes (CaSDs) are widely used in studies of brain function. VSDs are fluorescent molecules that bind to cell membranes and exhibit a shift in their excitation and / or emission spectra when changes in membrane potential occur. VSDs provide a method for monitoring precise electrical activity where it is not possible, or not desirable to insert a recording electrode (Shoham et al 1999). Most commonly used VSDs in brain imaging are based on aminonapthylethenylpyridinium (ANEP) dyes, which include di-4-ANEPPS or di-8-ANEPPS. The main advantage of VSDs is that they are able to detect fast changes in membrane potential, allowing detection of action potentials rather than slower calcium transients. However, a major limitation of VSDs that has prevented their widespread use for *in vivo* studies is their low signal to background (~0.5%) and poor performance with microscopy (Hillman 2007, Kuhn et al 2008).

CaSDs are also commonly used to study neural and glial activity, as calcium ions play an important role as second messengers in neurons as well as in synaptic transmission and astrocyte signaling. CaSDs non-discriminately label cortical cells and exhibit increases in fluorescence upon binding to intracellular calcium. The combination of SR101 or transgenic fluorescent proteins with calcium sensitive dyes such as Oregon Green BAPTA 1-AM (OGB-1AM), allows differentiated visualization of morphology and calcium activity in astrocytes and neurons (Wang et al 2006). Other calcium indicators that have different

excitation and emission wavelengths include Fluo-3, Fluo-4, Rhod-2, and ratiometric indicators Indo-1, and Fura-2 (Dustin 2000). Developments in transgenic animal technology have also produced genetically encoded calcium sensors which do not require exogenous labeling, thereby enabling more homogenous and consistent cell labeling staining (Heim et al 2007)[3].

In the absence of any exogenous dyes, brain tissue also contains a range of intrinsic fluorophores including metabolic coenzymes nicotinamide adenine dinucleotide (NADH) and flavin adenine dinucleotide (FAD), both of which exhibit unique spectral properties (Grosberg et al 2011, Radosevich et al 2008). NADH is a high energy compound that is produced during glycolysis, whereby glucose is converted into pyruvate. NADH and FAD are also the primary electron donor and acceptor, respectively, in the oxidative phosphorylation metabolic pathway. Both coenzymes can exist in two different redox states, only one of which is fluorescent. $FADH_2$, the reduced form of FAD, and the NAD^+, the oxidized form of NADH are not fluorescent. Thus, quantification of NADH and FAD changes during functional brain activation can in principle, provide valuable insight into brain cellular metabolism (Foster et al 2005, Kasischke et al 2004, Skala et al 2007).

Intravascular tracers are delivered intravenously to label the blood plasma and allow visualization of vessel diameter as well quantification of speed of red blood cells, which appear as black spots in the vessel (Kleinfeld et al 1998). Many fluorescent vascular tracers are often conjugated to large molecules, such as dextran polysaccharides, to prevent them from passing through the blood brain barrier.

---

[3] This review summarizes the properties of commonly used calcium sensitive indicators: Takahashi A, Camacho P, Lechleiter JD, Herman B. 1999. Measurement of Intracellular Calcium. *Physiological Reviews* 79: 1089-125

Table 1.1 Sources of fluorescent contrast used with two-photon microscopy

Fluorophore	Excitation λ	Emission λ	Labels	Delivery method
NADH/FAD	~740 nm	Blue/green	Metabolites	Intrinsic
Oregon Green BAPTA 1AM (OGB-1AM)	~850 nm	Green	Cortical cells	Cortical pressure injection
Sulforhodamine 101 (SR101)	~790 nm	Red	Astrocytes	Topical (under dura)
Texas Dextran Red (TDR)	~850 nm	Red	Blood plasma	Intravenous
Fluorescein (FITC-dx)	~780 nm	Green	Blood plasma	Intravenous

Chapter 2

Methods for *in vivo* imaging of neurovascular coupling

2.1 Introduction

Exposed rodent cortex models have been well established and widely used for optical brain imaging and neurovascular coupling research. The surgical and experimental procedures involved in these experiments are extensive and complex, and often include a number of physiological monitoring systems to ensure proper physiology and depth of anesthesia. Since animal preparations vary between different research groups, it is important to understand how physiological parameters and different anesthesia may affect the data collected. This is especially important when we compare results across studies using different preparations.

In this chapter, I describe the methodology that I established for conducting exposed cortex experiments to study *in vivo* neurovascular coupling and demonstrate how our imaging systems can be used to observe and measure the spatiotemporal dynamics of hemoglobin oxygenation, changes in blood vessel diameter, blood flow dynamics from the motion of red blood cells in superficial vessels of the exposed cortex, and local neuronal activity from the detection of a calcium sensitive fluorescent dye.

2.2 Animal procedures

This section will describe the general procedure used for the studies described in this thesis. In subsequent chapters, additional procedures that are performed for specific experiments are further detailed in their respective methods sections.

Sprague-Dawley rats (300 ± 40 g) are surgically prepared under isoflurane anesthesia (0.5-4% inhalation in oxygen) and then switched to intravenous alpha-chloralose (40 mg $kg^{-1}h^{-1}$) during stimulation and imaging. Animals are mechanically ventilated via tracheotomy with a 3:1 ratio of air to oxygen to avoid the respiratory suppression often caused by alpha-chloralose sedation. Femoral arterial and venous catheters are placed to allow continual blood pressure monitoring and delivery of intravenous alpha-chloralose. Following tracheotomy and vessel cannulation, the head is fixed in a stereotaxic frame and a portion of the skull (~ 5 mm x ~7 mm) is removed to expose the somatosensory cortex. The IV^{th} ventricle is opened to relieve intra-cerebral pressure prior to removal of the dura mater. Dental acrylic is then used to seal a glass coverslip with a drop of agarose in artificial cerebrospinal fluid over the exposed region, creating a window for imaging. For fluorescence imaging, the calcium indicator Oregon Green 488 BAPTA-1AM is pressure

injected into the cortex with glass pipettes (Picospritzer III, Parker Instrumentation). The dye is allowed to incubate for 1 hour prior to imaging. A detailed guide to surgical procedures and dye loading can be found in Appendix A.

After all surgical procedures are complete, the animal is transitioned off of isoflurane anesthesia and onto alpha-chloralose anesthesia. A bolus injection of intravenous alpha-chloralose is used to mediate this transition, during which blood pressure is closely monitored for dramatic drops or increases. Once the animal's blood pressure has stabilized, continuous intravenous infusion of alpha-chloralose is initiated. To prepare for imaging, LEDs and the CCD camera are positioned and focused onto the exposed cortex. For the experiments described in this thesis, blue (470 nm), (green 530 nm), and red LEDs were used to illuminate the cortex during imaging. To maximize reflectance signal detected by the camera, care is taken to optimize illumination of the exposed cortex by adjusting the height and angles of the LEDs. In cases where the exposed cortex is positioned at an angle relative to the camera lens, the stereotax is carefully propped to ensure a flat imaging plane.

Somatosensory pathways are activated via electrical forepaw or hindpaw stimulation. Electrodes are placed on the right forepaw or hindpaw and connected to an electrical stimulus unit (A360, World Precision Instruments) delivering 0.3 ms pulses at 3 Hz with 1.0 ± 0.1 mA amplitude. Each imaging run lasts 40 seconds and consists of a specified duration of stimulation that is preceded by 6 seconds of baseline recording (no stimulus) and followed by a period of post-stimulus recording. Prior to imaging, the stimulus amplitude is tested to ensure that the electrical stimulus is not painful. The depth of anesthesia, which is monitored by whisking activity and pain responses, can affect the acceptable stimulus amplitude.

2.3 Data collection methodology and analysis

2.3.1 Data acquisition

This section will provide a brief overview of the data collection methodology followed by a detailed demonstration of the oxygenation, vasomotor, and calcium dynamics that can be extracted from the acquired images.

The duration of an entire imaging experiment ranges between 7-11 hours. Despite all physiological monitoring measures, the quality of an animal's physiology will inevitably exhibit changes throughout the experiment. Minimizing the amount of time spent on the surgical preparation has often resulted in longer periods of stable physiology for imaging. Keeping this in mind, "sets" of stimulus runs that will be analyzed together are acquired as close in time as possible throughout the experiment. This ensures that the rat's physiology is similar across these runs.

Functional maps obtained from wide field OISI highlight regions of greatest hemodynamic change and can be used to assess the quality of the hemodynamic response during data acquisition. If subsequent two-photon imaging is performed, functional maps can be used to guide placement of the rat under the two-photon objective. When acquiring two-photon data, care is taken to avoid photo-bleaching or damaging an area of interest when multiple stimulus runs are acquired in the same field of view. To avoid damage, the power is lowered for consecutive runs and for imaging in superficial layers of the cortex. Control runs without stimulation are frequently taken to avoid confounding affects that laser power may have on cellular dynamics. At the end of imaging for a certain field of view,

a high resolution stack is often acquired to provide 3-D information about vasculature structure and cellular distribution in the region of interest. In general, the timeline of an experiment is as follows:

Table 2.1 Timeline for *in vivo* imaging experiment

Surgery (2-3 hrs)	Anesthesia switch (0.5 hrs)	Acquisition of OISI data (2-4 hrs)	Acquisition of 2-photon data (2-4 hrs)
• tracheotomy • femoral lines • craniotomy • injection of dyes if necessary • cranial window • stimulus electrodes	• turn off isoflurane • inject alpha-chloralose bolus • begin IV alpha-chloralose infusion	• position camera and LEDs • test stimulus amplitude • acquire data	• transport animal and physiological monitoring equipment to two-photon room • position animal under objective • locate region of interest based on OIS images • acquire data

2.3.2 Oxygenation dynamics

Ultra-fast imaging of the exposed cortex with multispectral illumination allows us to visualize wide field dynamics of blood oxygenation in individual arteries, veins, and discrete regions of the parenchyma simultaneously in a single imaging run. We converted our 470 nm and 530 nm image sets to images of oxy- and deoxyhemoglobin (HbO_2 and HbR, total hemoglobin HbT = Hb O_2 + HbR) using the Modified Beer Lambert Law and standard HbO_2 and HbR absorption spectra (Prahl 1998). We utilized average path length estimates provided by a Monte Carlo simulation of light propagation in brain tissue (Dunn et al 2005).

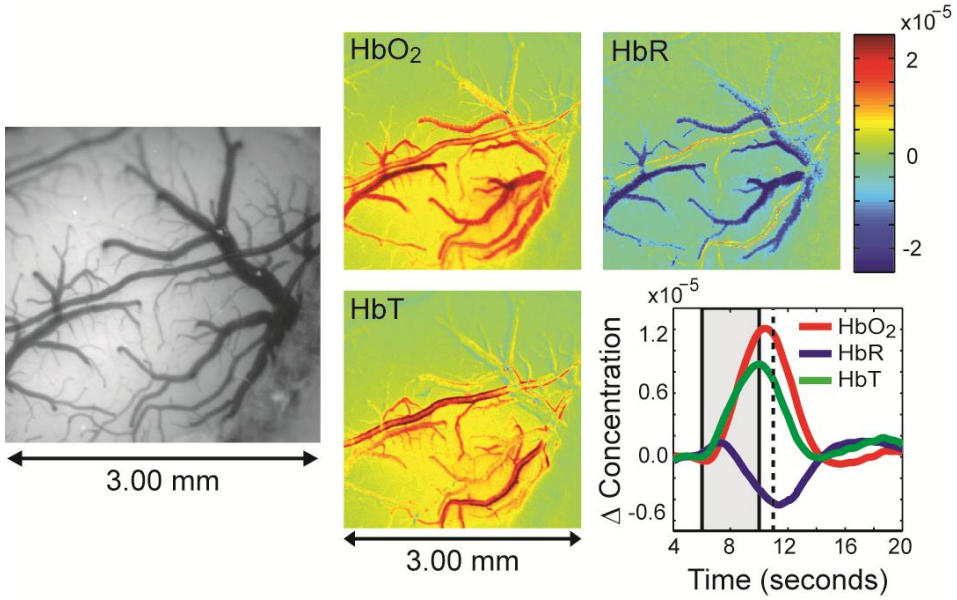

Figure 2.1 Oxygenation changes during somatosensory stimulation
Gray scale image of exposed rat somatosensory cortex. Images showing concentrations of HbO2, HbR, and HbT at t = 11 seconds (corresponds to dotted line on time course). Time courses showing the average change in HbO2, HbR, and HbT concentration across the entire field of view. Timing of hindpaw stimulus is shown in grey region. Figure taken from Bouchard et al 2009.

Since data was acquired with three LEDs (470 nm, 530 nm, and 630 nm), but conversion strictly only requires two wavelengths, data was converted with all three possible pairs of wavelengths in order to confirm proper and consistent conversions.

The high spatial and temporal resolution of our imaging system makes it possible to clearly visualize and measure the evolution of blood oxygenation in individual vessels. Figure 2.1 shows a gray scale image of an example field of view and the resulting converted $\Delta[HbO]$, $\Delta[HbR]$, and $\Delta[HbT]$ images at 11 seconds just following the end of stimulation. From these maps, we are able to see that the spatial distribution of HbO_2, HbR, and HbT differs between the arteries, veins, and parenchyma. We can further explore temporal oxygenation dynamics by extracting the time courses of HbO_2, HbR, and HbT

concentrations from the whole region (Figure 2.1) or from specific regions such as arterioles, veins and the parenchyma (Hillman et al 2007). Arterial, venous, and parenchymal regions can be readily distinguished based on their differing spectroscopic properties. The RGB image in Figure 2.2a was created by setting the red channel to the ratio of the 530 nm image to the 470 nm image, the green channel to 530 nm image, and the blue channel to the ratio of the 470 nm image to the 530 nm image. This image shows arteries in red, veins in purple, and parenchyma in green and yellow (Bouchard et al 2009).

2.3.3 Vascular and blood flow dynamics

Our optical imaging system allows us to take fast, wide field images of cortical surface vessels with sufficient resolution to quantify not only changes in blood oxygenation, but also vessel diameter and blood flow velocity simultaneously across the entire field of view. This makes it possible to capture many aspects of vascular dynamics from a single imaging data set. Figure 2.2 demonstrates our ability to zoom in on different regions of the wide field image to extract oxygenation, vasomotor, and blood flow dynamics on a data set collected at 60 fps. Close up HbO images in Figure 2.2b show the mixing of blood from two vein branches with different oxygenation levels. From the oxygenation maps in Figure 2.1 and Figure 2.2b, we note that the more oxygenated blood is draining from the center of the activated parenchyma (bottom left of images), while the blood draining from regions outside of the activated area (upper right of images) is less oxygenated relative to baseline.

In addition to spectroscopic analysis of individual vessels, we are also able to track changes in vessel diameter during the stimulus run from only the 530 nm data set (Figure 2.2c-d).

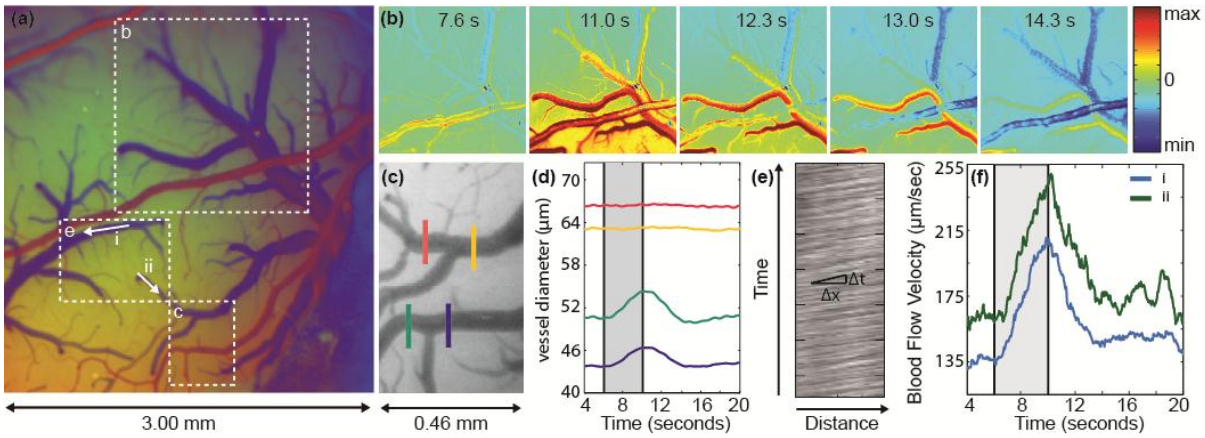

Figure 2.2 Quantification of vascular dynamics
(a) RGB image created using baseline 470 nm and 530 nm images allow veins (blue) and arteries (red) to be easily distinguished. Selected regions are shown in more detail in (b)-(f). (b) Mixing of oxy- and deoxyhemoglobin from different vein branches combining into a single larger vein. (c) Cross sections of vein and artery used for vessel diameter analysis shown in (d). (d) Time courses of vessel diameters. (e) Matrix of line scans showing movement of red blood cells as dark stripes. (f) Time course of blood flow velocity in veins i and ii labeled in (a). Data was collected at 60 fps and averaged across 20 trials. Figure taken from Bouchard et al 2009.

The cross sectional diameters shown by the lines in Figure 2.2c are plotted over time in Figure 2.2d and were calculated from the normalized full width half minimum of the image intensity along a line perpendicular to the vessel at each point. Comparing these vessels with the ratio map in Figure 2.2a, we see that the arteries exhibit a significant vasodilation whereas the veins do not (Hillman et al 2007).

The high spatial and temporal resolution of our data also allows us to extract blood flow velocity in surface veins from the movement of red blood cells in the blood plasma. Figure 2.2e shows a line segment along a vein that is plotted over time. The dark stripes correspond to red blood cells traveling along the length of the vessel, and the slope of the lines is proportional to the speed at which the red blood cells are traveling (Kleinfeld et al 1998). Simple correlation analysis of these space-time plots permits accurate calculation of

both the speed and direction of flow in any selected vessel segment (Hillman et al 2007). Flow dynamics in two separate vein branches from a single run are shown in Figure 2.2f, indicating faster flow in the smaller vein. These analyses can similarly be applied to all vessels in the field of view to provide information on the spatial extent of diameter and flow dynamics. Our data sets are also suitable for wide field optical flow tracking algorithms (Duan et al 2008).

2.3.4 Calcium dynamics

Increases in intracellular $[Ca^{+2}]$ through calcium channels are observed during both neural activity and astrocyte signaling (Stosiek et al 2003, Takata & Hirase 2008). Neurovascular studies have used calcium-sensitive fluorescent dyes, such as Oregon Green 488 BAPTA 1-AM, as an alternative to voltage-sensitive dyes to study neuronal and glial activity during the hemodynamic response (Takano et al 2005, Wang et al 2006). The activity of OGB-1AM can be detected with both wide-field camera imaging as well as with two-photon microscopy, making it possible to study calcium dynamics on different length scales.

Figure 2.3 demonstrates our ability to measure both hemodynamic and fluorescence dynamics in parallel using wide-field OIS and fluorescence imaging. Figure 2.3a shows images of the exposed cortex injected with fluorescent calcium indicator Oregon Green 488 BAPTA 1-AM under 530 nm and 490 nm illumination. A 500 nm long pass filter in front of the camera means that during blue illumination, the camera sees green fluorescence emission from the calcium sensitive dye, whereas during green illumination, the camera sees green reflectance, providing a measure of HbT dynamics.

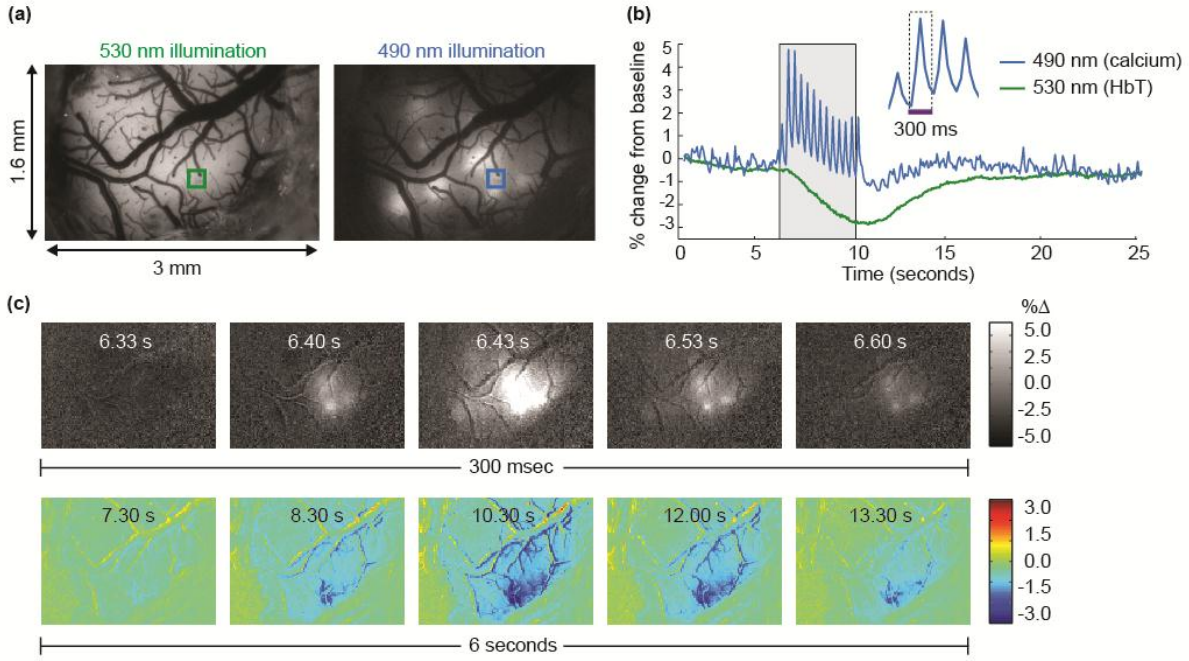

Figure 2.3 Wide-field imaging of calcium activity
Left: Exposed somatosensory cortex under 530 nm illumination. Right: The same field of view under 490 nm illumination and 500 nm long pass emission filter shows injection sites of Oregon Green 488 BAPTA 1-AM calcium indicator. (b) Time courses of selected regions of the cortex as shown in green and blue boxes in (a). Duration of electrical hindpaw stimulation is shown in gray. Close up of individual calcium "spikes" is shown in inset. (c) Top: Images of the cortex under 490 nm illumination during the evolution of a single calcium spike shown in (b inset) lasting over period of 300 ms. Bottom: Images of the cortex under 530 nm illumination showing the evolution of the hemodynamic response over a period of 6 seconds. Data was taken at 30 fps and 25 ms exposure time averaged across 10 trials. Figure taken from Bouchard et al 2009.

Time courses of both calcium sensitive dye fluorescence and 530 nm reflectance for a selected region of the parenchyma can be extracted and plotted together to show the temporal relationship between neuronal activity and the hemodynamic response (Figure 2.3b).

From these time courses, we can see rapid changes in calcium sensitive dye fluorescence that correspond to each electrical pulse delivered to the hindpaw at 3 Hz, as well as the slow hemodynamic response that reaches its maximum amplitude at the end of the 4 second

stimulation period. The high temporal resolution of our system makes it possible to visualize the spatiotemporal evolution of both calcium and HbT dynamics on drastically different time scales. Figure 2.3c shows images of the full field of view during the evolution of a single calcium spike (over 270 ms) and the entire hemodynamic HbT response (over 6 seconds). For these images, the 530 nm signal was converted into HbT as described above (under the approximation that 530 nm is an isosbestic point for oxy- and deoxyhemoglobin). We note that the region of greatest activity during a calcium spike co-localizes well with the region of greatest HbT change. This data set was collected with two LEDs at 30 fps with a 25 ms exposure time. The examples presented above were published in a joint first author paper in Optics Express in 2009 (Bouchard et al 2009).

2.3.5 Two-photon microscopy

Two-photon microscopy makes it possible to observe cellular level activity and vascular dynamics up to depths of 500 μm in the living brain. We use transgenic models expressing fluorescent proteins and cell specific dyes such as SR101 to target specific cells that have been implicated in neurovascular coupling. Figure 2.4 show examples of various fluorophores being used to co-label neurons, interneurons, astrocytes, and smooth muscle actin with intravascular tracers labeling the blood plasma. The multiple detector channels (red: 350-505 nm, blue: 505-560 nm, green: 560-650 nm) on our two-photon microscope allow many of these forms of fluorescent contrast to be acquired in parallel. In addition, high resolution z-stacks can be acquired to allow 3-D reconstructions of a volume of brain tissue. This technique has allowed us to conduct a detailed study of the distribution and morphology of neuronal and astrocytic cell bodies and processes (McCaslin et al 2011).

Wide-field OISI and two-photon microscopy can be performed on the same rat to obtain both vascular and cellular dynamics on different length scales. OISI allows us to localize the regions of greatest neuronal and hemodynamic activity (Figure 2.3). Using these images as a guide, we are able to use two-photon microscopy to study calcium dynamics at a cellular level for both neurons and astrocytes in the vicinity of the observed vascular changes. By comparing cellular level calcium dynamics with the timecourses of vascular change, we are able to correlate calcium events with phases of hemodynamic changes. In addition, two-photon microscopy of fluorescent vascular tracers can offer more precise measurement of vessel diameter dynamics, by avoiding potential confounds of hemoglobin absorption present during OISI. Further discussion of *in vivo* data acquired using two-photon microscopy is detailed in Chapter 4.

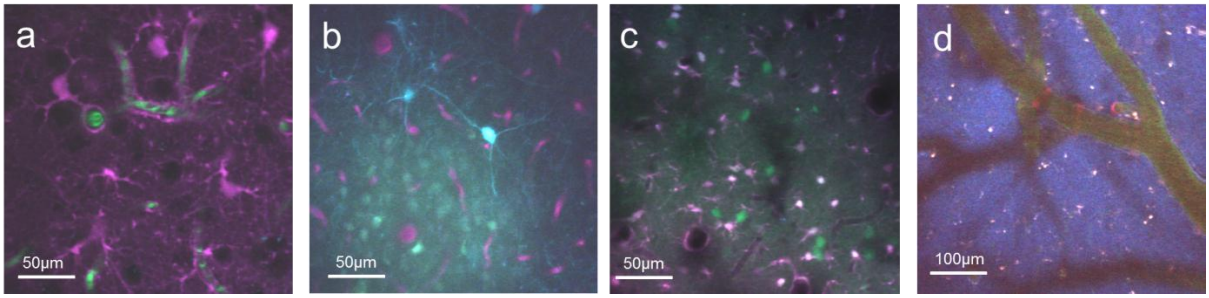

Figure 2.4 Two-photon microscopy of cortical cells *in vivo*
(a) Astrocytes labeled with SR101 encircle diving vessels with their cell bodies and processes. Blood vessels are labeled with FITC-dx. The dark holes represent unlabeled neuronal cell bodies. (b) GFP expressing somatostatin interneurons are found to be scarce among a dense region of cell bodies labeled with OGB-1AM, and do not appear to associate with blood vessels, labeled here with DTR. (c) Co-labeling of astrocytes and neurons with SR101 and OGB-1AM. (d) Rings of smooth muscle actin labeled with RFP encircling arterioles labeled with FITC-dx and NADH intrinsic fluorescence.

Chapter 3

High-speed vascular dynamics of the hemodynamic response

3.1 Introduction

Understanding the detailed vascular dynamics that comprise the hemodynamic response to sensory stimulation is a critical first step towards developing a robust model for neurovascular coupling and its associated cellular mechanisms. While a range of cellular mechanisms have been proposed to underlie control of neurovascular coupling, a comprehensive model that reconciles different observations has yet to be developed. To fit in such a model, it is essential that candidate mechanisms exhibit reaction times, spatial ranges, and speeds of propagation that are consistent with the vascular manifestations of the 'hemodynamic response.' Thus, we apply the tools developed in Chapter 2 in an investigation of the hemodynamic response itself.

In this chapter, we utilize high-speed and high-resolution optical imaging of exposed rodent somatosensory cortex to explore and characterize the spatiotemporal dynamics of surface vessels during functional hyperemia. Our approach allows us to study the hemodynamic response in individual vessels and in discrete regions of the parenchyma with the resolution necessary to precisely characterize spatial and temporal features of the response. Specifically, we explore when and where the first hemodynamic changes occur in response to stimuli, the direction and speed at which these changes propagate in arterioles and regions of the parenchyma, and the relative timing at which each of these compartments return to its original baseline state. From these results, we conclude that the hemodynamic response is initiated in the parenchyma and then spreads rapidly to surface arterioles. Following the initial onset, we find evidence that this response spreads spatially outwards via the dilation of targeted arterioles and the propagation of vasodilation is independent of the direction of blood flow within each arteriole. We also find evidence that the signal's decay is more spatially uniform, as opposed to targeting vessels, which in turn causes the periphery of the responding region to return to baseline first. We hypothesize that different underlying cellular mechanisms/signaling pathways are responsible for the response initiation and the response decay. Our results place tight constraints on theories that describe the hemodynamic response, enabling us to evaluate whether potential cellular mechanisms are likely to be involved in neurovascular coupling.

3.2 Background

Orchestration of the hemodynamic response most likely involves cellular signaling mechanisms that communicate to the local vasculature that changes in blood flow are

required. Cellular systems capable of actuating and propagating dilations and constrictions must also be present, with a distribution and connectivity that is consistent with the spatiotemporal spread and decay of the hemodynamic response.

A range of candidate mechanisms has been studied in recent years. *In vivo* and *in vitro* studies at the cellular level have used high resolution imaging techniques, such as Dodt gradient contrast imaging and two-photon microscopy, with specific attention being paid to astrocytes, interneurons and pericytes (Cauli et al 2004, Peppiatt et al 2006, Schummers et al 2008, Wang et al 2006, Winship et al 2007). These studies have focused on isolated cell-vessel interactions, exploring which cell types are capable of eliciting various vasomotor dynamics in neighboring vessel segments. Similarly, hemodynamic changes at the level of individual vessels have been characterized with in-vivo microscopy (Devor et al 2007, Hillman et al 2007, Kleinfeld et al 1998, Stefanovic et al 2008, Villringer et al 1994, Wang et al 2006). However, while many mechanisms have been proposed as a result of these studies, none of them have been validated as being consistent with the actual behavior of the vascular network during the hemodynamic response. We believe that this inconsistency is due, in part, to a current lack of detailed knowledge about the vessel-specific behavior that constitutes the hemodynamic response. To date, questions such as the following have not been accurately addressed: When and where does the hemodynamic response start? How, where and at what speed does it propagate? And, how do 'return to baseline' dynamics differ from the response initiation dynamics? With proper knowledge of these parameters, it should be possible to more accurately assign potential cellular mechanisms to the different aspects of hemodynamic response orchestration.

Optical intrinsic signal imaging (OISI) of the exposed cortex offers a method for exploring wide-field spatial and temporal characteristics of the hemodynamic response within the superficial layers of the cortex (see Figure SB.1 for an example[4]). OISI images represent a 2D, superficially weighted sum of signals from the surface vasculature and the deeper microvasculature of the parenchyma. Many OISI studies to date have imaged through thinned skull at relatively slow speeds and used different wavelengths of light to capture 'activation maps' of the hemodynamic response in the cortex. (Berwick et al 2005, Das & Gilbert 1999, Grinvald et al 1986, Sheth et al 2005). We recently developed an approach to OISI that offers high-resolution, high-speed imaging of exposed cortex, allowing the rapid responses of individual vessels to be observed (Bouchard et al 2009). Our OISI technique, implemented in rodent somatosensory cortex, allows the study of changes occurring in almost all superficial vessels in and around the region of activation simultaneously. In order to perform a comprehensive characterization of vascular dynamics during functional hyperemia, we have combined this imaging technique with a new approach to spatiotemporal analysis that overcomes confounds in timing measurements due to response amplitude and baseline variability.

3.3 Methods

3.3.1 Animal methods

The experiments in this study were conducted using exposed cortex model in adult rats under alpha-chloralose anesthesia. Details of this method are provided in Chapter 2. Briefly,

[4] Supplemental figures for Chapter 3 are found in Appendix B

a craniotomy was performed to expose the somatosensory cortex and a cranial window was created to minimize contamination and brain motion during imaging. A tracheotomy was performed to allow mechanical ventilation and placement of femoral arterial and venous catheters enable continuous blood pressure monitoring and delivery of intravenous fluids. Electrical hindpaw stimulation was delivered in 3 ms pulses at 3 Hz with 1.0 ± 0.1 mA amplitude. All animal procedures were reviewed and approved by the Columbia University Institutional Animal Care and Use Committee.

3.3.2 Optical imaging methods

A ~3 x 3 mm region of the exposed cortex was imaged using our high-speed OISI system. The system utilizes a Dalsa 1M60 CCD camera configured to acquire in synchrony with strobing blue and green light emitting diodes (LEDs) mounted with 470 ± 5 nm and 530 ± 5 nm filters respectively (MBLED, MGLED, FB470, FB530, Thorlabs). Dual wavelength data were acquired either at 60 or 50 frames per second (equivalent to 30 fps or 25 fps for each LED) with a 5 ms exposure time and 256 x 256 pixel resolution. Details of the system are described in (Bouchard et al 2009). Each imaging run consisted of 6 seconds of pre-stimulation, 4 seconds of stimulation, and 12 seconds of post-stimulation. Forepaw and hindpaw stimulation were presented in sets of 10 runs. A total of 5 rats were used in this study.

3.3.3 Analysis methods

General Methodology We developed a method of analysis specifically to study the timing characteristics of the hemodynamic response to functional stimulus. Typical time courses of

total hemoglobin concentration changes Δ[HbT] following somatosensory stimulation are shown in Figure 3.1C. The baseline is recorded prior to stimulation, followed by the onset, rising slope, peak, falling slope, and return-to-baseline of the response.

To understand where and when the hemodyamic response begins, we need a method of quantifying the "onset time" of the Δ[HbT] response. Many studies to date have attempted to characterize the overall timing of the hemodynamic response pattern by estimating the time-to-peak (TTP, or to some % of the peak) of the response within different regions or compartments (Berwick et al 2005, Blood et al 2002, Sheth et al 2005, Vanzetta et al 2005). However, as illustrated in supplemental Figure SB.3, the TTP or other threshold-based measures may or may not be related to the time at which the response is initiated. For example, if two regions were to exhibit identical onset times and rates of increase, but the post-stimulus decay of one began before the other, then the TTP would be completely unrelated to the signals' true onset times (Figure SB.3 A). The various combinations of onset time, onset slope, peak amplitude and inflection point all influence the TTP and its relation to the true onset time. With so many free parameters describing the structure of these complex responses, a single statistic (eg. TTP) cannot be used as a reliable measure to characterize all the variations of interest.

In our approach, we estimate when the response signal in each pixel deviates from its baseline state. This allows us to determine when the signal in each region has 'onset', i.e. transitioned out of its baseline state, up to a specified level of confidence. An analogous calculation is used to determine the time at which the signal returns to its baseline state. Our technique estimates the earliest moment at which we can confidently observe a

transition out of (or into) the baseline state. However, this method may still be affected by the rate at which signals rise, if baseline signals exhibit nonzero variance. For example, two signals with identical onset times and identical noise levels but different rates of increase will yield different apparent onset times (Figure 3.1G). Alternatively, two signals with identical time-courses but different levels of baseline noise will also yield different apparent onset times (Figure 3.1H). We therefore apply a second level of processing to compensate for this effect. Details on this technique are provided below.

Pre-processing All analysis was performed using Matlab™. Data sets from each run were co-registered between consecutive frames and low pass filtered at 5Hz to minimize variance due to motion artifacts related to breathing and heart rate. All analysis was performed on single-run data sets that were mean-normalized by their average baseline value.

Since 530nm is an isobestic point for hemoglobin absorption, the baseline-normalized signal acquired with this wavelength (I/I_0) should be independent of changes in oxygenation and thus provide only a measure of Δ[HbT] concentration when converted using the Beer Lambert law:

$$\Delta[HbT] = -\frac{1}{\alpha}\ln\left(\frac{I}{I_o}\right) \qquad \text{Eq. 1}$$

where

$$\alpha = \frac{(\varepsilon_{HbO,530} + \varepsilon_{HbR,530})}{2} x_{530}. \qquad \text{Eq. 2}$$

α is a constant that is expected to be approximately spatially and temporally invariant, and depends on x_{530} (an estimate of the mean pathlength of 530 nm light in the rat cortex) and

$\varepsilon_{HbT,530}$, the mean molar extinction coefficient for HbO and HbR at 530 nm. Since α is dependent on the choice of a light propagation model and the accuracy of estimates of the molar extinction coefficients, we analyzed and display our data in terms of $\alpha\Delta[\mathrm{HbT}]$, which is linearly proportional to $\Delta[\mathrm{HbT}]$ (Hillman 2007). We began by carefully ensuring that our multispectral-converted $\Delta[\mathrm{HbT}]$ signals (derived from both blue (470 nm) and green (530 nm) data) corresponded accurately to changes in $[\mathrm{HbT}]$ calculated using Eq. 1. However, we chose to utilize only data acquired at 530 nm to avoid the potential confounds of inaccurate conversion of spectral data into hemoglobin concentrations (Kohl et al 2000, Sirotin et al 2009). While oxygenation dynamics can readily be extracted from our dual-wavelength data, our primary goal here was to understand the timing of vascular responses as indicated by changes in vessel diameter or hematocrit, both of which can be determined from measures of $\Delta[\mathrm{HbT}]$.

Calculation of response onset and return 'tau' (τ) We model our measured signals as having two states: a *baseline state* and a *stimulated state*. We start our analysis by characterizing the signal variability for each pixel under baseline conditions for the 3 seconds prior to stimulation. Figure 3.1D-E displays the probability distribution function (PDF) of baseline total hemoglobin absorption for parenchyma and artery regions computed using a kernel density estimator. When pixel $\Delta[\mathrm{HbT}]$ levels are well beyond the PDF observed in the baseline, it is improbable that a pixel is still in the baseline state. At every time point we calculate the probability that a pixel's signal has departed from the baseline $\Delta[\mathrm{HbT}]$ PDF, this is computed as the integral of the PDF for values above the observed level (p-value = 1 – cdf, the cumulative distribution function). Figure 3.1F shows

how p-values of the selected pixels change over time. We define onset τ (τO) as the time after stimulation when a pixel is first observed in the stimulated state at the 90% confidence level. A similar analysis is done to estimate the time of the return transition, denoted *return* τ (τ_R). We use τ to denote an estimate of the time of events. In practice, τ values are computed by determining the time at which the un-normalized, smoothed (12^{th} order polynomial fit) time course in each pixel crosses a threshold based on that pixel's baseline variance. Supplemental Figure SB.4 shows a map of threshold values for the 90% confidence level. We note that while there is heterogeneity across threshold values between vessels and parenchyma, we do not observe any systematic spatial differences across the exposed cortex.

For each run in every rat, we computed the τ_O and τ_R of every pixel. Averaging each pixel's τ values over runs for a single rat generates a "τ map" depicting the average times at which each pixel is observed to transition between baseline and stimulated states (Figure 3.2A-B). Regions that do not exhibit significant changes in [HbT] are shown in black.

Correcting τ values for initial rate of change The calculated τ_O values described above characterize the moment when the first *observable* hemodynamic response occurs in the tissue. Prior to τ_O, we cannot claim to observe changes that are distinguishable from baseline noise. However, the calculated τ_O is not only influenced by the signal's true onset time, but also by the level of baseline variance and the initial slope of the signal as well (Figure 3.1G-H, Figure SB.3).

This effect can be visualized by generating a simulated data set using an average representative time-course from the data for each rat. At every pixel the representative

time-course is scaled such that its amplitude matches the amplitude (A) of the original signal at time t_A (Figure 3.1I). Thus, every pixel in the simulated data set has an identical true onset time but varying rates of change, which are prescribed from the original data. If we calculate a map of τ using this simulated data, but with threshold values (m) determined from the baseline variance at every pixel of the original data, we observe a range of apparent onset times that are due only to differences in spatial variations of onset slopes (Figure 3.1C-D). These simulated (τ_{sim}) maps illustrate how much our original estimates of τ are influenced by spatial variations in the rate of signal change. We can thus use these maps as a means to correct our original (τ_{orig}) maps, since regions where τ_{orig} maps differ from τ_{sim} maps are likely to be regions where there are genuine differences in true onset.

More formally, if we assume signals are linear between the true onset time and time t_A (Figure 3.1 I), then the relationship between the τ_{orig}, the τ_{sim}, and the corrected τ (τ_{corr}), highlighted in gray in Figure 3.1 I) can be written as:

$$\tau_{corr} \approx \frac{A(\tau_{orig} - \tau_{sim})}{A - m} + t_0 \qquad \text{Eq. 3}$$

where t_0 is the true onset time of the simulated response curve. The amplitude A of the signal at time t_A and the baseline threshold m are both specific to each pixel and are determined by the original data. The value of t_A will affect the appropriateness of our linear approximation. For this analysis, we set $t_A = 2$ seconds following the start of stimulation. By applying this correction, we generate τ_{Ocorr} maps that provide an estimate of "true onset" decoupled from the signal's rate of change. The same method is applied to obtain a baseline return τ_{Rcorr}, by using a value of $t_A = 6$ seconds following the start of stimulation.

In summary, the existence of baseline noise places a constraint on what is observable during a single experimental run, if we are not willing to make additional assumptions about the structure of the data below the noise level (τ_{orig}). However, the true timing of the signal onset is a meaningful parameter with regards to the physiology of response initiation. Thus, if we are willing to make assumptions regarding the behavior of the signal below the noise level, we can make an estimate what the true onset time would be independently of the signal's initial rate of change (τ_{corr}).

Distinction of vascular compartments We use the differing baseline oxygenation properties of the arterial, venous, and parenchymal regions revealed in 470nm and 530 nm baseline images to effectively isolate compartments for further analysis. This method is described in detail in (Bouchard et al 2009). To explore which compartment has a faster observable onset time, we overlay parenchyma and arterial masks with onset τ and return τ maps to obtain distributions of compartment-specific τ values.

Quantification of signal onset and return τ propagation speed Speed of τOcorr and τRcorr propagation can be quantified by linearly regressing τcorr values on linear distance from the center of the responding region (Figure 3.3B-E). The inverse slope of the fitted regression line is then the estimated speed of τOcorr and τRcorr in units of mm/s. We also investigate the directions of τOorig and τRorig propagations by taking the sign of the regression slope as a function of distance from the center of the responding region (Figure 3.4 D-E).

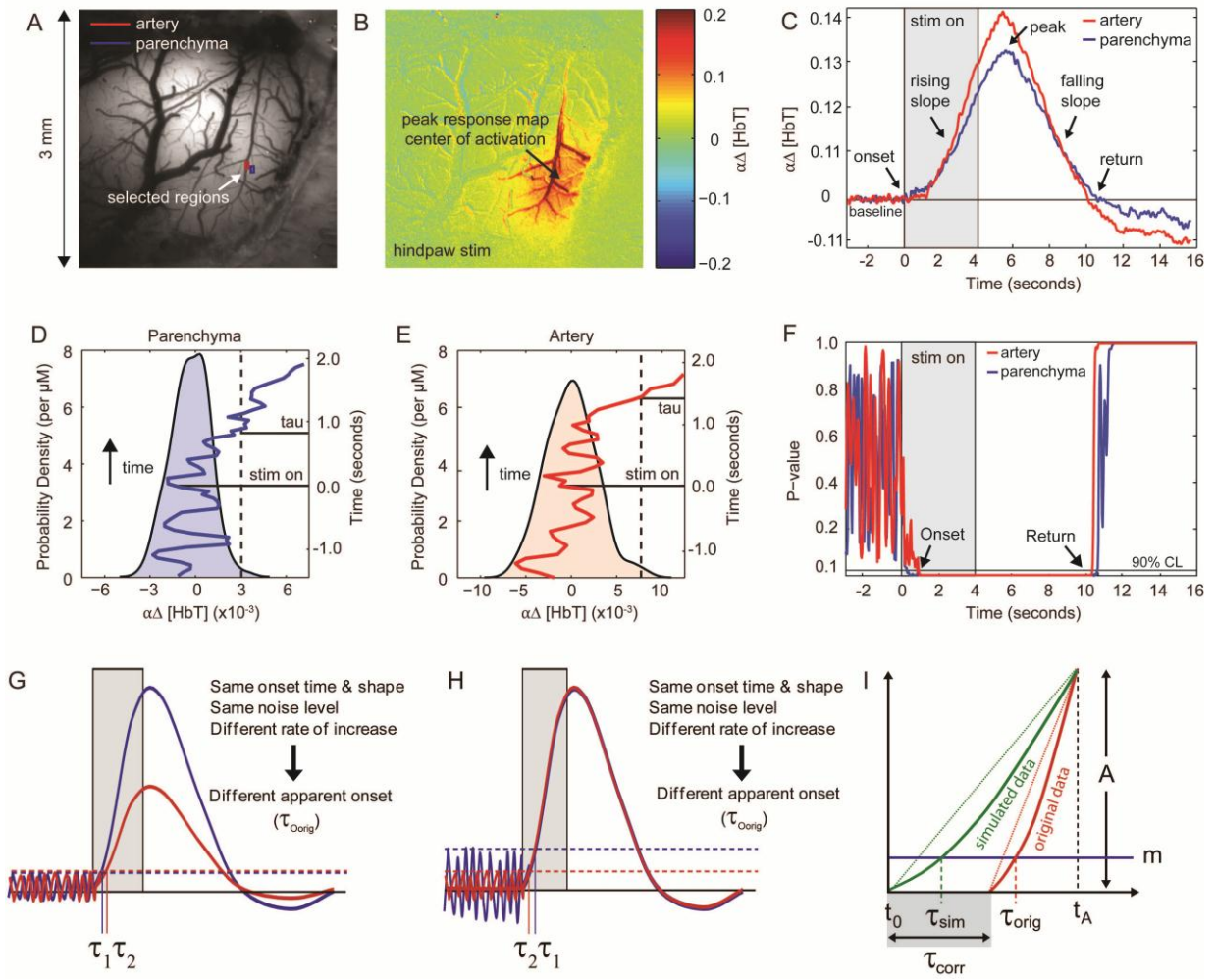

Figure 3.1 Quantification of response timing methods

(A) Image of exposed cortical surface. (B) Functional map showing region of largest signal change following hindpaw stimulation. (C) Δ[HbT] response from selected artery (red) and parenchyma (blue) regions in (A) obtained using 530 nm illumination (single trial). Stimulation period is shown in gray. (D-E) Baseline PDFs constructed from 3 seconds of natural baseline signal for selected artery and parenchyma regions respectively. The dotted vertical lines indicate the 90th percentile of the baseline distributions. A segment of the Δ[HbT] signal is overlaid on the PDFs, with time on the vertical axis. The tissue is no longer in the baseline state with 90% confidence when the Δ[HbT] signal crosses the dotted 90th percentile line. (F) Plot of p-values (p-value = 1-cdf) computed for each of the time courses shown in (C). (G-H) Schematics showing potential confounding factors associated with measuring relative response onset times. (I) Schematic showing derivation of correction factor. Noise level thresholds are denoted by m. τ_{sim} and τ_{orig} are the calculated τ values for the simulated and original data sets respectively, τ_{corr} is the estimated true onset time of the original data relative to t_0, the true onset of the simulated data, and t_A is the time at which the simulated data and the original data are normalized to the same amplitude A.

3.4 Results

3.4.1 Comparison of original, simulated, and corrected τ maps

Figure 3.2A-F displays τ_O and τ_R maps calculated from the original data (A-B), simulated data (C-D), and after applying the rate-of-change correction factor (E-F). τ_{Oorig} maps show spatial timing gradients with minima at the center of the responding region and maxima in the periphery, while τ_{Ocorr} maps show greater spatial uniformity. In contrast τ_{Oorig} maps are very similar to τ_{Osim} maps, suggesting that the spatial gradients in the τ_{Oorig} maps may be due to spatial variations in signals' rates of change (C-D). As expected, the fastest growing signals from the simulated data set are also the pixels with the fastest τ_{Osim} (recall that all pixels having identical onset times by construction). This is especially noticeable in the central artery which exhibits early τ_{Osim} in contrast to its relatively later τ_{Orig}.

Comparison of τ maps also suggests that the τ_{Ocorr} is generally faster than τ_{Oorig}. This is expected because the true time of onset should occur before we observe it (in the presence of nonzero noise). In addition, the correction reduces the variance in τ_{Ocorr} (relative to τ_{Oorig}), resulting in a cleaner separation in the distributions of artery and parenchyma τ_{Ocorr} across rats (Figure 3.2K).

τ_{Rorig} maps and τ_{Rcorr} both show spatial gradients with periphery regions exhibiting earlier return-to-baseline than central regions. However, we note that the regions exhibiting the latest in τ_{Rorig} and τ_{Rcorr} are slightly shifted from each other, with the central arteriole exhibiting earlier τ_{Rcorr} in contrast to its relatively later τ_{Rorig}.

In contrast to the similarities between τ_{Osim} and τ_{Oorig}, the differences in τ_{Rsim} and τ_{Rorig} maps suggest that spatial variations in signals' rates of change (τ_{Rsim}) may not be primarily responsible for the spatial gradients observed in τ_{Rorig}. The relatively small gradient observed in τ_{Rsim} is on the order of 2 seconds, which is comparable to the spatial gradient observed in τ_{Osim}. This is as expected since the shape of the response curve used to create the simulated data set does not vary between pixels. In comparison, the larger gradients observed in τ_{Rorig} and τ_{Rcorr} may suggest that the shape of the response decay as it returns to baseline differs more significantly between central and peripheral regions.

While applying the correction described in Eq. 3 changes the distribution of parenchyma and artery τ_O and τ_R values, the relative order of timings between compartments remains the same for both original and corrected τ_O and τ_R values.

3.4.2 Corrected onset and return τ of central response

We consistently observe that the central parenchyma region exhibits both the first measureable signal onset and the latest return to baseline, while central arterial regions exhibit later signal onset and earlier baseline return. Figure 3.2G-H shows histograms of onset and return τ_{corr} values for masked arterial and parenchyma regions from the central region (see right inset). A greater proportion of parenchyma pixels exhibit earlier onset τ_{corr} and delayed return τ_{corr} compared to arteriolar pixels.

Across rats, the average median τ_{Ocorr} is 0.537 ± 0.066 seconds for the parenchyma response and 0.748 ± 0.131 seconds for the arteriolar response (Figure 3.2K). The average onset lag (arterial τ_{Ocorr} minus parenchymal τ_{Ocorr}) is 0.211 ± 0.087 seconds (Figure 3.2 M).

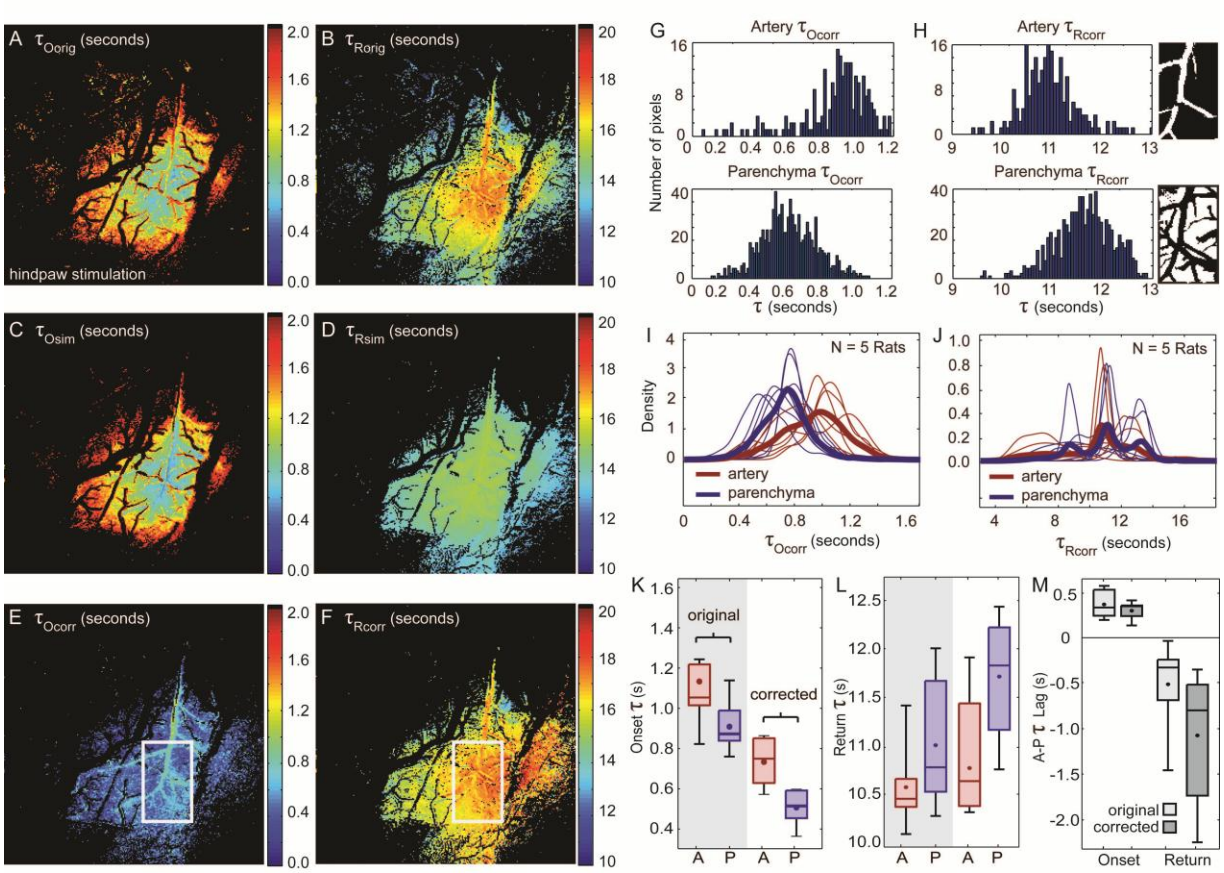

Figure 3.2 Onset and return τ results

(A-B) τOorig and τRorig maps. The stimulus is presented at t = 0 s and ends at t = 4 s. (C-D) τOsim and τRsim maps constructed from simulated data set. (E-F) τOcorr and τRcorr maps with white box indicating center region of activity. This masked region is studied in more detail in (G-M). (G) Histograms of τOcorr for arterial (top) and parenchyma (bottom) compartments extracted from the central region of interest. (H) Histograms of τRcorr for arterial (top) and parenchyma (bottom) compartments. Insets show artery (top) and parenchyma (bottom) masks used to differentiate compartments, with veins excluded from both. (I-J) Smoothed histograms of τOcorr and τRcorr for 5 rats are shown. τOcorr distributions are consistent across rats whereas τRcorr distributions are more variable across rats. Bold lines represent mean density functions. (K-L) Median τorig and τcorr values computed from central region indicated by the white box in (E-F). (M) τorig and τcorr lags between artery and parenchyma compartments. For all boxplots, bounding boxes show the inter-quartile range with the solid line indicating the median and the dot indicating the mean value. Whiskers show the extent of data for all 5 rats.

This analysis was repeated for the τ_{Rorig} and τ_{Rcorr}. The arterial region exhibited average median τ_{Rcorr} of 10.910 ± 0.875 seconds while the central parenchyma exhibited later τ_{Rcorr} of 11.899 ± 0.825 seconds (Figure 3.2L). The lag between the τ_{Rcorr} of the arterial and parenchymal regions was -0.989s ± 0.615 seconds (Figure 3.2M). Figure 3.2 I-J displays smoothed histograms for artery and parenchyma onset and return τ_{corr} from all 5 rats as well as their average (bold lines).

In both compartments, the onset τ_{corr} distributions are remarkably similar across rats. This similarity is what produces the narrow ranges of median onset τ_{corr} in Figure 3.2 K. Histograms for return τ_{corr} in both compartments exhibit greater variability (Figure 3.2H). As a result, we observe a wider range of median return τ_{corr} in Figure 3.2 L. We note that the major veins in Figure 3.2 A-B appear black, indicating that no statistically significant changes in $\Delta[HbT]$ were detected in these regions under our stimulation paradigm (Bouchard et al 2009, Hillman et al 2007).

The onset and return analysis above was limited to the central region of activation. We now extend our τ analysis to study the spatial spread of the response in both the center and periphery of the responding region.

3.4.3 Signal propagation speed and direction

The initiation of the response appears to occur simultaneously across all responding locations in the parenchyma. Subsequent propagation in major arterioles occurs rapidly in a direction away from the center of activity and is independent of the direction of blood flow.

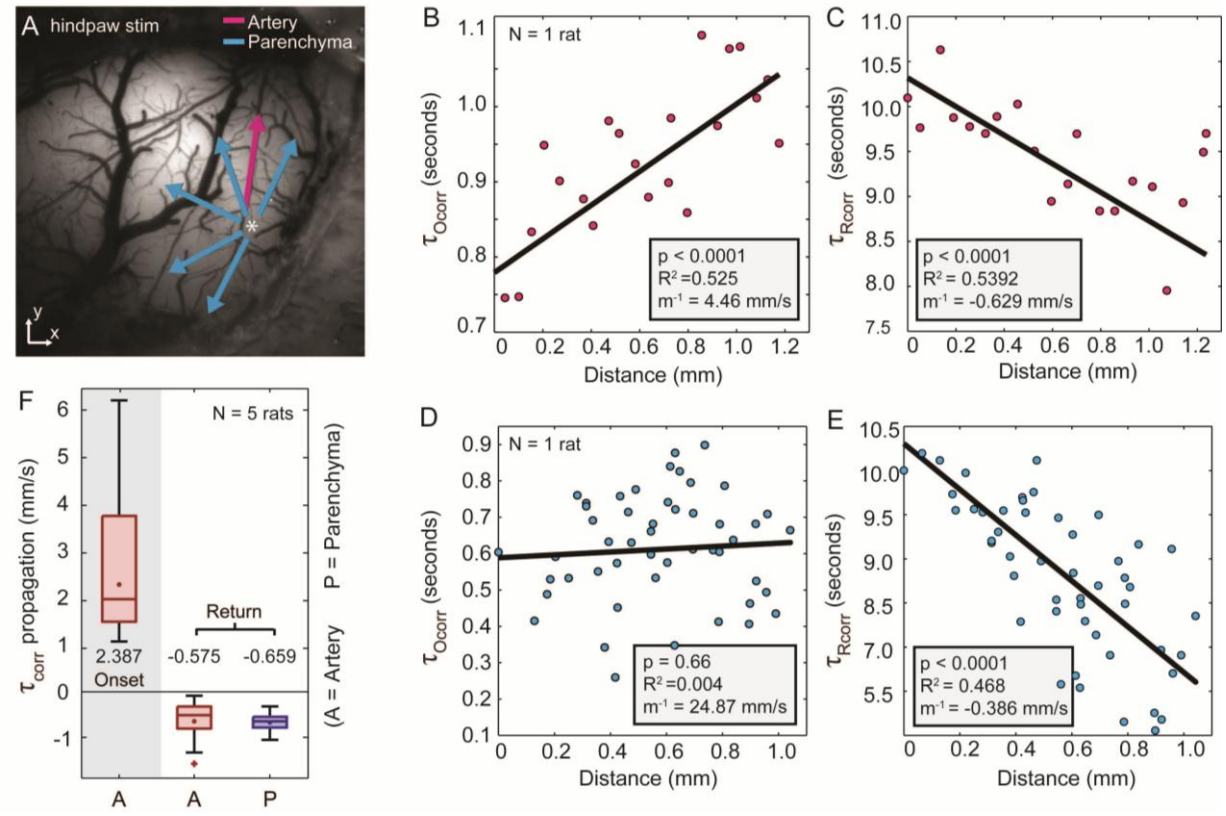

Figure 3.3 τcorr propagation dynamics

(A) Image of the exposed cortex. Pink and blue arrows indicate vector directions used to compute propagation speeds. (B-E) τOcorr and τRcorr values selected from arterial vector in (A) are plotted as a function of radial distance from the center of activation. (B-C) shows arterial propagation and (D-E) show parenchyma propagation. The inverse slope of the linear regression represents the onset and return propagation speed in mm/s. (F) Summary of propagation speeds computed over 5 rats. Boxes show inter-quartile range with solid line indicating the median and the dot indicating the mean value. Whiskers show the extent of the data. Onset propagation speeds in the parenchyma are excluded due to insignificant p-values ($p>0.1$). This indicates that any propagation that does occur in the parenchyma is faster than we can reliably measure.

The return-to-baseline in both compartments is first observed in peripheral regions and occurs last at the center of the responding region.

Arrows in Figure 3.3A indicate artery and parenchyma regions along which τ_{Ocorr} and τ_{Rcorr} are plotted in Figure 3.3 B-E. Linear regression of τ_{Ocorr} on radial distance and τ_{corr} on radial distance provides measures of propagation speed. All regression fits exhibited significant p-values ($p < 0.1$) except for onset in the parenchyma (Figure 3.3 D), indicating that any propagation within the parenchyma occurs faster than we can reliably measure. In addition to this constraint, we also discard measured propagation speeds greater than 6.5 mm/s, as this is at the limit of our temporal resolution when imaging ~0.5 mm vessel segments at 25 fps. Eliminating the trials where $p > 0.1$ or speed > 6.5 mm/s, we estimate average arterial τ_{Ocorr} propagation speed to be 2.387 ± 1.65.mm/s. We estimate the average rate at which τ_{Rcorr} returns to baseline along arterioles to be -0.575 ± 0.46 mm/s, and across parenchyma to be -0.659 ± 0.21 mm/s (Figure 3.3 F). Within the artery, τ_{Ocorr} propagation speeds were consistently found to be faster than τ_{Rcorr} return rates, and the relationship between these two measures across 5 rats is shown in Supplemental Figure SB.5. We find that while some rats exhibit fast propagation speeds and others exhibit slow propagation speeds, the ratios between onset propagation speeds and the rates of return to baseline are comparable for different rats. Further investigations across rats did not reveal significant correlations between propagation speed and blood pressure or body weight (Figure SB.6).

We emphasize here that propagation of τ_{Ocorr} and τ_{Rcorr} represent a spatial propagation of a transition between the baseline and stimulated states. The τ_{Ocorr} and τ_{Rcorr} maps do not characterize any dynamics occurring between the response initiation and return-to-

baseline, and following the return to baseline, and so do not reflect the ultimate amplitude of changes in those regions. Further, τ_{Rcorr} does not represent the time of initial vasoconstriction.

3.4.4 Dynamics of the response amplitude

Following the response initiation, the fastest growing $\Delta[HbT]$ signals are observed at central responding regions, while signal decay rates are more uniform across both central and peripheral regions.

The results above indicate that the first hemodynamic change in response to stimulation occurs nearly simultaneously throughout the parenchyma, followed by rapid propagation of vasodilation along the major artery feeding the region. However, despite the spatial uniformity of τ_{Ocorr}, we nevertheless observe spatial differences in rate of signal growth and peak amplitudes throughout the responding region (Figure 3.4). These differences are effectively captured in τ_{Oorig} maps and extracted $\Delta [HbT]$ signals, which may provide insights into the location of the "driving force" behind the response evolution.

Figure 3.4B-C shows time-courses generated by sampling the $\Delta[HbT]$ data at different locations along the arteriole transecting both hindpaw and forepaw regions as shown in Figure 3.4A. Pink and white arrows indicate the locations of the responding forepaw and hindpaw regions respectively, and corresponding functional maps can be seen in Figure 3.4 D-E. These plots demonstrate that peak response amplitudes (and rates of change) are greatest near the center of the responding region and decrease along the artery further away. We also note that the pattern of peak amplitudes as a function of distance from the

center of the responding region in a single artery is the same for both forepaw (Figure 3.4 D) and hindpaw (Figure 3.4 E) stimulation, regardless of the absolute location of the responding region along the vessel and the direction of blood flow.

Following the return-to-baseline, regions along the vessel exhibit a brief signal undershoot that corresponds to vasoconstriction. Arterioles at the periphery of the responding region exhibit small peak amplitudes (dilations) and large undershoots (constrictions), while central arterioles exhibit larger peak amplitudes and smaller undershoots (Figure 3.4 F-G). The relative order of undershoot amplitudes also mirrors the relative order of τ_{Rcorr} along the artery. Peripheral regions with earliest τ_{Rcorr} have the smallest peak and largest undershoot amplitudes. Central regions with the latest τ_{Rcorr} have the largest peak and smallest undershoot amplitudes.

To further investigate how the response evolves just following τ_{Ocorr}, we computed the direction of propagation of τ_{Oorig} and τ_{Rorig} along branches of the arterial tree. While these measures do not necessarily correspond to the initial onset propagation, they do reflect the spatial gradient of 'vasodilatory signal strength' insofar as the end of the branch that exhibits the fastest increase in dilation is likely to be the end that is closest to the source of the signal that is mediating vasodilation (the "driving force"). Figure 3.4D-E displays functional maps indicating the location of Δ [HbT] increases for each stimulus type. The directions of τ_{Oorig} (pink arrows) and τ_{Rorig} (blue arrows) spatial gradients under the two stimulation paradigms are depicted on the magnified images of the major artery and its branches, with white asterisks marking the center of the responding region for each. For hindpaw and forepaw stimulation, the direction of the τ_{Oorig} gradient is independent of

whether the vessel segment is upstream or downstream of the responding region. In many, but not all segments the direction of the τ_{Oorig} gradient switches when the stimulus is changed from forepaw to hindpaw.

Our τ_{corr} maps show that peripheral branches are the first to return to baseline. In most cases, the τ_{Rorig} gradient is in the opposite direction to the τ_{Oorig} gradient for a given stimulus, again showing that these gradients develop irrespective of the direction of blood flow. Two vessel segments can be seen to have τ_{Oorig} and τ_{Rorig} gradients in the same direction in Figure 3.4E, but different directions in Figure 3.4D.

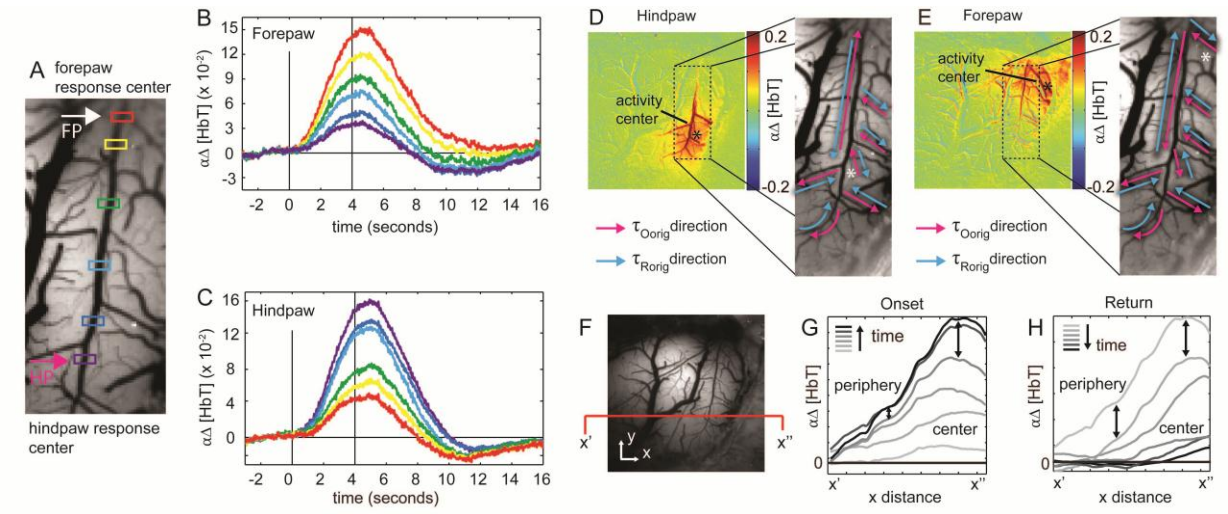

Figure 3.4 Response amplitude dynamics
(A) Artery transecting both hindpaw (pink arrow) and forepaw regions (white arrow). (B-C) Δ[HbT] time courses plotted for the color-coded points along the vessel in (A) during forepaw (B) and hindpaw (C) stimulation. Time courses represent the average over 10 runs (unfiltered). (D-E) Directions of τOorig (pink arrows) and τRorig (blue arrows) spatial gradients are shown in the major surface artery and immediate arterial branches during hindpaw (D) and forepaw (E) activation. Arterial blood flow direction is from top to bottom. (F) Gray scale image showing cross section x'-x". (G-H) Cross sectional signal from x'-x" plotted at 20 time-frame intervals during the onset (G) and the return (H). Signal growth is faster in the center than in the periphery during the onset, but signal decay is more spatially uniform (until baseline is reached) during the return to baseline.

Finally, because the hemodynamic response is a highly spatiotemporal phenomenon we can also visualize its dynamics from an alternative perspective. The cross-sectional Δ[HbT] signal across x'-x" shown in Figure 3.4C is plotted at 20 frame intervals of during the signal rise (Figure 3.4D) and decay (Figure 3.4E). This plot allows us to look at the differential changes in signal as a function of spatial location relative to the responding region. During the signal rise, we notice that signal amplitude grows much faster in the central regions as compared to signal growth in peripheral regions. However, the decay phase following the signal peak exhibits a relatively constant rate of change in both central and peripheral regions.

3.4.5 Summary of findings

Our results indicate that the first hemodynamic changes in response to somatosensory stimulation occur as a uniform Δ[HbT] increase in parenchymal regions. This initial response remains parenchyma-specific for no longer than 200 ms before spreading rapidly to major pial arterioles (Figure 3.3). Following the initial response onset, we saw that further spread of the response appears to occur via a secondary phase of rapid retrograde vasodilation along only those branches that feed the responding region (Figure 3.4). At parent arteries, propagation of this vasodilation continues both upstream and downstream along the superficial arterial tree. The direction of this propagation is therefore independent of the direction of blood flow and appears to be governed primarily by the relative location of the activated cortical region.

The return-to-baseline is first observed at the periphery of the responding region. This is true for both arterial and parenchyma compartments. After returning to baseline, peripheral segments of the parent artery and branches feeding non-responding cortical regions undershooting briefly before returning back to their initial baseline state. The last region to return to baseline is the central parenchyma region, which exhibits a sustained $\Delta[\mathrm{HbT}]$ increase following return-to-baseline of the feeding arteriolar tree. These results are consistent with pictorial evolution of the hemodynamic response shown in supplemental Figure SB.1.

3.5 Discussion

In order to properly evaluate hypotheses about the cellular mechanisms governing the hemodynamic response, we must first understand what the hemodynamic response to somatosensory stimulation represents at the vascular level. Combined, our results imply that the cellular mechanism(s) underlying the hemodynamic response must be able to (1) act initially, and rapidly on capillaries and/or pre-capillary arterioles, (2) propagate rapid vasodilation along the arteriolar network at average speeds of ~2.4 mm/s, (3) account for propagation of vasodilation along arterioles in directions that are independent of the direction of blood flow, and (4) mediate vasoconstriction such that vessels at the periphery return to baseline first. We discuss each of these implications below:

3.5.1 Initial parenchyma hyperemia

Our results suggest that capillary hyperemia is a major contributor to the ensemble Δ[HbT] response. Although such increases in parenchymal Δ[HbT] have been repeatedly observed *in vivo* with optical imaging methods (Berwick et al 2005, Blood et al 2002, Culver et al 2005, Devor et al 2003, Hillman et al 2007, Jones et al 2004, Nemoto et al 2004, Sheth et al 2005, Sirotin et al 2009, Vanzetta et al 2005), the occurrence of capillary hyperemia is often overlooked due to the lack of a known mechanism capable of actuating such an observation (Buxton et al 1998, Hoge et al 1999).

Actuation mechanisms for a parenchymal HbT increase For an increase in parenchymal HbT to occur, it is necessary for there to be an increase in the number of red blood cells (RBCs) per unit volume of tissue at any point in time. One way for this to occur would be for capillaries to increase their diameters, which would allow more plasma, and hence more red blood cells per unit length to be carried within a capillary. Two photon and confocal microscopy studies (Chaigneau et al 2003, Hutchinson et al 2006, Kleinfeld et al 1998, Stefanovic et al 2008, Villringer et al 1994) have previously demonstrated that capillaries can exhibit changes in both their diameters and their speed of flow during hypercapnia and functional stimulus. However, these studies were unable to conclude whether this 'dilation' occurs passively, as a result of initial upstream arteriolar dilation (Vanzetta et al 2005) or actively, via physical regulation of microvessel diameters (Iadecola et al 1997, Sheth et al 2005).

Our results indicate that initial functional hyperemia of the parenchyma occurs *prior* to dilation of upstream pial arterioles, suggesting that the initial onset of the hemodynamic response might indeed be directly and *actively* initiated by the capillaries themselves. While apparent lack of smooth muscle at the capillary level makes this seem unlikely, a recent study suggested that pericytes may be capable of physically modulating the diameters of microvessels (Peppiatt et al 2006). This hypothesis is also attractive, since it allows for almost arbitrary positioning of initial flow control, and spatially couples sensing, signaling and actuating mechanisms at the site of peak metabolic activity and nutrient exchange (Borowsky & Collins 1989, Klein et al 1986).

In order for *passive* capillary dilation to occur, a part of the vascular network other than the pial arterioles would need to actively decrease its resistance. (Tian et al 2010) recently reported that deep segments of pre-capillary arterioles can be seen to dilate prior to pial branches, which is consistent with retrograde propagation of dilation. Such changes could feasibly cause increases in capillary flow (and / or diameter) prior to observable dilations of pial vessels, however it is not clear whether changes in capillary tone or HbT precede these changes and therefore whether these deep arteriolar dilations could in fact represent back-propagated signals from capillaries. (Stefanovic et al 2008) showed that capillary diameters increase during functional stimulus, but used steady-state stimulus and so could not explicitly examine the dynamics of the early parenchymal HbT response that we observe prior to arteriolar dilation.

Besides capillary dilation, another explanation for parenchymal HbT increases might be an increase in capillary hematocrit, for example due to an *increase* in post-capillary resistance, causing red blood cells to be trapped within the capillary beds while plasma is

able to leave. A further possibility might be that changes in capillary hematocrit could be modulated by changes in capillary water permeability. Fluctuations in venous hematocrit that could be consistent with these mechanisms have been previously observed using two-photon microscopy (Hillman et al 2007).

In addition to a rapid parenchymal HbT increase, our results also revealed sustained elevation of HbT in a localized region in the center of activation after stimulus cessation (Figure 3.2F and Figure SB.1). This sustained increase in HbT following the return of arteriolar dilation to its baseline is consistent with a mechanism that forces extra RBCs into each capillary during the high-flow phase of the response, only to have them get trapped once flow has reduced upon arteriolar constriction. (Berwick et al 2008) observed a similar sustained localization of increased $\Delta[\mathrm{HbT}]$ in the stimulated barrel following electrical whisker stimulation. They suggest that this later phase of the response may be a spatially specific and less transient indicator of neuronal activity than very early changes.

Relevance to the initial dip It is important to note how our findings relate to the 'initial dip' (a previously noted initial increase in HbR thought to indicate increase in oxygen consumption prior to increases in flow) (Malonek & Grinvald 1996). A recent study by (Sirotin et al 2009) demonstrated that traditional OISI measurements at 610 nm to 630 nm can provide misleading time-courses that do not specifically reflect changes in HbR, but are contaminated by early changes in HbT. To summarize; initial decreases in detected signal perceived as increases in HbR can be readily explained by simultaneous (or even faster) increases in HbT. Sirotin et al. demonstrated in awake behaving primates, that multispectral OISI data could be converted to changes in HbO, HbR and HbT that were

consistent with our findings, and did not exhibit an initial increase in HbR. As a result, much of the recent literature that has utilized OISI at these wavelengths and identified the 'initial dip' spatial extent as the center of the responding region may in fact have been measuring an early, rapid and localized increase in HbT.

If the first changes in the parenchyma in fact corresponded to an increase in HbR in the absence of an active increase in HbT, one would also need to observe a concurrent decrease in HbO. This feature of the hemodynamic response is not routinely observed, and was not a noticeable feature in our 470 nm imaging data which would be sensitive to this oximetric change. This leads us to conclude that if an increase in HbR does occur early during the response to stimulus, it is accompanied by an active increase in HbT in the parenchyma, which robustly precedes changes in the diameter of pial arterioles. Nevertheless, it should be noted that since our analysis of the earliest initial onsets ($\tau_{O\text{corr}}$) pushes our data to the limits of its statistical power, we cannot unequivocally know that these small rapid changes have no oximetric component at all. Equally, if fast scattering changes were occurring in the cortex during neuronal firing, our analysis would not be able to distinguish between their effects and those of an HbT increase.

3.5.2 Retrograde propagation

Following the initial onset of parenchyma hyperemia, we observe retrograde propagation of vasodilation along arterioles at the cortical surface at a speed on the order of 2.4 mm/sec. These observations support the existence of mechanisms that actuate control along vascular paths between capillaries and surface arteries, rather than signaling networks that

establish a direct communication between active neurons and surface arteries (Vanzetta et al 2005) or diffusive molecular signals that act non preferentially on vessels (Roy & Sherrington 1890).

Previous *in vivo* imaging studies have generally acquired images at rates that were too slow to detect propagation direction, although several have suggested that their results indicated either retrograde or anterograde vasodilations (Duling & Berne 1970, Iadecola et al 1997, Sheth et al 2005). Our higher frame rate, high-resolution imaging and statistical analysis have allowed us to more clearly characterize and quantify propagation of vasodilation in somatosensory cortex. While retrograde vasodilation was previously described in response to direct stimulation of parallel fibers in the cerebellum (Iadecola et al 1997) measurements of propagation speeds in hamster cheek pouch vessels suggested likely rates of 200 μm/sec (Duling & Berne 1970). We have now determined that retrograde propagation in cerebral arterioles in-vivo in response to functional stimulus occurs at over 10 times that rate, explaining why such propagation had not been detected previously at slower imaging speeds.

Interplay between arteriolar and parenchymal propagation dynamics

Just after initial onset of the response in the parenchyma, given by τ_{Ocorr}, our results seem to indicate the presence of a secondary "wave" of actuation that is responsible for spatial differences in rate and amplitude of vasodilations along arterial vessels and throughout the parenchyma. This is to be expected since as dilation spreads along pial arterioles and their branches, regions fed by these vessels will receive increased flow, on top of any initial

increases in Δ[HbT]. Increases in Δ[HbT] in peripheral parenchyma are also consistent with this model, since their patterns appear to more closely follow the contours of the arteriolar branches than being isotropic (Figure 3.2A-B, Figure 3.4 D-E).

In most cases, we find that only those arteriolar branches that appear to feed the initially responding parenchyma region exhibit a secondary retrograde vasodilation, while those feeding peripheral regions do not. This is consistent with the cortical angioarchitecture presented by (Nishimura et al 2007), who showed that each penetrating arteriole is associated with a spatially distinct domain in the microvasculature.

Our results also suggest that the vascular path between capillaries and each surface arteriole may serve as the signaling conduit between the active region and more distant vessels. This vascular path back to parent pial arteries may provide a convenient "road map" indicating which vessels are required to dilate in order to orchestrate a neatly localized hemodynamic response. Mechanistic hypotheses that fit this scheme include signal transduction via endothelial gap junctions in vessel walls (Bartlett & Segal 2000) and networks of pericytes or glial cells that are closely integrated with vasculature (McCaslin et al 2010, Peppiatt et al 2006).

3.5.3 Second mechanism responsible for return to baseline

Previous studies have focused mainly on the rising (vasodilation) phase of the response, often neglecting to address the constriction phase that returns blood flow to its baseline state. We find that the response decay does not seem to result simply from a lack of dilatory actuation, but rather from active constriction that causes Δ[HbT] to undershoot the baseline before returning to normal after stimulus cessation.

Our results reveal several differences in spatiotemporal behavior between the two phases (onset/dilation and return/constriction). In particular, we note that the response grows the fastest in the central responding region relative to the periphery whereas the response decay occurs at a more spatially uniform rate (Figure 3.4 G-H). Figure 3.4 B-C show that during the onset phase, all responding regions reach their peak amplitudes in approximately the same amount of time. During the decay phase however, the peripheral regions return to baseline in less time than the central regions, leading to the staggered returns to baseline captured in our τ_R maps. A more subtle but consistent feature of these plots is the slightly earlier peak inflection time for peripheral regions compared to central ones suggesting that the 'decision' to begin constriction may actually originate at the periphery. The large variability of τ_{Rorig} and τ_{Rcorr} values across rats, compared to the low variability of τ_{Oorig} and τ_{Ocorr} values (Figure 3.2J), suggests that the response initiation is a much more controlled and consistently regulated than the return phase. Together, these results indicate that distinctly different underlying signaling pathways and cellular mechanisms may be responsible for the dilate and constrict phases of the hemodynamic response.

Different mechanisms for the "excitatory" and "inhibitory" phases of the response may be required to suit different purposes. Onset signaling along the vascular network may provide the most direct, targeted pathway to allow rapid, localized flow increases by dilating only the most necessary arteriolar branches. However, since return-to-baseline is less time-critical, the inhibitory vasoconstrict signal does not necessarily need to travel along the same network. A wide-ranging inhibitory domain (not organized along the vascular tree)

would not directly constrict the specific vessels that had initially dilated, but would guarantee the eventual return to baseline of vessels within the entire cortical region, while also potentially acting to constrain the area over which vasodilate signals are able to spread initially. The presence of two spatiotemporally independent dilate / constrict mechanisms would explain anomalies such as the vessel segments in Figure 3.4 A-B that in one case reverse directions between onset and decay gradients, and in the other exhibit gradients of onset and return in the same direction.

The pattern of dilation and constriction that we observe agrees well with the center-surround pattern of hemodynamics described by Devor et al. and recently supported by Boorman et al. (Boorman et al 2010, Devor et al 2007). Both reported that arteriolar constriction and decreases in $\Delta[\mathrm{HbT}]$ are accompanied by neuronal inhibition, as indicated by voltage sensitive dyes and electrode array recordings. As noted by Boorman et al. and Devor et al, the presence of inhibition in peripheral regions could relate to interneuron involvement. Cauli et al. demonstrated that several species of interneurons are capable of mediating vasoconstriction, such as somatostatin interneurons whose morphology (soma located around layer III/IV with dense, wide-reaching projections to layer I) lends itself well to this hypothesis (Cauli et al 2004, Karagiannis et al 2009).

A hemodynamic response which is a balance between two effects; one dilatory and one constrictory, is an attractive model since few physiological systems can achieve homeostasis with only an excitatory mechanism in the absence of an inhibitory one. Natural oscillations in baseline blood flow could also represent the normal settling back and forth between these two effects (Mayhew et al 1996, Raichle 2009, White et al 2009).

3.5.4 Methodological Conclusions

Previous OISI studies of cortical hemodynamics have focused on studying spatiotemporal dynamics of the timing and amplitude of the signal peak. The peak of the hemodynamic response is an obvious feature in the measured response signal; however the peak time and peak amplitude result from the confluence of numerous effects including the signal onset and rates of signal change before and after the peak (Figure 3.4, Figure SB.3). The unknown spatiotemporal dynamics of these very different effects can confound the meaning of the response peak.

Further, each feature of the hemodynamic response, such as onset, rate of change, and peak timing and amplitude may represent distinct physiological mechanisms or events. It is therefore important to treat these measures independently of each other. For example, it is easy to mistake fast signal growth for fast signal onset. Because the response onsets occur on such a rapid time scale, the visual effect of response growth and peak amplitude in a series of images or time courses quickly dominates the subtle differences exhibited in onset transitions between compartments. The fast arteriolar and slow parenchyma signal peak time that we observed may therefore explain why some studies reported initial arteriolar $\Delta[HbT]$ responses that subsequently spread to the parenchyma (Nemoto et al 2004, Vanzetta et al 2005).

Here we used an analysis methodology that seeks to overcome the influence of peak amplitudes and rates of change on onset determination. Our τ_{Oorig} measures represent the time at which the effects of the response actuating mechanisms are first observable via OISI given the baseline variability. To better understand the precise physiological correlates

underlying response initiation, we make an estimate (τ_{corr}) of what the true onset time would be given what we can observe (τ_{orig}) and a structured model of the response (τ_{sim}). By using these measures in addition to studies of peak amplitude and timing, we have been able to develop a more complete picture of the hemodynamic response.

In summary, we have conducted a thorough characterization of the hemodynamic response through the use of high-speed multispectral optical imaging. We conclude that the hemodynamic response is initiated at the capillary level and then propagates back along targeted arterioles in the vascular network. We hypothesize that a different underlying mechanism is responsible for the response's decay back to baseline, and show evidence for a decay phase that acts non-preferentially across the responding region. Our results advance a fundamental understanding of the hemodynamic response as well as our ability to determine the potential cellular neurovascular coupling mechanisms that are responsible for orchestrating the observed vascular changes.

Chapter 4

Distinct phases of the hemodynamic response

4.1 Introduction

In this chapter we extend our studies of the hemodynamic response to the cellular level using two-photon microscopy. Previously, we characterized the spatiotemporal properties of the hemodynamic response following 4 seconds of electrical hindpaw stimulation (3Hz, 1mA). Specifically, we were interested in identifying the hemodynamic events that occur during initiation of the blood flow response in order to understand the cellular mechanisms actuating them. Our results indicated that the hemodynamic response is initiated at the capillary level and then spreads rapidly along diving arterioles up to surface pial arterioles. Based on these observations, we hypothesized that a cellular pathway capable of rapidly conducting a vasodilatory signal *along* the vasculature is required.

Astrocytes appear to be well suited for this role as a number of studies have demonstrated that astrocytes are 1) intimately connected to both neurons and the vasculature, creating a sheathing of astrocyte endfeet around diving arterioles and capillaries (McCaslin et al 2011, Xu et al 2008) and 2) capable of releasing vasodilatory factors that influence smooth muscle tone (Anderson & Nedergaard 2003, Bonvento et al 2005, Wang et al 2006, Zonta et al 2003). We subsequently designed a series of experiments to investigate the possibility that astrocytes are involved in coordinating the initial vasodilation observed during the hemodynamic response.

Our preliminary results found calcium-dependent astrocyte responses to be infrequent and difficult to observe following a 4 second stimulus. Reviewing the previous literature on *in vivo* astrocyte activity, we note that astrocyte calcium responses have only been reported following long durations of sensory stimulation (1 minute of whisker stimulation (Wang et al 2006) and 5 seconds of visual stimulation (Schummers et al 2008)). However, these reported astrocyte calcium responses were not fast enough (delayed by ~3-4 seconds) to account for the rapid and repeatable vasomotor responses that are observed immediately following stimulus onset (< 1 second). This temporal mismatch suggests that astrocytes cannot be responsible for the initial blood flow changes observed almost immediately after stimulus onset and implies that an additional mechanism is required (Cauli & Hamel 2010, Iadecola 2004).

While our experimental findings cannot implicate astrocytes in mediating the rapid blood flow responses at the stimulus onset, they do provide evidence that astrocytes may play a role later in the stimulation period. This idea that multiple mechanisms may orchestrate the hemodynamic response agrees with our previous interpretation of the

different spatiotemporal properties associated with the response onset and return-to-baseline (Chen et al 2011). We postulate that different mechanisms and / or signaling pathways are responsible for initiating the increase in local blood perfusion and for returning the tissue to its resting state. Previous investigations using stimulus durations longer than 8 seconds have similarly hypothesized that different "hemodynamic phases," characterized by their different spatial and temporal patterns, are produced by distinct underlying cellular mechanisms (Berwick et al 2008, Harris et al 2010, Kennerley et al 2011).

Collectively, these findings motivated us to extend our studies characterizing the spatiotemporal features of the hemodynamic response to include the blood flow responses elicited by varying stimulus durations. If there exists a sequence of different cellular mechanisms that are recruited to control early and late portions of the blood flow response, then a better understanding of the hemodynamic changes that occur during longer stimuli may provide insight into the contributions of these underlying mechanisms. This chapter will present our investigations of (1) astrocyte reactivity and (2) the hemodynamic responses elicited by a range of stimulus durations.

4.2 Methods

The animal preparation and imaging systems used in the experiments presented in this chapter are similar to the methods described in Chapter 2. Briefly, Sprague-Dawley rats are anesthetized with isoflurane during tracheotomy and placement of femoral arterial and venous catheters, allowing mechanical ventilation, blood pressure monitoring and delivery of intravenous fluids. A craniotomy is then performed to expose the somatosensory cortex,

and a cranial window is constructed prior to imaging. For two-photon imaging of cortical cell dynamics, calcium indicator Oregon Green 488 BAPTA-1 AM (OGB-1AM) is pressure injected into the cortex and astrocyte specific dye SR101 is applied topically (details of dye loading procedures is provided in Appendix A). OGB-1AM is a non-specific calcium indicator which is loaded into all cortical cells, neurons and astrocytes alike. SR101 staining allows us to differentiate intracellular calcium dynamics originating from astrocytes and all other cortical cells. After dye loading and construction of a cranial window, the animal is switched to intravenous alpha-chloralose anesthesia during imaging. Electrical hindpaw stimulation is delivered in 1 ± 0.2mA, 0.3ms pulses at 3Hz for the specified stimulus duration. As discussed in Chapter 2, wide-field camera imaging of calcium dynamics is first performed using appropriate emission filters and imaging parameters. This allows us to identify the regions of greatest calcium and hemodynamic changes, which are subsequently positioned under the two-photon microscope objective.

In these experiments, stimulus durations between 0.5 – 12 seconds are used during OISI of hemodynamics. All imaging runs include six seconds of baseline data collection (no stimulus), followed by the stimulus period and a post-stimulus period such that the total imaging time is forty seconds per run. Four second and twelve second stimulus durations are used during two-photon imaging of calcium dynamics.

4.3 Calcium-dependent astrocytes responses

Recent studies have proposed that astrocytes may play a role in vascular control based on their interactions with both neurons and with the cortical vasculature, as well as their potential for detecting changes in cellular metabolism (Anderson & Nedergaard 2003,

Attwell et al 2010, Petzold & Murthy 2011). Despite the growing body of literature on astrocyte-vascular associations, the experimental preparations used to observe astrocyte activity accompanying vascular changes have been inconsistent across accounts, making them difficult to interpret (Schummers et al 2008, Takano et al 2005, Wang et al 2006, Winship et al 2007, Zonta et al 2003). The few *in vivo* studies that used sensory stimulation to evoke astrocyte calcium responses were performed in the visual cortex, barrel cortex, and somatosensory cortex (Schummers et al 2008, Wang et al 2006, Winship et al 2007). Other studies have used alternative methods of eliciting increases in astrocytic intracellular calcium, including calcium uncaging (Takano et al 2005) and high intensity electrical pulses (Zonta et al 2003). Thus, discrepancies in reported astrocyte reactivity may be due in part to differences in experimental and stimulus paradigms.

We therefore attempt to investigate astrocytic calcium reactivity using our own experimental paradigm, which allows us to conduct both high-resolution OISI of the wide-field hemodynamic response in addition to two-photon microscopy of cellular level dynamics. Figure 4.1 shows *in vivo* two-photon microscopy of OGB-1AM during 12 seconds of 3Hz electrical hindpaw stimulation. Co-staining of cortical cells with OGB-1AM and SR101 allows us to distinguish calcium changes exhibited in astrocytes from calcium changes in other cortical cell types. The timecourses in Figure 4.1 are averaged over selected regions in the field of view (color coded). The neuronal responses appear as sharp, repeated increases in intracellular calcium levels corresponding to each electrical pulse of stimulation.

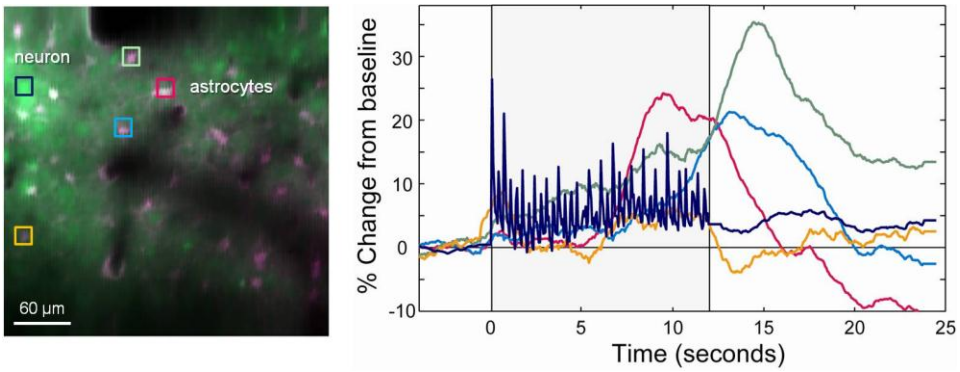

Figure 4.1 Neuron and astrocyte calcium dynamics
(Left) Neurons (green) are labeled with OGB-1AM, while astrocytes (pink) are co-labeled with OGB-1AM and SR101. This image was taken in a central responding region of the somatosensory cortex, approximately 250µm below the surface. (Right) OGB exhibits increases in fluorescence with increases in intracellular calcium. Timecourses of fluorescence change are averaged over the selected regions as color-coded in the image to the left. Neuronal spiking is observed throughout the stimulus period and delayed astrocytic calcium responses are seen approximately 5 seconds after the start of stimulation.

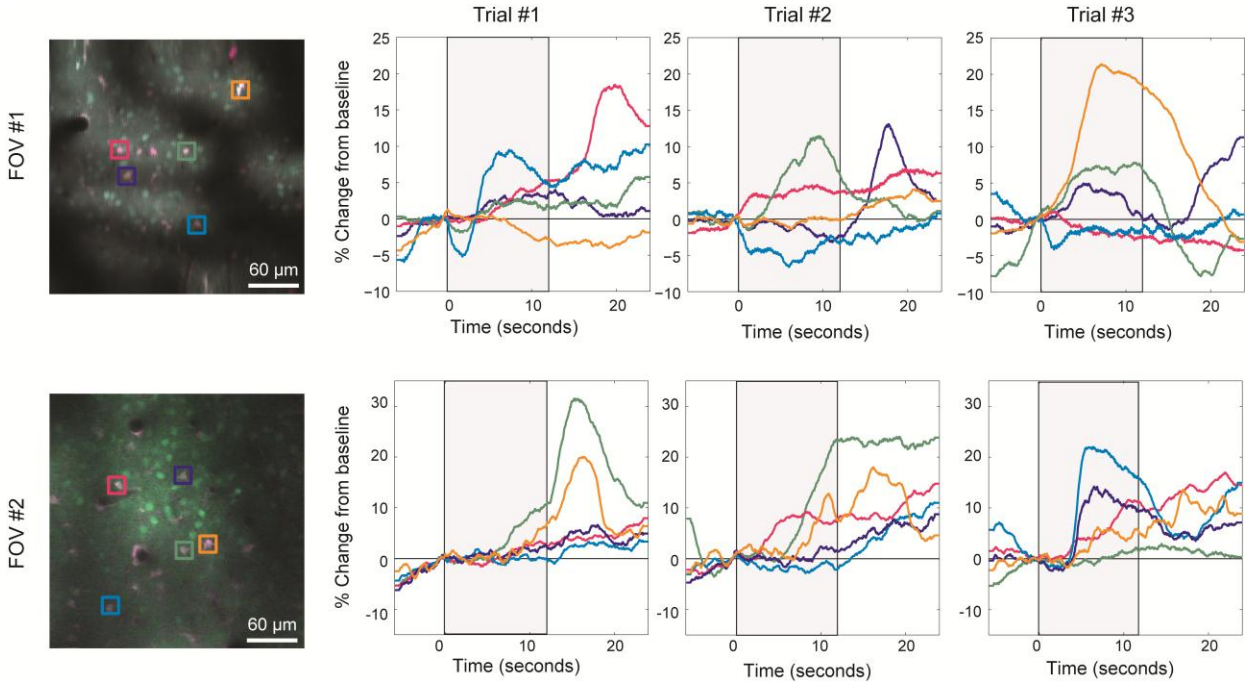

Figure 4.2 High level of variability in astrocyte calcium responses
Calcium responses are shown for selected astrocytes from two different fields of views (FOV). Each trial represents the calcium responses recorded for a single presentation of a 12-second electrical hindpaw stimulus. Timecourse colors correspond to selected astrocytes in images on the left. The timecourses show that only a subset of astrocyte in both FOVs exhibit calcium responses. In addition, the temporal dynamics of calcium responses among responding astrocytes is also highly variable

We found that astrocyte calcium responses are generally not observed following short stimulation periods (2-4 seconds, not shown). Upon increasing stimulus duration to 12 seconds, we observe increases in astrocytic calcium concentration that begin 3-5 seconds after stimulus onset. These responses exhibit a relatively slow rise to their peak response and sometimes remain elevated for approximately 2-3 seconds before returning to baseline. These observations are consistent with the findings that astrocytes in the visual cortex exhibit a stimulus-locked calcium increase that is delayed ~3-4 seconds from onset of visual stimulation (Schummers et al 2008), and astrocytes in the barrel cortex exhibit somatic calcium increases that are delayed by ~3 seconds after the onset of whisker stimulation (Wang et al 2006).

Interestingly, a qualitative observation of our data suggests that not all astrocytes in a given field of view exhibit calcium responses, and the same astrocytes do not consistently exhibit calcium responses across trials (Figure 4.2). The location of the astrocyte with respect to active neurons or diving vessels also did not appear to influence whether or not an astrocyte exhibited a response. This high level of variability seems to indicate that astrocyte signaling pathways do not consistently recruit the same cells each time. Rather, these observations are consistent with a regional level of signaling that may depend on the local environmental conditions surrounding the vicinity of neural activation. Although we have not quantified the spatial and temporal variances of astrocyte responses, these qualitative observations are consistent with finding reported by Wang et al 2006, which show a wide distribution of astrocyte response durations (9-36 seconds), as well as of onset (2-15 seconds) and peak (3-21 seconds) delays relative to the start of stimulation. They also reported that while one minute of whisker stimulation produced only a single calcium

response in the majority astrocytes sampled, a subset of astrocytes also exhibited a second calcium response before the end of stimulation (Wang et al 2006). This study did not comment on the relationship between astrocytes and blood flow changes, but did suggest that the delay in astrocyte response may be due to the time required for glutamate to accumulate in sufficient concentrations.

Together, this evidence suggest that the astrocyte calcium responses are neither fast nor consistent enough to account for the rapid onset of blood flow changes that we observe within ~300-400 ms of stimulus onset in the pial arterioles (Chen et al 2011). Although astrocytes are known to be closely associated with blood vessels, they have not been found to have any direct connectivity with pial arterioles, further suggesting that astrocytes are not responsible for mediating rapid pial arteriole dilation (McCaslin et al 2011). Nevertheless, astrocyte calcium responses reported here and in previous studies suggest that astrocytes may still play a role in modulating blood flow in later portions of the response (3-6 seconds after stimulus onset). Specifically, the timing and variability of astrocyte responses, as well as their sensitivity to neurotransmitters and their ability to produce vasoactive substances support their eventual involvement in blood flow modulation. It may also be possible that astrocytes influence blood flow in a calcium-independent manner, or that astrocytes exhibit small enough calcium changes that are undetectable using a calcium sensitive indicator. However, these cases are beyond the scope of the present study.

To guide subsequent investigations, we reason that if astrocytes are indeed involved in modulating the hemodynamic response then: 1) another mechanism must be responsible for earlier portions of the response, 2) astrocyte contribution to the hemodynamic response

should become apparent during longer stimulations, and 3) the hemodynamic response before and after astrocyte activation should exhibit different spatiotemporal qualities. We investigate the hypothesis that distinct mechanisms are responsible for controlling temporally shifted "phases" of the hemodynamic response by looking for evidence of these mechanisms in the blood flow changes elicited by different stimulus durations. Specifically, we study differences between short and long stimulus responses across 3 dimensions of the data: spatial pattern (section 4.4), variability (section 4.4), and response amplitude (section 4.5).

4.4 Hemodynamic 'phases' arise during prolonged stimulation

Previous studies have found that the hemodynamic response to prolonged stimulation follows a timecourse that exhibits an initial 'peak' followed by a 'plateau' before returning to baseline (Ances et al 2000a, Berwick et al 2008, Harris et al 2010, Matsuura & Kanno 2001). Berwick et al. further reported that the delayed plateau is more spatially localized to regions of neural activity than the initial peak in rodent whisker barrel (Berwick et al 2008), a finding that we produced in rat somatosensory cortex (Figure 4.3). For simplicity, we term the observed peak and plateau portions of the blood flow response, the 'phases' of the hemodynamic response.

The timecourses in Figure 4.3A-B show the hemodynamic response to 2 and 12 second stimulation in "central" and "peripheral" locations, relative to the active region of the somatosensory cortex. We use the central and peripheral regions as rough measures of proximity to neural activity. The central region of the hemodynamic response corresponds

to the location of greatest neuronal activity (evidence from calcium imaging Figure SC.1[5]); whereas peripheral regions may be influenced primarily as a result of dilation of major branches of the arteriolar tree, and less so by localized neuronal activity.

The images in Figure 4.3 C-D show the Δ[HbT] maps for the 2 and 12-second hemodynamic responses at discrete time points following the start of stimulation. As we expect, the initial phase of the responses are very similar for the first ~1-2 seconds after stimulus onset, displaying extensive recruitment of pial arterioles. The Δ[HbT] maps begin to differ 2-3 seconds after the 2-second stimulus ends, when the 2-second response returns to baseline. In the center of the responding region, the 12-second response reaches peak at a similar time as the 2-second response, but maintains a sustained response at reduced amplitude before returning to baseline at the end of stimulation. The peripheral responses exhibit a single peak response, and are the same for both 2 and 12-second stimulus durations (Figure 4.3 B-D).

This spatiotemporal pattern is consistently observed across rats for a range of stimulus durations. Figure 4.4 show timecourses for center and peripheral Δ[HbT] responses to 2, 4, 8, and 12 seconds of stimulation across 5 different rats. The fact that the response to a long stimulus does not appear to be a simple scaling of the response to a short stimulus implies that there is an additional level of complexity to the mechanisms regulating the blood flow response. From a mechanistic point of view, these observed hemodynamic could be explained by at least two different frameworks.

[5] Supplemental figures for Chapter 4 can be found in Appendix C

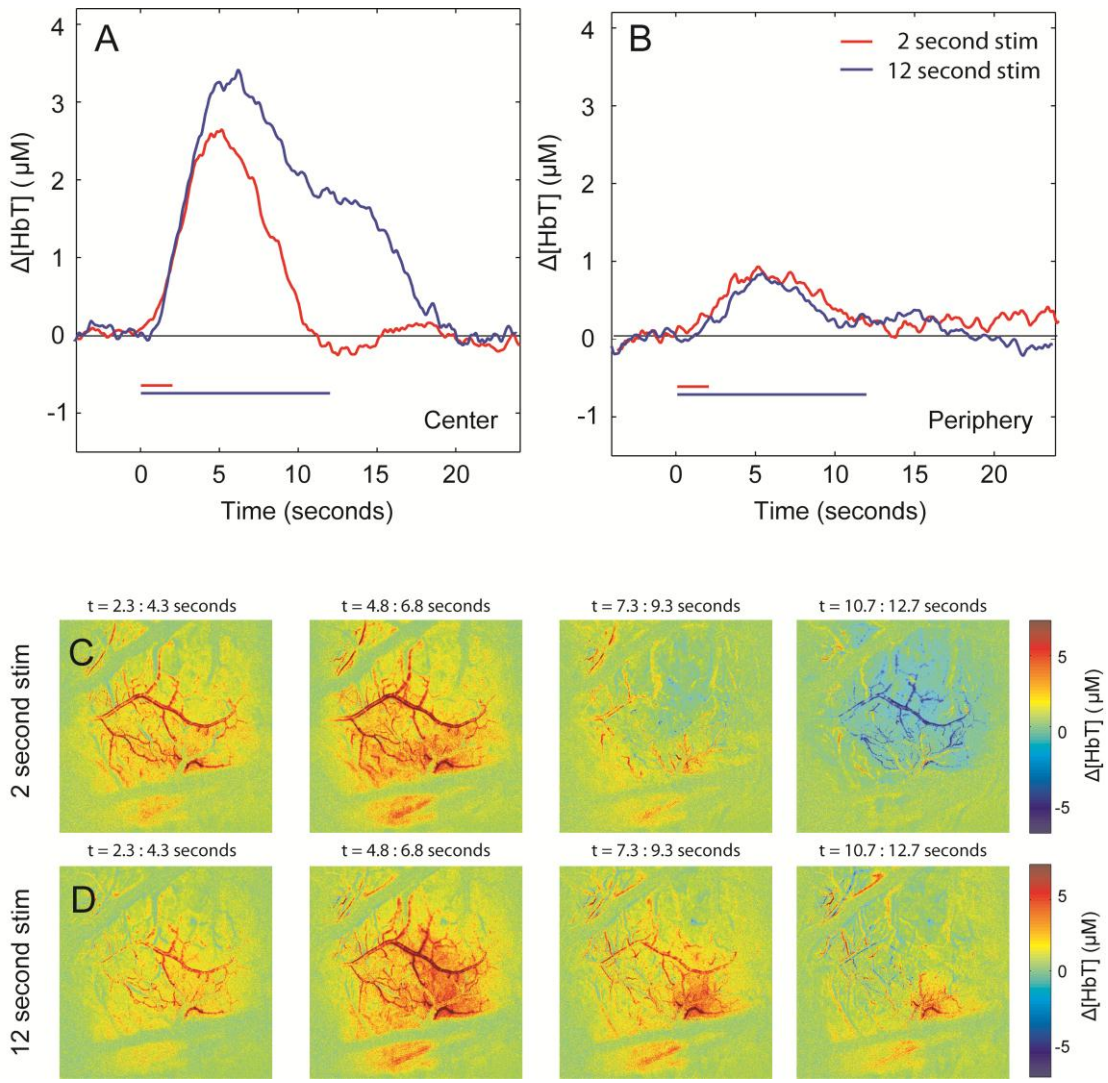

Figure 4.3 Spatiotemporal evolution of 2 and 12- second stimulus responses
(A-B) Timecourses showing the central and peripheral Δ[HbT] response to 2 second (red) and 12 second (blue) stimulus. (C-D) Δ[HbT] maps illustrate the spatial evolution of the hemodynamic response to a 2 second (C) and 12 second (D) hindpaw stimulus.

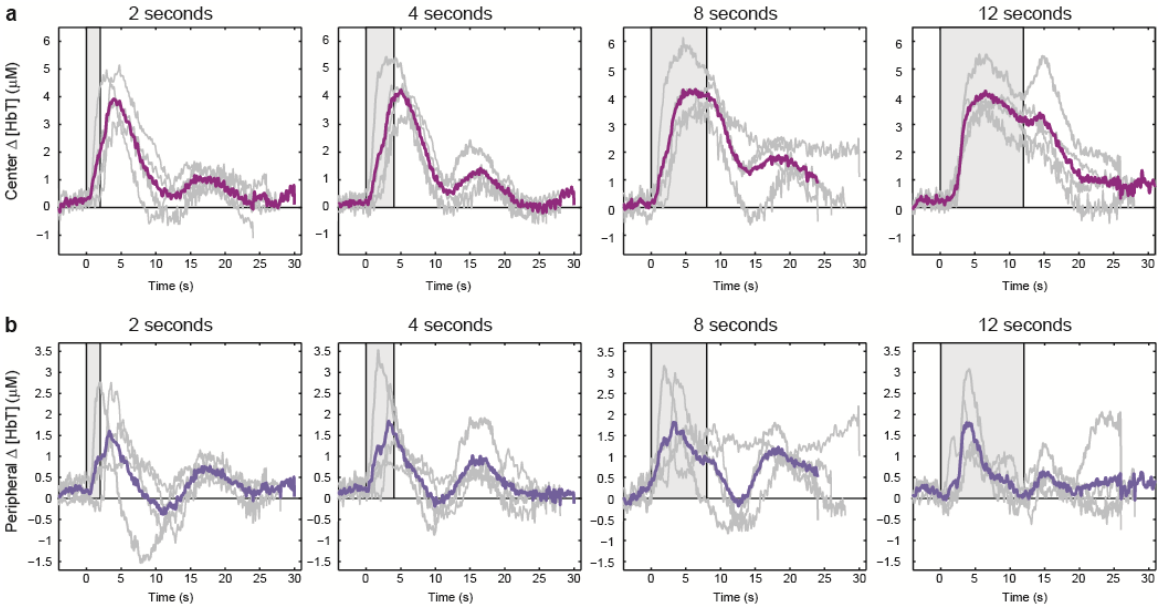

Figure 4.4 Center and peripheral Δ[HbT] responses
(a) Δ[HbT] responses selected from the 'central' responding hindpaw region for 5 rats are shown in light gray. The average timecourse is shown in bold. A 'plateau' phase arises for stimulus durations lasting eight or more seconds. (b) Δ[HbT] responses selected from the 'peripheral' responding hindpaw region for 5 rats are shown in light gray. The average timecourse is shown in bold. The peripheral responses do not exhibit a 'plateau' phase, even for longer stimulus durations.

The first explanation is that the response is orchestrated by a single cellular mechanism which exerts its influence in a space and time dependent manner. For example, this may be the case if a particular mechanism were capable of adjusting its influence as a function of metabolite levels, or oxygen levels over time. Nevertheless, there are several reasons for why this explanation does not seem likely (Cauli & Hamel 2010, Iadecola 2004). None of the cortical cells possess the connectivities and distribution that would be required of a single mechanism orchestrating the entire hemodynamic response. For example, astrocytes are capable of interacting with both neurons and vasculature, but they do not possess any direct contacts with the pial vessels and generally communicate with each other through slow propagating calcium waves (Anderson & Nedergaard 2003). Our results on astrocyte

reactivity, discussed in the previous section, also imply that astrocytes cannot be solely responsible for orchestrating the entire blood flow response. Pericytes are primarily found on capillaries, pre-capillary arterioles, and post-capillary venules, making them capable of influencing blood flow only at those discrete locations (Hirschi & D'Amore 1996). In addition, a large number of studies have attempted to abolish the hemodynamic response by inhibiting a single cellular mechanism or signaling pathway, but were only able to attenuate the amplitude of the response (Bernardinelli et al 2011, Dirnagl et al 1993, Harris et al 2010, Higley & Contreras 2007, Lecrux et al 2011, Leithner et al 2009, Lindauer et al 1999, Peng et al 2002, Shimamoto et al 2004).

The second explanation, and more likely explanation, is that the distinct spatiotemporal patterns of the hemodynamic phases are attributed to different cellular mechanisms which exhibit different reaction times and spatial extents of influence. The idea that there may be distinct mechanisms underlying different phases of blood flow control has been proposed in recent literature (Berwick et al 2008, Calcinaghi et al 2011, Cauli & Hamel 2010, Iadecola 2004, Kennerley et al 2011), but not directly tested. Using evidence from OISI of vascular responses to long stimulus durations in whisker barrel, Berwick et al., suggest that different but complementary mechanisms may be responsible for the "initial-diffuse" and "prolonged-restricted" hemodynamic responses (Berwick et al 2008). Integrating findings from existing literature in their review article, Cauli and Hamel suggest that a combination of neuronal and astroglial messengers acting in sequence probably mediate the hemodynamic changes (Cauli & Hamel 2010). More recently, experimental studies have attempted to 'de-couple' the hemodynamic phases by selectively inhibiting a single mechanism that corresponds to either the early or late phases of the response (Calcinaghi et al 2011, Kennerley et al 2011).

Kennerley et al. use hypercapnic induced pre-dilation of arterioles to inhibit the initial rapid vasodilation of pial arterioles. However, they discovered that this method also affects the underlying neural activity, making it difficult to determine whether true de-coupling of the phases was observed. Calcinaghi et al. report that the early hemodynamic response is not attributable to activation of astrocytic metabotropic glutamate receptors (mGluR5), but did not comment on the role of mGluR5 in later portions of the response.

While these studies contribute towards our understanding of blood flow control, the properties defining the hemodynamic phases remain imprecise and based on qualitative observations. Hypotheses describing the distinct mechanisms underlying vascular control continue to be speculative. In many cases, this is because the findings from pharmacological experiments were not definitive in implicating explicit mechanisms of control, making results difficult to interpret. In addition, the possibility of a multi-phase framework has been discussed, but not be directly supported with experimental evidence (Kennerley et al 2011).

To build upon the idea of multiple mechanisms of blood flow control, we survey the literature for reports on the hemodynamic response to prolonged stimulation. It is interesting to note the subtle discrepancies among these studies (Ances et al 2000a, Berwick et al 2008, Harris et al 2010, Matsuura & Kanno 2001). Matsuura et al. found that the blood flow response of the plateau was 43.4 ± 24% of the peak amplitude, while the timecourses reported by Berwick et al., and Harris et al., show that the plateau actually exhibits a second peak that is comparable to the first peak's amplitude (Berwick et al 2008, Harris et al 2010, Matsuura & Kanno 2001). Across studies, it appears that the initial phase of the

response exhibits consistent spatial and temporal patterns, yet the temporal shape of the plateau phase is less well-defined.

If two mechanisms indeed underlie control of the different phases of the response, then the different phases should exhibit inherently different properties and characteristics (as suggested by the different hemodynamic features reported across studies). One way that we can observe these mechanistic properties is to measure how variable each phase of the response is over time. To investigate these differences more thoroughly, we quantified the variability of the peak and plateau Δ[HbT] response amplitudes over 20 imaging runs in a single rat throughout the course of an experiment (Figure 4.5).

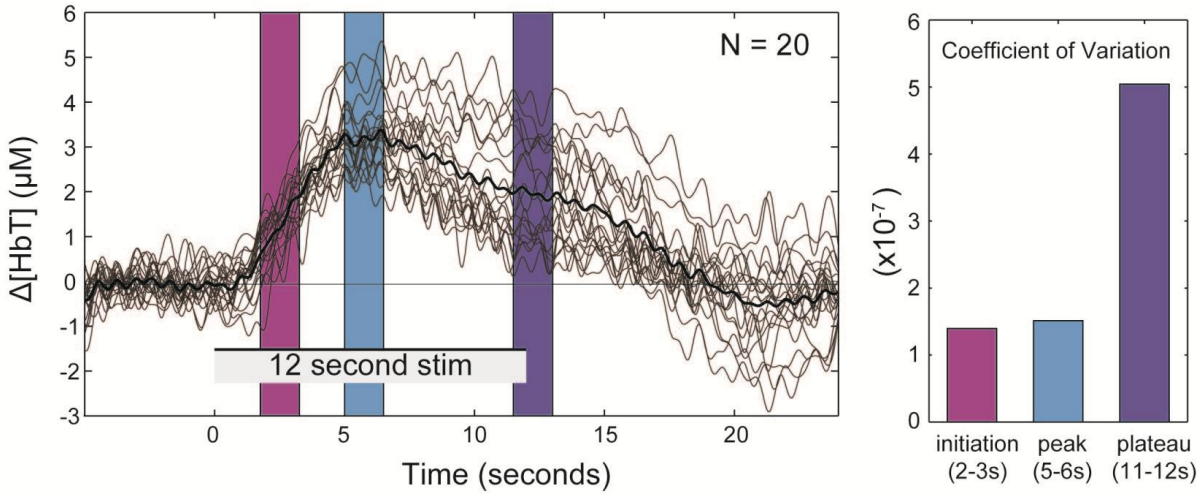

Figure 4.5 Variability of the hemodynamic response
(Left) Δ[HbT] single-trial timecourses for a 12 second stimulus collected over the course of an experiment are overlaid on top of each other, with the average timecourse shown in black. (Right) Bar plot showing the coefficient of variation computed over a 1 second interval for the color-coded intervals shown. The plateau amplitudes are approximately 4 times more variable than the peak amplitudes.

The coefficient of variation (variance/mean) bar plot in Figure 4.5 shows that the amplitude of the plateau response is ~ 4 times more variable than the amplitude of the initial peak. If we hypothesize that the initial peak is a reflex-like response to cortical input but the later phase is more tuned to subsequent cortical activity or energy demands, then the second phase should indeed vary more from one stimulus run to the next, depending on the current state of the neural tissue. In the context of cellular mechanisms, we attribute the source of variance in the Δ[HbT] to properties of the actuating mechanisms underlying them. The low variability measured in the peak response indicates a mechanism that exhibits highly repeatable actuation. In contrast, the mechanism responsible for maintaining the plateau response appears to be more sensitive to variations in cortical processing or brain physiology which changes throughout the experiment.

4.5 Transitions between short and prolonged stimulus duration

The hemodynamic response to prolonged stimulation exhibits interesting spatiotemporal and variability features that can be used to inform our investigations of underlying cellular mechanisms. To better understand the conditions that recruit each potential mechanism, we examined the transition between a "single-phase response" to a "multi-phase response" by using a range of different stimulus durations. The timecourses in Figure 4.6 and Figure SC. 2 show the central and peripheral responses relative to the hindpaw region for stimulus durations varied between 0.5 to 14 seconds in two different rats. The temporal dynamics of this data closely resembles the BOLD-CBF responses obtained for stimulus durations ranging between 1-30 electrical pulses by (Hirano et al 2011).

From our previous analysis, we know that the hemodynamic response in arterioles and parenchyma can be very different (Chapter 3). Thus, we decompose the average center signal and average periphery signal into their arteriolar (red-yellow spectrum) and parenchymal (blue-green spectrum) components for further analysis (Figure 4.7). The most obvious difference between central arteriolar and parenchymal responses is in their dynamic ranges. As stimulus duration increases, the arteriolar and parenchymal response amplitudes appear to saturate at different maximal levels around the same stimulus duration. In the periphery, both arteriolar and parenchymal responses exhibit smaller amplitudes than in the center.

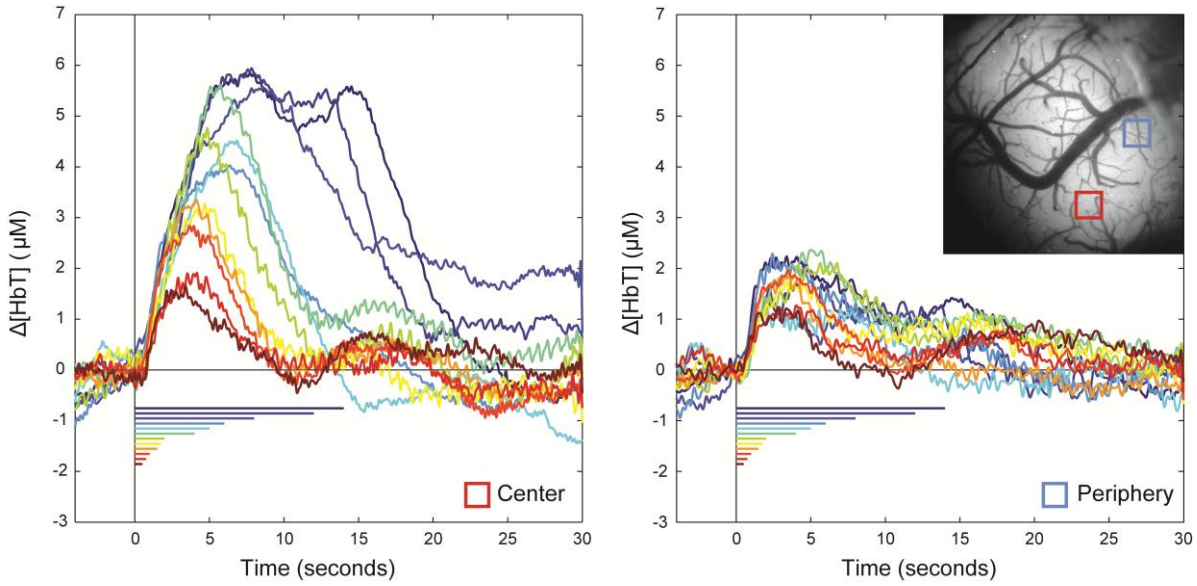

Figure 4.6 Hemodynamic responses to a range of stimulus durations
Central and peripheral Δ[HbT] responses to 0.5, 0.75, 1, 1.5, 1.75, 2, 4, 5, 6, 8, 12, and 14 second stimulus durations. Timecourses are averaged over a central region and a peripheral region (inset, red and blue squares).

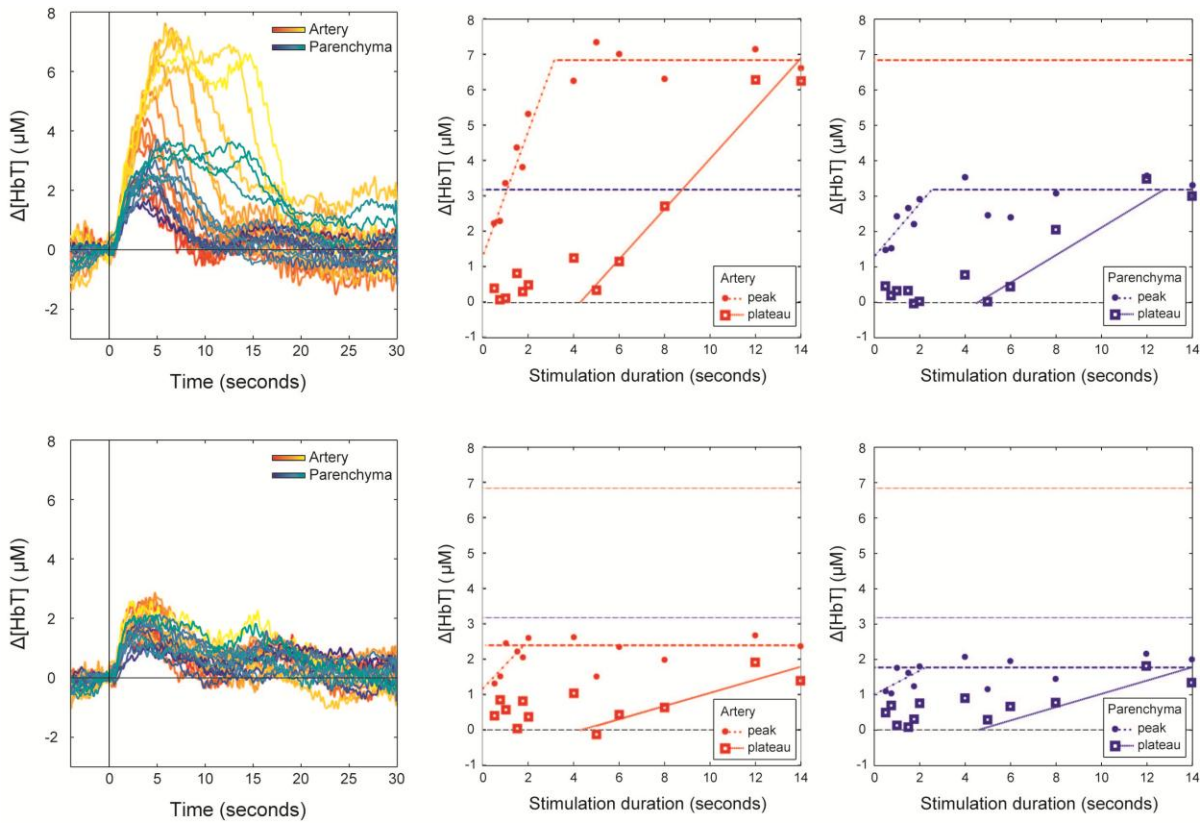

Figure 4.7 Arteriolar and parenchymal hemodynamics
(Top) Central Δ[HbT] responses decomposed into arterial and parenchymal components. The scatter plots show arteriolar (red) and parenchymal (blue) Δ[HbT] amplitudes as a function of stimulus duration for the peak and plateau phases of the response. The horizontal dotted lines represent the theoretical saturation point for each vascular compartment. (Bottom) Peripheral Δ[HbT] responses decomposed into arterial and parenchymal components.

To study these trends in amplitude more carefully, we plot the peak and plateau as a function of stimulus duration (we measure peak amplitude at the maximal turning point and the plateau amplitude 10-12 s following the start of stimulation). Maximal saturation levels are approximated as shown by the horizontal dotted lines, and linear regression lines are fitted to the remaining observations. The central arteriolar peak response scales linearly with stimulus duration until the peak amplitude reaches the saturation level for stimuli longer than ~4 seconds. The central parenchyma response saturates at slightly shorter

stimulus durations and reaches a lower saturation level. In the periphery, the arterial response is smaller and more constant across stimulus durations and the parenchymal response is similar in both trend and amplitude.

We hypothesize that the central arterial response saturates due to vasodilation signal reaching a maximal level since the plateau response reaches the same maximal level at longer stimulus durations. This saturation level is not necessarily equivalent to the maximal physical diameter of the arteriole, but rather the upper limit of the arteriole's natural dynamic range. It is not clear whether the parenchyma saturation is a direct result of arteriolar saturation, or whether a physical saturation of capillary blood flow is also reached. Similarly, it is also unclear from this data alone whether saturation has truly been reached above a certain stimulus duration threshold or instead, that the relationship between response amplitude and stimulus duration changes above this threshold. Thus, a more generalized observation is that the relationship between Δ[HbT] amplitude (A) and stimulus duration (S) is different for responses to stimulus durations less than and stimulus durations greater than a threshold duration (T): $\frac{dA}{dS(S<T)} \neq \frac{dA}{dS(S>T)}$.

Looking at the center arteriolar plots in Figure 4.7, we note that the x- and y- intercepts of the peak and plateau regressions do not intercept the origin. This is important because: 1) The non-zero y-intercept of the peak regression shows that as the stimulus duration approaches zero, there remains a finite, non-zero response in all regions. This observation suggests that there is a unitary hemodynamic response that must result, even for the tiniest cortical input, consistent with a reflex-like response to cortical input. 2) The x-intercept of the plateau regression shows the minimum stimulus duration that is needed to elicit a

secondary plateau response. It is also interesting to note that the stimulus duration at which the plateau phase appears to be elicited is also around the stimulus duration at which the peak arteriolar response saturates.

Additional experiments replicating this data in additional rats will be required to further develop hypotheses about the necessary conditions required to trigger recruitment of a secondary mechanism. These experiments provide an analytical paradigm for building a more detailed characterization of the hemodynamic and for interpreting subsequent findings in the context of energetic or temporal dependencies of the blood flow control mechanisms.

4.6 Conclusions & implications

4.6.1 Summary of findings

In this chapter, we explored the idea that the hemodynamic response consists of distinct 'phases' that are characterized by their spatiotemporal properties and attributable to different underlying cellular mechanisms. We studied the astrocyte calcium dynamics and blood flow dynamics in response to prolonged somatosensory stimulation. Astrocyte calcium responses appeared delayed by 2-3 seconds from stimulus onset, suggesting that astrocytes are not responsible for the initiation of the blood flow response but could play a role in the later phases of the blood flow response. To further develop this hypothesis, we conducted investigations of the blood flow response following a range of stimulus durations. We found that the blood flow response to short and prolonged stimulus durations manifested different spatiotemporal properties in spatial pattern, variability, and

amplitude. These findings further support the hypothesis that multiple distinct mechanisms are recruited throughout the course of the hemodynamic response. Our findings are also consistent with existing literature describing the hemodynamic response to prolonged stimulation, and provide further details into the defining qualities of the hemodynamic phases.

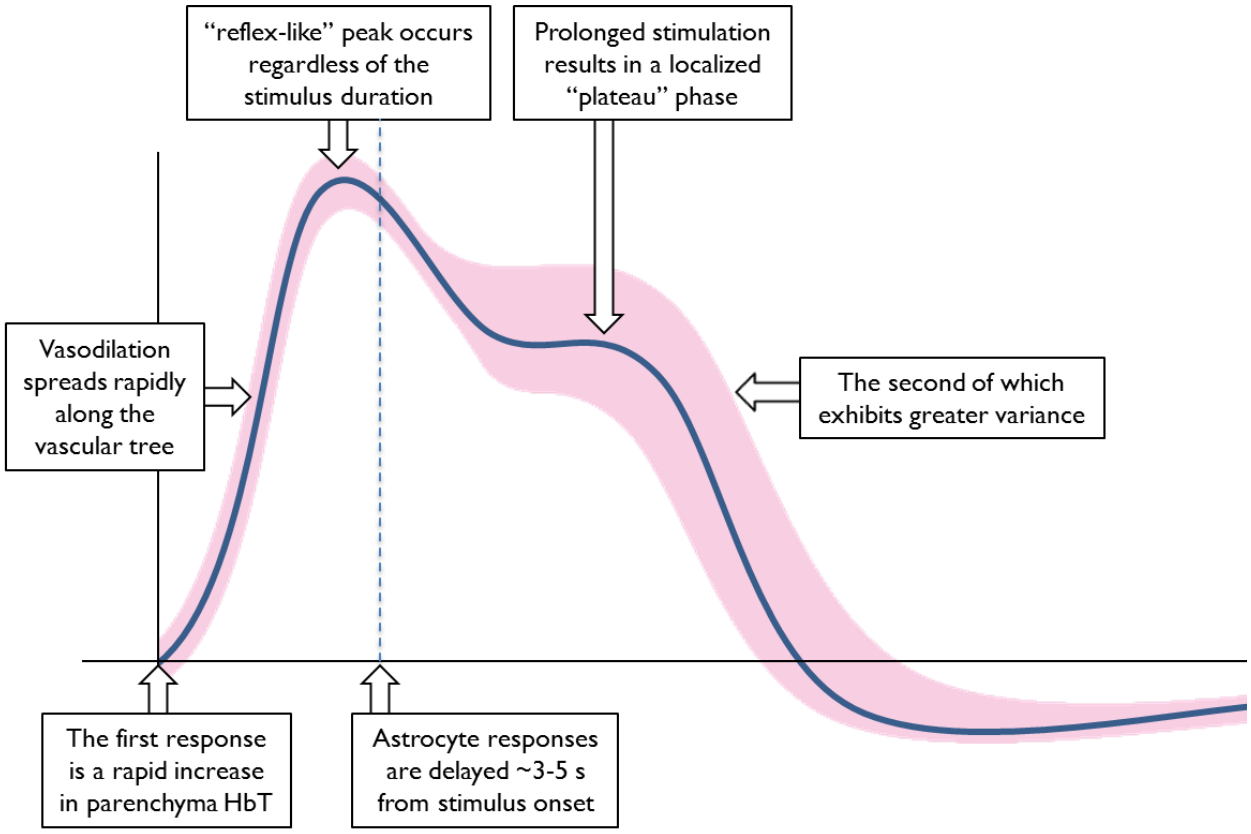

Figure 4.8 Summary of multi-phase descriptive model
This schematic summarizes the key features of the hemodynamic response (blue timecourse). The pink envelope represents the signal variance at each point in time. Identifying specific properties of the blood flow response will enable us to create a theoretical framework that can help guide further investigations of the cellular mechanisms underlying the response.

We integrate the findings from Chapters 3 & 4 into a descriptive model of the evolution of the hemodynamic response (Figure 4.8): The first response to somatosensory stimulus is a rapid increase in parenchyma Δ[HbT] which rapidly spreads along the vascular tree to the surface pial arteries through conducted vasodilation. Around 2-3 seconds after stimulus onset, the Δ[HbT] response reaches a peak regardless of stimulus duration. If stimulation continues, a plateau phase that is spatially localized to the region of neural activity is observed. The amplitude of the plateau phase is more variable over time than the initial peak amplitude. Interestingly, astrocyte calcium responses exhibit a similar delay and level of variability as the latter portion of the blood flow response during prolonged stimulation (> 4-5 seconds after stimulus onset) (Chapter 4.3).

Methodological conclusions We have demonstrated that analysis of hemodynamic responses obtained through wide field OISI can provide useful insights into the mechanisms underlying the observed blood flow changes. Specifically, studying how increasing stimulus durations map to changes in the observed hemodynamic response may elucidate the relationship between incremental increases in neuronal activity and changes in blood flow. Changing stimulus parameters (duration, amplitude, frequency, pulse width) can be used as a natural method to perturb metabolic and energetic demands of the brain tissue, without the use of chemicals or other artificial stimuli (further discussed in Chapter 7.4.1).

4.6.2 A Multi-phase model of neurovascular coupling

Based on the key features of the hemodynamic response (highlighted in Figure 4.8), we construct a framework for neurovascular coupling that allows different phases of the hemodynamic response to be motivated by different neuronal or metabolic conditions. Figure 4.9 shows a theoretical depiction of a multi-phase model of blood flow control that is based on our empirical findings (Figure 4.8). The first phase exhibits consistent reflex-like characteristics and appears to involve signaling mechanisms that follow the vascular tree (highlighted in blue in Figure 4.9 A, B & C). The far-reaching spatial pattern of the early $\Delta[\mathrm{HbT}]$ response can be attributable to rapidly propagating vascular changes at the pial arteries that extend to peripheral regions that would otherwise not be "active". In the case of prolonged stimulation, a second phase of the hemodynamic response is elicited by a slower cellular mechanism that is more sensitive to energetic or metabolic feedback from active neurons (highlighted in green in Figure 4.9 A, B & D).

In this model, the action of the first phase begins to subside 3-4 seconds after the stimulus onset (corresponding to the TTP), possibly due to a temporal property inherent in the underlying mechanism. This 'turning off' of the first mechanism causes the response in the periphery to return to its baseline state. In the meantime, if increased neural activity has continued in the central regions, a second mechanism acts locally to maintain an elevated level of blood perfusion throughout the duration of the stimulation.

The fact that the observed hemodynamic response is a continuous 'peak' and 'plateau' without a significant break in between the phases suggests that there is temporal overlap in the actions of the two mechanisms. If the onset of the second mechanism is delayed relative

to the start of stimulation, then this overlap could be mediated by the gradual decay or deactivation of the first mechanism. An alternative explanation is that both first and second mechanisms are recruited at the stimulus onset, but the second mechanism exhibits a gradual 'ramp up' or a slower time constant than the first mechanism. In the case of short stimulation, the second phase may never 'ramp up' enough that it can be distinguished from the first phase.

At the cellular level, this framework depends on the existence of two distinct mechanisms: one that signals along the vasculature and a second that is capable of sensing increased neural activity and that acts locally and independently of the pial vessels. It is difficult to further establish the properties of these two mechanisms based existing observations alone. In the context of this framework, one way to study these mechanisms would be to experimentally inhibit one of the hypothesized mechanisms (Chapter 5). Assuming that the hemodynamic contributions of the two mechanisms add linearly, the entire hemodynamic response could then be decomposed into its first and second phase contributions. With this knowledge we could more accurately define a framework for the hemodynamic phases that is characterized by 'hemodynamic response functions' (HRF) with specific onset times and rates of action for each mechanism, rather than by qualitative features of the manifested blood flow response. Such a model could explain many of the paradoxical findings in neurovascular coupling literature to date, particularly since key studies have used a range of different stimulus types, frequencies and durations that may recruit different mechanism to varying degrees (Cauli & Hamel 2010 for review).

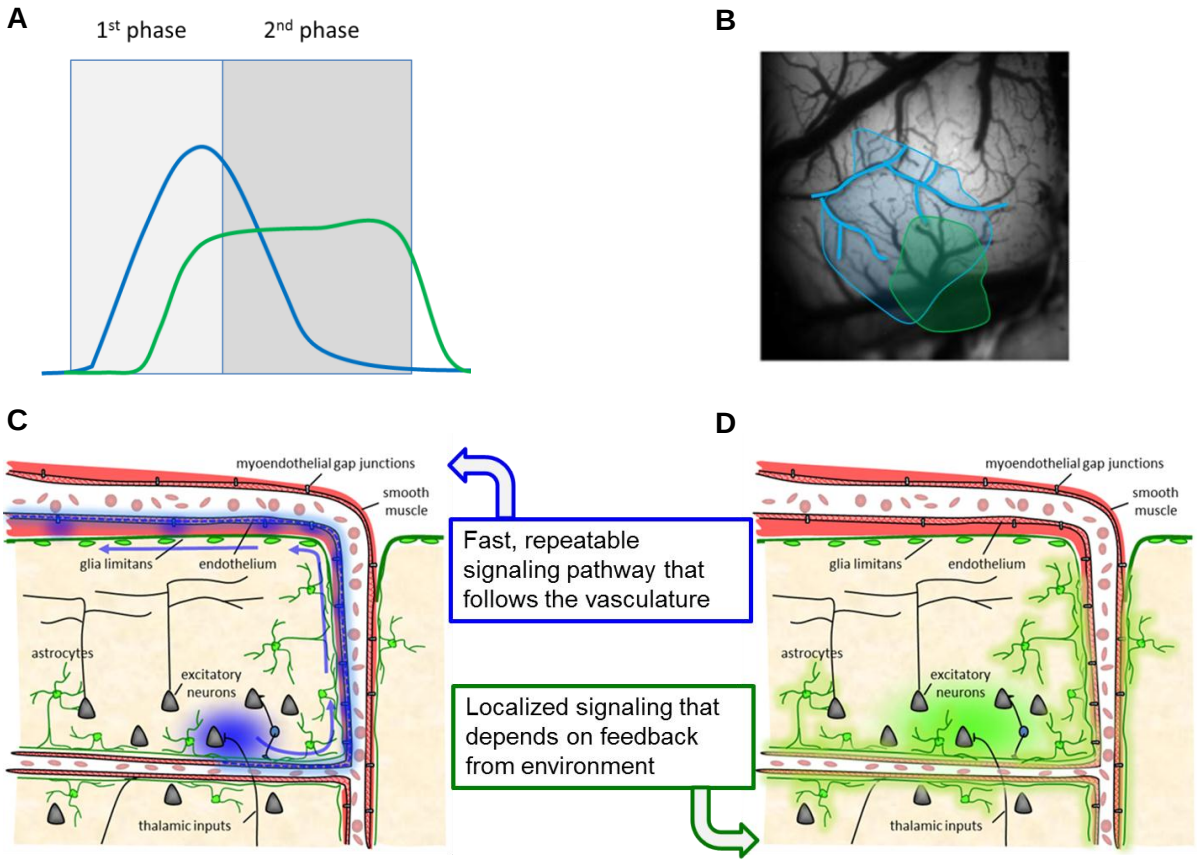

Figure 4.9 Theoretical framework for neurovascular coupling
(A) Timecourses showing temporal structure of blood flow responses attributable to theoretical 1st (blue) and 2nd (green) phase mechanisms. (B) Map demonstrating the corresponding spatial spheres of influence exerted by each mechanism. The 1st phase would theoretically extend along surface pial arterioles, recruiting even vessels that are further away from the location of active neurons. Alternatively, the 2nd phase would be spatially localized to the parenchyma region surrounding the active neurons. (C-D) Schematic of 1st and 2nd phase mechanisms at the cellular level. The mechanisms must exhibit properties that agree with the observed behavior of the blood flow response.

Chapter 5

A critical role for arterial endothelium in neurovascular coupling

5.1 Introduction

In the previous chapter, we described the properties of the different hemodynamic phases that arise during prolonged stimulation and outlined a model for neurovascular coupling that relies on the recruitment of at least two distinct signaling pathways or cellular mechanisms. This model is based on the empirical findings of Chapters 3-4 and includes detailed constraints governing the mechanism underlying the first phase of the hemodynamic response. In this chapter, we develop the hypothesis that a key component of the early cortical response involves vasodilatory signals transmitted through the arteriolar endothelium. We use a well-established light-dye injury model to selectively disrupt the

arteriolar endothelium and find that the early sensory-evoked arteriolar vasodilation is substantially attenuated, while the later phase of the response remain relatively unchanged. This result demonstrates a critical role for endothelial signaling in neurovascular coupling and provides experimental evidence that multiple neurovascular mechanisms are recruited during extended stimulation.

5.2 Background

The hemodynamic response to stimulus exhibits several interesting features when examined at high spatial and temporal resolution. The initial phase of the response includes parenchymal hyperemia followed by rapid, retrograde dilation of specific branches of the arteriolar tree feeding the active region. This dilation can spread through the vasculature up to a millimeter away from the center of the responding region within ~400 ms of the stimulus onset (Chapter 3). Irrespective of stimulus duration, this arteriolar dilation decreases after 3-5 seconds. If the stimulus ends before this point, blood flow returns to baseline. If stimulation persists, blood flow is maintained at an intermediate level and is generally more localized as a region of capillary hyperemia, returning to baseline at cessation of stimulation (Chapter 4, Berwick et al 2008, Matsuura & Kanno 2001).

Astrocytes have been proposed to play a role in neurovascular coupling owing to their perivascular connectivity and their ability to sense glutamate and to release vasoactive substances (Attwell et al 2010, Schummers et al 2008, Takano et al 2005, Wang et al 2006). However, as discussed in Chapter 4, there is a general consensus that astrocytic calcium responses are neither fast nor consistent enough to account for the early pial arterial dilation of the hemodynamic response. Therefore, while the properties of astrocytes make

them intriguing candidates for sustaining blood flow during prolonged stimulation, they are unlikely to be involved in mediating the early pial arterial dilation during functional stimulus.

We propose here that the spatiotemporal features of the hemodynamic response are consistent with the presence of an alternative mechanism governing, at least, the brain's 'first response' to cortical input. This mechanism must be capable of rapidly mediating dilation of key branches of pial arteries driving a significant localized blood flow increase that peaks around 3-5 seconds, irrespective of stimulus duration. In this chapter, we hypothesize that the arterial endothelium is a critical component of this mechanism.

Although previously speculated upon, the explicit involvement of the vascular endothelium in neurovascular control has not been directly demonstrated *in vivo* (Andresen et al 2006, Girouard & Iadecola 2006, Hannah et al 2011). Involvement of endothelial cells in functionally modulating cortical blood flow provides elegant explanations for many features of neurovascular coupling: Firstly, endothelial cells are tightly coupled to each other via gap junctions, forming an integrative route by which signals could plausibly travel continuously from capillaries to pial arteries via diving arterioles (Andresen et al 2006, Sarelius & Pohl 2010). Myoendothelial gap junctions (MEGJs) and/or activation of smooth muscle potassium channels allow this signal to be relayed to peripheral smooth muscle cells, actuating dilation of the vessel from within (Andresen et al 2006, Little et al 1995, Wölfle et al 2011). A recent study demonstrated that endothelial hyperpolarization could mediate propagated arterial vasodilation in cremaster muscle without attenuation over distances of 1-2 mm despite decaying hyperpolarization gradients, owing to an effect in which maximal dilation is induced by membrane potentials above a certain threshold.

The resulting almost instantaneous propagated response has spatial and temporal properties that are remarkably consistent with the dynamics of early cortical arterial dilation (Wolfle et al 2011). Such a propagated response would likely select the shortest route along which to dilate specific arteriolar and arterial branches, generating rapid and localized increases in blood flow (Andresen et al 2006, Sarelius & Pohl 2010). Initiation of endothelial signaling at the capillary level would be consistent with capillary beds being the locations of greatest demand for nutrients, and the fact that the capillary endothelium is not obstructed by smooth muscle cells.

Secondly, endothelial hyperpolarization can be induced experimentally using acetylcholine (ACh) and can also be initiated by K+ ions, adenosine, adenosine and uridine triphosphate (ATP and UTP) (Andresen et al 2006, Dietrich et al 2009, Duza & Sarelius 2003, Marrelli et al 2003, Rosenblum 1986, Winter & Dora 2007, You et al 1997), all known neurotransmitters and/or co-transmitters. Endothelium-driven blood flow increases could therefore be initiated via a neurogenic pathway, consistent with recent findings that the hemodynamic response is largely independent of local availability of glucose and oxygen (Cardoso et al 2012, Lindauer et al 2010, Wolf et al 1997).

Finally, endothelial cells possess many of the same signaling pathways that trigger vasodilation as astrocytes and neurons, such as production pathways for prostaglandins (PGs), epoxyeicosatrienoic acid (EETs), nitric oxide (NO), and arachidonic acid (AA) (Andresen et al 2006). Studies using pharmacology to block such pathways in other cell types may thus have also affected the endothelium (Cauli & Hamel 2010, Girouard & Iadecola 2006, McCaslin et al 2011, Takano et al 2005). Demonstration that the vascular endothelium plays a vital role in generating the cortical hemodynamic response to

functional stimulus could therefore explain many observed features of neurovascular coupling, while also providing a compelling new target for therapeutic interventions.

In this chapter, we test the hypothesis that the vascular endothelium is a key component of neurovascular coupling using *in vivo* multi-spectral OISI (MS-OISI) of the exposed somatosensory cortex in combination with light-dye (LD) disruption of the vascular endothelium. Used widely in studies of the peripheral vasculature, LD treatment is a standard method to selectively disrupt the arterial endothelium and prevent propagated vasodilation via endothelial hyperpolarization. LD treatment uses strong blue light focused on intravascular dextran conjugated fluorescein (FITC-dx) to generate hydroxyl radicals that damage communication between endothelial cells while leaving smooth muscle and other surrounding cells intact. Our findings characterizing the hemodynamic response to electrical hindpaw stimulation before and after LD disruption indicate that vascular endothelium-dependent vasodilation plays a critical role in mediating early stimulus-evoked cortical blood flow changes.

5.3 Methods

5.3.1 Animal preparation & light-dye treatment

The animal surgical preparation performed prior to LD treatment is described in Chapter 2. Light-dye injury to the endothelium involves introducing an intravascular sensitizing agent, such as a fluorescent dye, into the luminal space where it can contact the endothelium. Excitation of the sensitizing agent with intense light produces free oxygen

radicals that react with neighboring endothelial cells that eventually causes disruption of the cellular membrane[6].

To prepare for LD treatment, rats were slowly injected with 0.5 mL 1% dextran conjugated fluorescein isothiocyanate MW 70kDa (FITC-dx) in saline through the femoral vein catheter (~ 1.2 mL/hr). After 5 minutes of equilibrium, the endothelium was disrupted over a ~2mm diameter spot by exciting the dye with a 473nm blue LED coupled to a 400μm optical fiber for a period of 6-7 minutes. The blue light spot was positioned over the desired region to be treated prior to injection of FITC-dx and the power at the cortical surface was measured to be ~ 6mW/mm^2. The optimal duration of illumination to achieve selective endothelial disruption using this experimental set up was determined through a series of preliminary studies. Specific endothelial damage was investigated at the end of each experiment with pharmacology controls and propidium iodide labeling of damaged nuclei. All animal procedures were reviewed and approved by the Columbia University Institutional Animal Care and Use Committee.

5.3.2 Optical intrinsic signal imaging

A $\sim 3 \times 3$ mm region of the exposed cortex was imaged using our MS-OISI system consisting of a Dalsa 1M60 camera and synchronized light emitting diode (LED) strobed illumination (Bouchard et al. 2009). Data was acquired using red (630nm centered, M625L2, Thorlabs) and green (530 nm centered, M530L2, Thorlabs) LEDs with a 534/43nm filter in front of the green LED (NT67-031, Edmund Optics). Dual wavelength data were acquired at 74 fps (equivalent to 37 fps for each LED) with a 5 ms exposure time

[6] A background overview on the LD technique is provided in Appendix D.

and a 512 x 512 pixel resolution. Each imaging run lasted 40 seconds and consisted of 6 seconds of pre-stimulation, 12 or 2 seconds of stimulation, and 22 or 32 seconds of post-stimulation, respectively. Sensory evoked hemodynamic responses were recorded before and after light dye disruption. A 496 nm longpass emission filter (FF01-496/LP-25, Semrock) was placed in front of the CCD camera to allow fluorescent imaging of the FITC-dx during blue light illumination. Negligible absorption of green LED light was found for FITC-dx at *in vivo* concentrations.

5.3.3 Data processing and analysis

The collected 630 nm and 530 nm reflectance data was converted to $\Delta[HbO]$ and $\Delta[HbR]$ using the modified Beer Lambert law with wavelength dependent pathlength factors calculated using Monte Carlo simulations (Hillman 2007, Sirotin et al 2009). Data was temporally filtered at 5 Hz, and typically averaged over 10 repeated stimulus runs. Time-courses were averaged over a region with both pial arteries and parenchyma (corresponding to capillary signal). Diameter calculations were performed on raw 530 nm reflectance data. The vessels examined for diameter measurements were roughly the same resting size (same degree of branching). Diameter was calculated as the full width of the vessel profile.

5.3.4 Pharmacology & propidium iodide labeling

We used pharmacological controls and propidium iodide labeling order to assess endothelial damage and confirm that smooth muscle cells were not disrupted. Topical application of 0.1mM acetycholine (ACh), an endothelium-dependent vasodilator, and 0.1

μM sodium nitroprusside (SNP), a endothelium-independent vasodilator that acts directly on smooth muscle cells, was used to induce endothelial dependent and independent vasodilation respectively (Budel et al 2003, Leffler et al 1994, Wölfle et al 2011). A field of view containing both light dye treated and non-treated vessels was imaged for 1 minute following application of ACh or SNP. After each imaging run, the brain was flushed with ACSF and allowed to return to baseline for 15 minutes. Control and treatment dilations were assessed in arteries of similar resting diameter. Only vessels that exhibited intact smooth muscle-dependent dilation to SNP, but not endothelial dependent dilation to ACh where included in the study.

We used a membrane impermeant fluorescent dye, propidium iodide (PI) to assess the extent of LDT disruption on endothelial and smooth muscle cells. This DNA stain is excluded from healthy intact cells and taken up by cells in which the plasma membrane has been compromised. At the end of the LDT experiments, ~1mL of 2μM of PI was infused intravenously over the course of 20 minutes and also applied topically to the cortical surface. After 20 minutes of incubation time, the animal was deeply anesthetized with 4% isoflurane and perfused with phosphate buffered saline (PBS) to clear any residual FITC-dx from the vasculature. The brain was then removed post mortem and fixed in 4% paraformaldehyde for 24 hours. Two-photon images of light dye treated and non-treated pial arteries were acquired using 900-1020 nm excitation wavelength.

5.3.5 Pre-dilation control

To determine how increases in baseline arterial diameter affect the hemodynamic response, we used topical application of 1-2 μM ACh to induce an increase in baseline diameter in the absence of LD treatment. Control responses to 12 s stimulation were first recorded as previously described. The cranial window was then removed such that ACh could be applied to the exposed cortex. Immediately after ACh application, a layer of agarose was applied and the cranial window was re-sealed to minimize brain motion during imaging. Responses to 12 s stimulation were then recorded at ~ 10 minute intervals for 1-1.5 hours after ACh application.

5.3.6 Electrophysiology

Local field potentials (LFPs) were recorded to obtain a measure of neural responses in the somatosensory cortex before and after LD treatment. A tungsten microelectrode (0.005 mm diameter, 0.5 MΩ, A-M Systems) mounted on a micromanipulator was stereotaxically inserted into the cortex to a depth of ~400-500 μm in the center of the responding region identified through pre-LD MS-OISI imaging. Electrode signals were recorded using Spike2 software (CED, UK). LFP signals were filtered (0.1-100 Hz) and processed using Matlab™.

5.4 Results

5.4.1 Early arterial dilation is significantly attenuated by LD treatment

Identical stimulation runs were acquired before and after LD disruption of the vascular endothelium. Pre-LD responses were used to identify responding pial arteries to be subsequently targeted using LD treatment. Raw MS-OISI data was converted to Δ[HbO], Δ[HbR], and Δ[HbT] = Δ[HbO] + Δ[HbR] using the modified Beer-Lambert law with Monte Carlo-derived wavelength dependent path length factors (Cardoso et al 2012, Chen et al 2011, Hillman 2007, Sirotin et al 2009). Spatiotemporal patterns of Δ[HbT] are assessed through 'functional maps' that show the change in Δ[HbT] for a given time-window relative to baseline and time-courses extracted from selected regions of these spatial maps (example: Figure 5.1 d&e). We consider changes in Δ[HbT] to be measures of physical changes in vessel tone that are independent of changes in oxygen extraction (Chen et al 2011, Hillman 2007, Sirotin et al 2009).

Consistent with previous studies (Berwick et al 2008, Chen et al 2011), the hemodynamic response to 12 second stimulation prior to LD treatment was found to exhibit an early peak in Δ[HbT], corresponding to the rapid and early dilation of pial arteries (Figure 5.1 c & e). The classic 'peak and plateau' shape of the Δ[HbT] temporal response in Figure 5.1e has previously been reported for stimulus durations lasting longer than 8 seconds (Berwick et al 2008, Kennerley et al 2011, Matsuura & Kanno 2001). After LD treatment, pial arterial dilation is dramatically attenuated, although parenchymal hyperemia can still be discerned (Figure 5.1d and Supplemental Figure SD. 3).

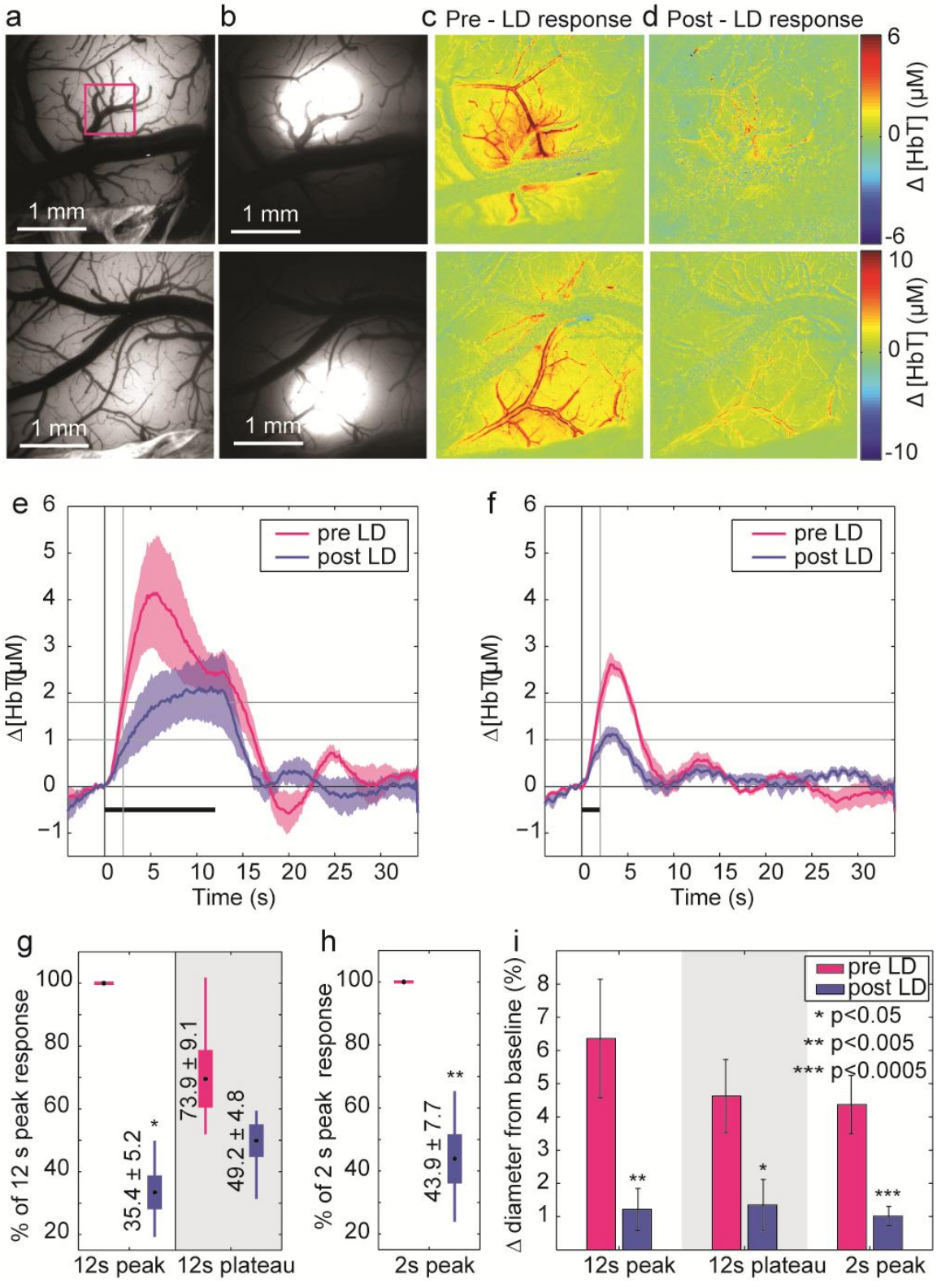
a
b
c Pre - LD response
d Post - LD response
1 mm
Δ [HbT] (μM)
6
0
-6
10
-10
e
f
pre LD
post LD
Δ[HbT](μM)
Time (s)
g
% of 12 s peak response
35.4 ± 5.2
73.9 ± 9.1
49.2 ± 4.8
12s peak
12s plateau
h
% of 2 s peak response
43.9 ± 7.7
2s peak
i
Δ diameter from baseline (%)
* p<0.05
** p<0.005
*** p<0.0005

Figure 5.1 The hemodynamic response before and after LD treatment
(a) Images of the exposed somatosensory cortex. (b) Blue light spots used for LD-treatment. (c) Pre-LD treatment functional maps showing Δ[HbT] relative to baseline during the "peak" averaged between 4 to 6 s after stimulus onset. (d) Post-LD treatment functional maps showing "peak" Δ[HbT] relative to baseline (shown on the same color scale as (c)). (e) Pre and post-LD Δ[HbT] responses to 12 seconds of stimulation averaged over 6 rats (error bounds show SEM). (f) Pre and post-LD Δ[HbT] responses to 2 seconds of hindpaw stimulation averaged over 5 rats (error bounds show SEM). The same results including Δ[HbO] and Δ[HbR] are shown in supplemental Figure SD. 5. For (e) – (f), the stimulus duration is shown by the black bar. Each time-course represents a spatial average over a selected region of the hindpaw center. (g) Δ[HbT] amplitudes averaged over the "peak" (4-6 seconds) and "plateau" (10-12 seconds) time periods, shown as a percentage of the pre-LD 12-second "peak" response. (h) Δ[HbT] amplitudes averaged over the 2 second response "peak" (3-5 seconds) time period, shown as a percentage of the pre-LD 2-second peak response. For (g)-(h), black dots represent the mean, boxes show SEM, and whiskers show the range of data. * $p < 0.05$ ** $p < 0.001$. (i) Percent change in diameter of responding pial arteries pre and post-LD for 12-second "peak", 12-second "plateau" (over 6 rats), and 2-second "peak" (over 5 rats). Whiskers show SEM.

_The time-course of the post-LD response to 12 second stimulation does not exhibit the early peak response, but rather a gradual rise in Δ[HbT] that reaches an amplitude similar to that of the pre-LD 'plateau' response (Figure **5.1**e). These time-courses were averaged over the same spatial region as the pre-LD data, such that the Δ[HbT] increases for both pre- and post-LD indicate increased perfusion of the capillary bed, despite a lack of pial arterial dilation in the post-LD case.

Pre-LD responses to 2-second stimulation are similar in temporal shape to the early peak response to longer stimulation (Figure 5.1f). The post-LD response to 2-second stimulation exhibits an attenuated response time-course compared to the pre-LD response that is consistent in timing and amplitude with the early evolution of the 12-second post-LD responses, as demonstrated by the gray crossbars in Figure **5.1**e-f. Functional maps for responses to 2 second stimulation are shown in Supplemental Figure SD. 4.

The bar plots in Figure 5.1g-i summarize the LD-induced attenuation in Δ[HbT] response amplitude as a percentage of the pre-LD initial peak responses to 12-second and 2-second stimulation. These changes correspond to a ~65% attenuation of the 'peak' response ($p < 0.05$) and only a ~25% attenuation of the later 'plateau' response to 12-second stimulation. The peak Δ[HbT] response to 2-second stimulation was attenuated by ~56% after LD ($p < 0.001$).

To confirm that LD treatment specifically impaired dilation of pial arteries, the diameters of targeted arteries were also calculated directly from acquired high-resolution images. Prior to LD treatment, the investigated pial arteries had baseline diameters between 45-55 μm. Consistent with our Δ[HbT] results, arterial diameters increased by 6.4 ± 1.8% at the initial peak of the response to 12 second stimulation and were 4.6 ± 1.1%

above baseline during the plateau phase. After LD treatment, dilations were significantly attenuated to 1.2 ± 0.6% (peak, $p < 0.005$) and 1.4 ± 0.8% (plateau, $p < 0.05$) of their baseline diameters.

Dilatory responses to 2-second stimulation were also attenuated at their peak from a 4.4 ± 0.9% dilation to a 1.0 ± 0.3% dilation above baseline ($p < 0.0005$). However, this analysis did reveal one potential confound; LD-treatment itself induced a 26% (7.8 ± 1.2 μm) increase in pial arterial baseline diameter (Rosenblum & El-Sabban 1982), a change that is larger than the stimulus-induced vasodilation. Control experiments to address this confound are described below.

5.4.2 Control studies

An increase in baseline arterial diameter could arguably reduce the capacity of the artery to dilate in response to stimulus. Increased baseline diameters also cause a local increase in baseline blood flow, and therefore oxygen and glucose delivery, which can potentially affect stimulus response mechanisms and even underlying neuronal activity itself. The following control experiments demonstrate that none of these effects can explain the changes in spatiotemporal response that we observe in response to LD treatment.

To address whether the pre-dilation effect of LD-treatment was sufficient to attenuate arterial dilations in response to stimulus, we induced local pre-dilation in surface arteries using an alternative method (topical application of 1-2μM Acetylcholine, ACh) and evaluated the ability of the vessels to respond to stimulation as a function of their baseline diameters. ACh acts upon the endothelium to generate pre-dilation, and therefore like LD-treatment, should not alter the function of smooth muscle cells. After the application of

ACh, pial arteries gradually dilated by roughly 30 μm and eventually returned to their original baseline diameters over the course of approximately 1 hour. Throughout this period, hemodynamic responses to 12 second stimulation in the absence of any LD treatment were recorded.

The functional maps in Figure 5.2a reveal that contrary to the effects of LD-treatment, pre-dilation of pial arteries to an equivalent level of around +7-10 μm did not prevent stimulus-evoked dilation, nor did it affect the temporal shape of the response; leaving the initial peak and subsequent plateau of the response in place for pre-dilation levels less than +23 μm (Figure 5.2b). Even for pre-dilation levels greater than +20 μm, functional dilations of arterial branches were still observed. To summarize this data, we plot the amplitude of the peak Δ[HbT] responses observed across 3 rats as a function of their vessel's pre-dilation. Peak Δ[HbT] amplitudes are generally unaffected by increases in baseline diameters between 0 and +10 μm. At higher levels of pre-dilation, a gradual decrease in peak Δ[HbT] amplitude is seen as baseline diameters increase (Figure 5.2b-c). Equivalent results for our LD treatment measurements are plotted on the same axes and are found to be significantly different from this trend ($p < 0.0001$), suggesting that endothelial disruption, and not pre-dilation alone is responsible for LD-induced changes in functional hemodynamics (Figure 5.1).

In order to ensure that LD treatment did not affect sensory-evoked neural activity, electrophysiology recordings were performed in 2 rats before and after LD-treatment. Figure 5.3a-b shows time-courses of local field potentials (LFPs) recorded during 12 seconds of electrical hindpaw stimulation before and after LD treatment. Recorded responses were the same in both cases.

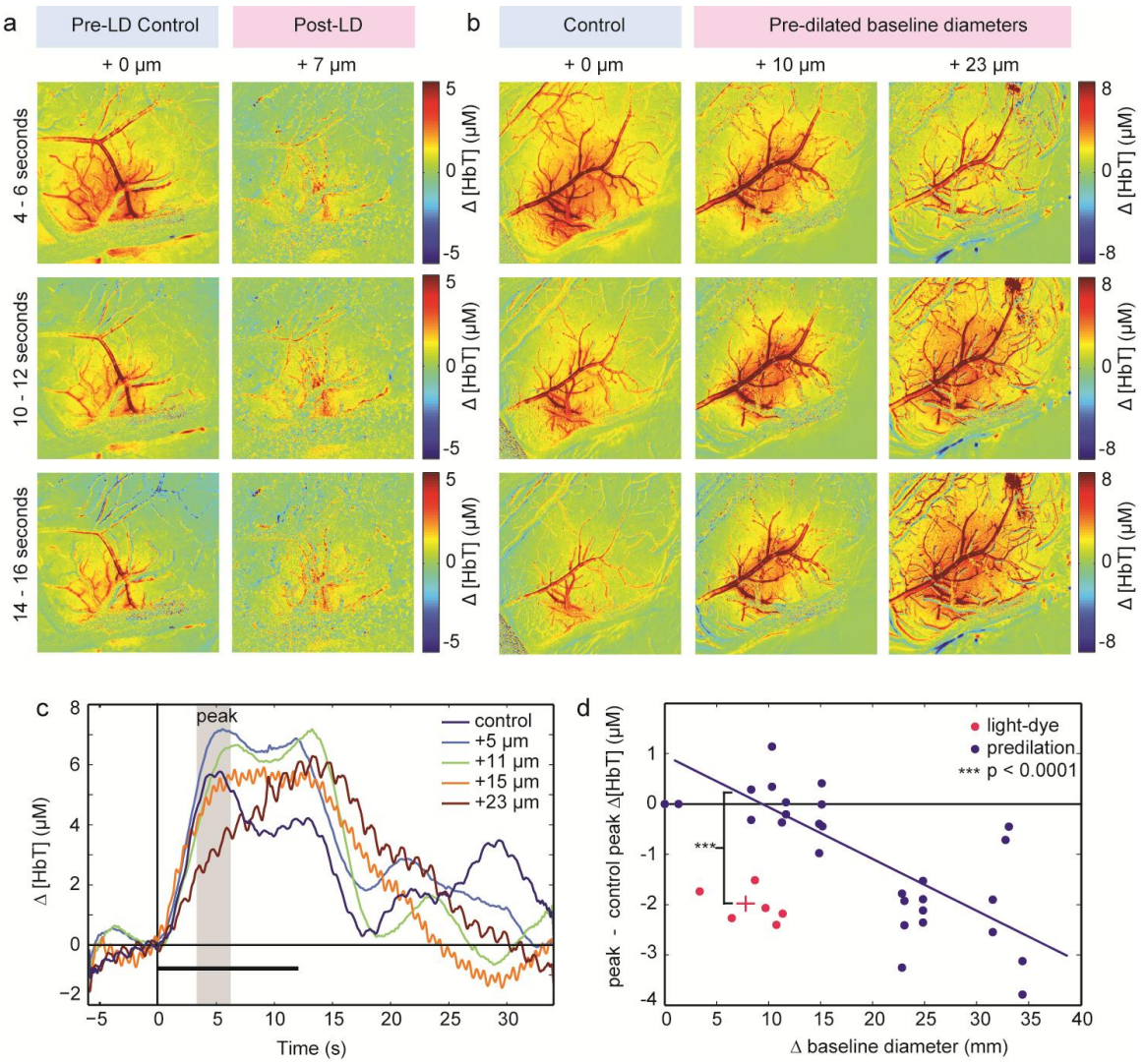

Figure 5.2 Pre-dilation does not significantly affect arterial responsiveness
(a) Functional maps showing pre-LD (control, left) and post-LD treatment (right) Δ[HbT] responses to 12 second stimulus averaged between 4-6 seconds (top), 10-12 seconds (middle), and 14-16 seconds (bottom) after stimulus onset. Post-LD functional maps lack dilation of pial arteries. (b) Functional maps showing Δ[HbT] response evolution when baseline diameters are pre-dilated using topical ACh by 0 µm (control), +10 µm, and +23 µm (left to right), all in the absence of LD treatment. Pial arterial responses are still observed, even in the presence of pre-dilated baseline diameters. (c) Δ[HbT] time-courses extracted from the same region in a single rat for increasing amounts of pre-dilation. (d) The change in peak Δ[HbT] amplitude (gray region in (c)) relative to the control peak Δ[HbT] from 3 rats is plotted for varying degrees of induced baseline pre-dilation (blue dots) and for LD experiments (pink dots). The solid regression line is the ordinary least-squares fit to the pre-dilation data (with no LD). The pink cross shows the mean and SEM of both variables for the LD data. Our comparison tests whether there is an additional effect of LD on peak amplitudes (relative to the effect of pre-dilation alone) while controlling for the influence of baseline dilation.

For both pre- and post LD-treatment, LFPs exhibit larger amplitudes at stimulus onset, and subsequently decay to lower amplitudes for the rest of the stimulus duration. Individual LFPs also did not exhibit significant differences in amplitude or shape throughout the duration of the stimulus period (Figure 5.3c).

As is common for LD treatment experiments in peripheral vessels (Bartlett & Segal 2000, Budel et al 2003, Koller et al 1989, Wolfle et al 2011), we also performed pharmacological controls to ensure that LD treatment was indeed only selectively disrupting the vascular endothelium and not smooth muscle cells. At the end of each LD experiment, endothelium-dependent dilator ACh and endothelium-independent dilator SNP were applied to the exposed cortex in turn. As expected, LD-treated pial arteries exhibited a loss of vasodilation in response to ACh application ($p < 0.005$), indicating endothelial disruption, but continued to dilate in response to SNP application, verifying that smooth muscle cells were intact and reactive (Figure 5.3d). Propidium iodide, a fluorescent membrane impermeant DNA stain was used to further confirm that LD-induced damage was confined to endothelial cells (Figure 5.3e) and did not also extend to the smooth muscle cells (Bartlett & Segal 2000). Neither intravenous delivery of FITC-dx nor blue light exposure alone affected the amplitude of the peak response to stimulus or the baseline diameter of pial arteries (Supplemental Figure SD. 6).

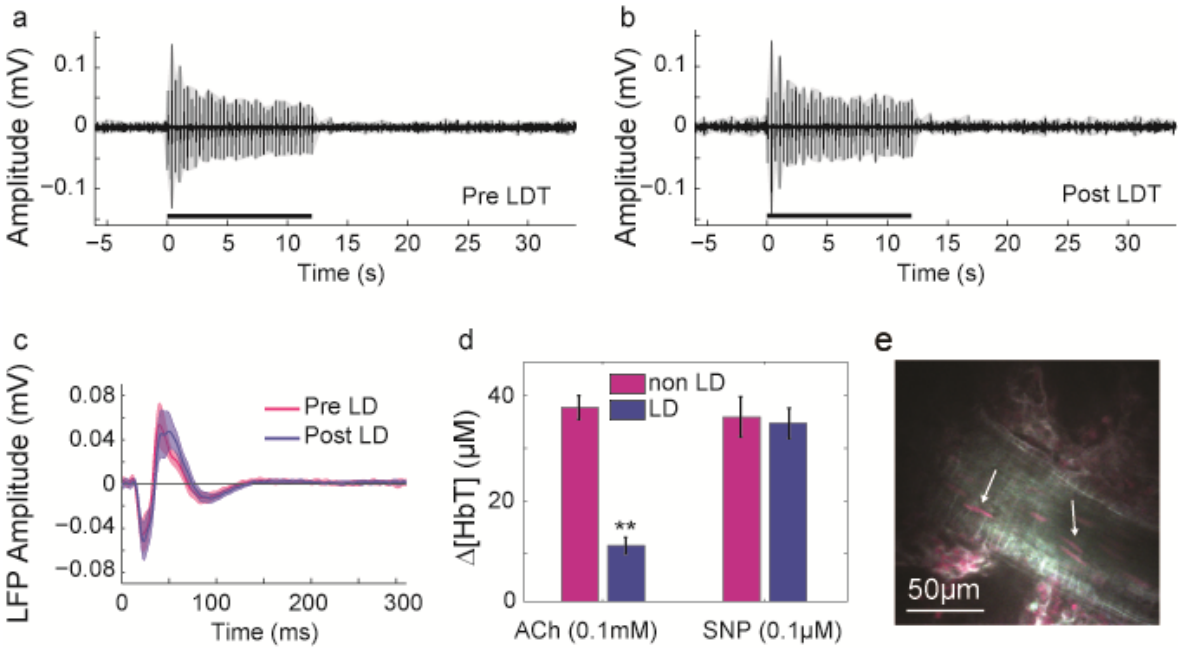

Figure 5.3 Neural activity and smooth muscle are unaltered by LD treatment
(a-b) Electrophysiological recordings of neural activity during 12 seconds of hindpaw stimulation before (a) and after (b) LD treatment. Black time-course represents the average over 10 single trial runs. Gray envelope indicates SEM. (c) Averaged individual local field potential (LFP) spikes from the time-courses in (a) and (b). Shaded regions show SEM. These results show that neural activity is not significantly altered by LD treatment. (d) Maximum Δ[HbT] change induced by topical cortical application of ACh (0.1mM) and SNP (0.1μM) following LD-treatment. LD values were extracted from within the treated blue light illumination area, whereas non-LD values were extracted from untreated, peripheral regions. Vasodilation to ACh in LD treated regions were significantly attenuated (** $p < 0.005$). The temporal dynamics of dilation to SNP in LD-treated and untreated regions were also unaffected (see Supplemental Figure SD. 7) (e) A typical ex-vivo two-photon microscopy imaging of propidium iodide staining of a pial arteriole after LD treatment. Arrows show longitudinal endothelial cell nuclei labeled with propidium iodide (red) indicating selective damage. Smooth muscle cells that wrap around the circumference of the vessel are not labeled, indicating no damage. Green signal is from residual FITC-dx after perfusion.

5.5 Discussion

In this chapter, we directly investigated the hypothesis that the arterial endothelium plays a crucial role in generating sensory-evoked increases in blood flow in the somatosensory cortex. We used light-dye treatment to selectively disrupt the endothelium of pial vessels, while leaving smooth muscle and neural activity unchanged. Our results demonstrate that the early spread of pial arterial vasodilation critically depends upon a healthy, intact endothelium.

The endothelium acting as a vasodilatory signaling pathway offers an elegant explanation for the early phase of the hemodynamic response, which is characterized by an early peak in blood perfusion that is localized to targeted pial arterioles. In particular, signaling along the vasculature allows for integrative and efficient vessel selection, eliminating the need for neuronal or glial processes to relay information from active neurons to pial arterioles at the cortical surface. The ability of the endothelium to rapidly conduct vasodilation millimeters away from the site of stimulation also provides a mechanism whereby a short neural stimulation can still elicit a 'reflex-like' blood flow response that exceeds the energetic demands of the tissue.

These findings are well supported by studies of endothelium in the peripheral vasculature (Bartlett & Segal 2000, Budel et al 2003, Koller et al 1989, Wolfle et al 2011) as well as by a growing number of studies exploring properties of the cerebrovascular endothelium (Andresen et al 2006, Cipolla et al 2009, Dietrich et al 2009, Dietrich et al 1996, Duza & Sarelius 2003, Hannah et al 2011, Janigro et al 1997, Koller et al 1989, Marrelli et al 2003, You et al 1997). In the peripheral vasculature, the vascular endothelium

has been well documented to mediate conducted vasodilation through the spread of hyperpolarization, even under nitric oxide (NO) and prostacyclin inhibition (Andresen et al 2006, Wolfle et al 2011). The mechanism underlying this conducted vasodilation is thought to involve the tight electrical coupling between endothelial cells via calcium sensitive K+ channels of small and intermediate conductances and/or the release of an endothelium derived hyperpolarizating factor (EDHF), with signals being relayed to smooth muscle cells via MEGJs (Andresen et al 2006, Hannah et al 2011, Marrelli et al 2003). Such K+ channels were recently identified in the endothelium of isolated cerebral penetrating arterioles and their role in regulating resting cerebral blood flow has been demonstrated *in vivo* through the use of pharmacological channel blockers (Hannah et al 2011). The possibility that gap junctions between arterial endothelial cells are sufficiently tight that they can propagate long-range signals is consistent with observations made by McCaslin et al of endothelial uptake and gap junction-mediated spread of astrocyte-targeted SR101. This uptake and transmission of dye was not observed in the more disorganized venous endothelium (McCaslin et al 2011).

The idea of an integrative vascular signaling pathway that fine-tunes local perfusion via retrograde vasodilation from capillaries, superposed on more global modulations in blood flow from innervation of larger vessels is well established in skeletal muscle literature (Sarelius & Pohl 2010). The existence of a similar system in the cortex is therefore likely, with larger-scale, more global cerebral blood flow modulations being mediated by established innervation of major vessels from the superior cervical, sphenopalatine and trigeminal ganglia, or the locus coeruleus, raphe or nucleus basalis (Girouard & Iadecola 2006, Iadecola 2004).

5.5.1 Multi-phase framework of cerebral blood flow control

Our results indicate that the disruption of arteriolar endothelium does not significantly affect the later phase of the hemodynamic response, suggesting the existence of a second mechanism that is independent of the endothelium. A potential two-phase mechanism for neurovascular coupling, composed of an initial reflex-like hyperemia that is dependent on endothelial hyperpolarization, accompanied by a second phase driven by slower and more environmentally responsive cells such as astrocytes, could explain a range of prior findings (Cauli & Hamel 2010, Kennerley et al 2011, Martindale et al 2005a). For example, neurovascular coupling studies that have attempted to attenuate the hemodynamic response through pharmacology have almost uniformly failed to block it completely, suggesting the presence of multiple neurovascular pathways (Cauli & Hamel 2010, Girouard & Iadecola 2006, Takano et al 2005, Wang et al 2006).

Studies using linear 'hemodynamic response function' (HRF) analysis to predict blood flow changes from electrophysiological recordings during stimuli of longer durations often fail to account for the later parts of responses, and numerous other spatiotemporal non-linearities of neurovascular coupling have been reported (Martindale et al 2005a),(Berwick et al 2008, Birn et al 2001, Martindale et al 2005a). If the response to prolonged stimulation is a superposition of vascular responses that are actuated by two mechanisms, then the difference between the pre-LD response and the post-LD response can be interpreted as the response that is eliminated by LD treatment.

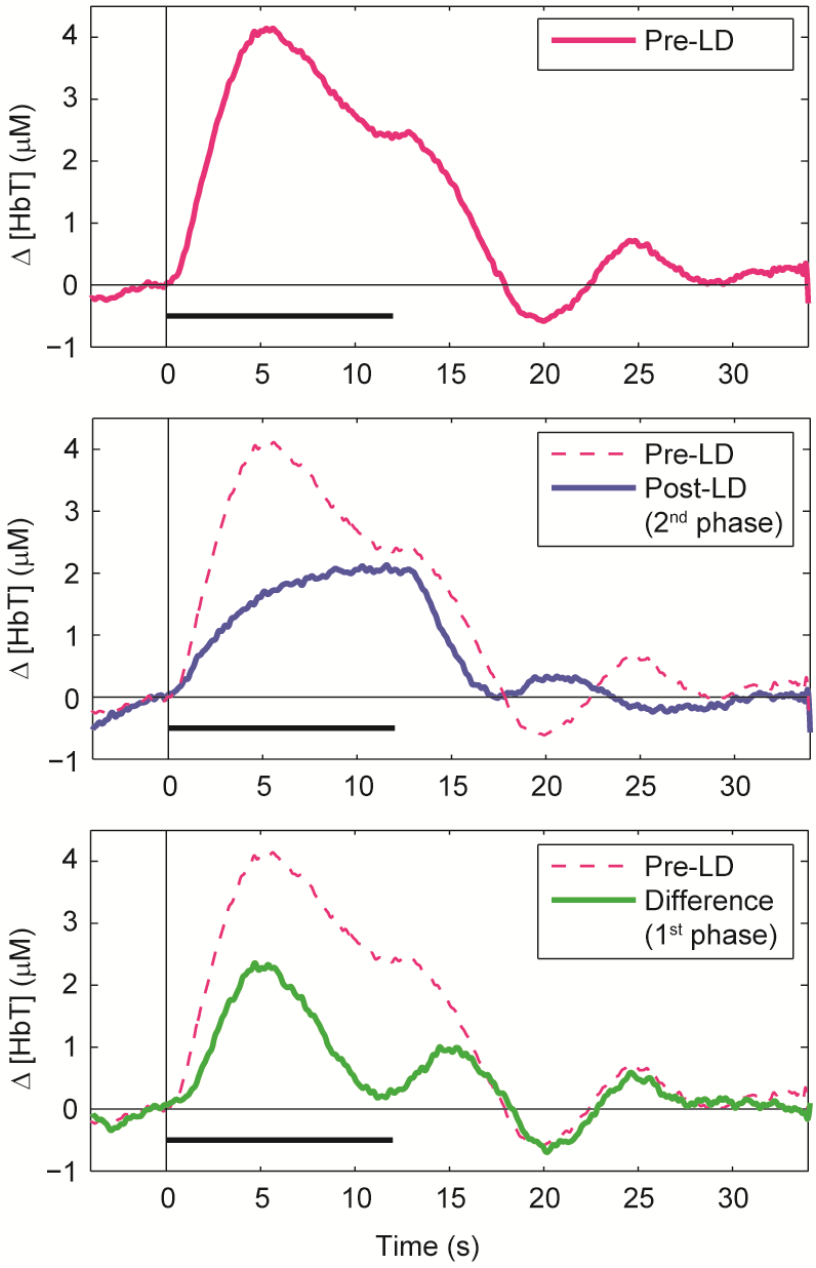

Figure 5.4 Decomposition of the hemodynamic response
Possible decomposition of the hemodynamic response The average 12 second pre and post-LD Δ[HbT] responses (from Figure 5.1e) are shown in pink (top) and blue (middle) respectively. The difference of the pre- and post-LD responses is shown in green (bottom). Conceptually, if LD treatment eliminates the "first phase" of the response, and the blue time-course represents an additional, additive slower response mechanism, then the green time-courses represent the fast, early, endothelium-dependent hemodynamic response. The green response resembles published 'hemodynamic response functions' (HRFs)(Kennerley et al 2011), as well as the response to short duration stimuli (Birn et al 2001, Cardoso et al 2012, Kennerley et al 2011, Yeşilyurt et al 2008).

We note that if we subtract the post-LD response from the pre-LD response to 12 second stimuli, to isolate the endothelial-related component of the response, we find a time-course that closely resembles the response to stimuli of short durations, and the HRF reported by others (Figure 5.4, (Birn et al 2001, Cardoso et al 2012, Kennerley et al 2011, Yeşilyurt et al 2008). A more complex, perhaps multi-component model where the fast endothelial-driven response represents the conventional HRF, but a second, slower component contributes significantly during prolonged activation could explain these prior findings. Further parametric studies are needed to determine how two different HRFs (fast and slow) might combine, since each could be driven by different neuronal or molecular input functions.

A potential multi-component model of neurovascular coupling also raises the question of which mechanisms might dominate during normal 'resting state' brain function, when the brain is not generating highly organized responses to discrete stimuli, but reacting to a wide range of different inputs and processes continually (Zhang & Raichle 2010). Further, certain stimulation and measurement paradigms might yield data that is preferentially weighted to either rapid initial and possibly neurogenic hyperemic responses, or to prolonged ones perhaps dependent on metabolic factors. Such a model may explain the widely varying, and sometimes paradoxical findings of studies that use stimuli of differing type, frequency, amplitude and duration.

5.5.2 Caveats

Our results strongly suggest a critical role of the endothelium as a signaling pathway involved in neurovascular coupling. However, we cannot rule out the possibility that other

cellular mechanisms, such as astrocytes or pericytes, also contribute to blood flow regulation. Compelling evidence has been presented that astrocytes and other cells such as pericytes and interneurons could play a role in neurovascular coupling (Cauli & Hamel 2010, Fernández-Klett et al 2010, Peppiatt et al 2006). Our finding, that the arterial endothelium is a critical component in generating early cortical hyperemia in response to stimulation does not preclude the involvement of some or all of these other cell types in governing different aspects of the response. For example, our findings do not elucidate the mechanism by which endothelial hyperpolarization might be initiated following peripheral somatosensory stimulation. We hypothesize that, upon thalamic input to the somatosensory cortex, local neurotransmitter release above some threshold generates a propagated vasodilatory response via the closest capillaries extending along the arteriolar tree to the pial arteries. However, it is also possible that additional cells could be required to generate second messengers in this signaling pathway (Abbott et al 2006, Andresen et al 2006, Armulik et al 2005, Attwell et al 2010, Cauli & Hamel 2010)[7].

Another caveat of our study results from the difficulties associated with performing LD treatment on an entire vascular bed *in vivo*. LD treatment is known to produce endothelial damage in small vessels faster than in larger vessels (Karlheinz S 1983, Miller et al 1992), and previous studies employing the LD technique have traditionally examined specific vessels of a certain caliber. Because we are studying a systems-level phenomenon and our results depend on the integrative vascular route between active neurons and the pial surface, we cannot simply choose specific arterioles to target in our study. Thus, it is possible that the extent of LD treatment used in these experiments may cause some smooth

[7] Further discussion of results can be found in Appendix D.

muscle damage for smaller caliber vessels in the illuminated field of view. However, the fact that our pharmacological controls do not completely abolish the endothelial-dependent vasodilation to ACh suggests that the level of LD treatment we are using is on the conservative side.

5.5.3 Conflicting studies

A recent study by Kennerley et al hypothesized that arterial dilation was a key component driving the early part of the somatosensory hemodynamic response (Kennerley et al 2011). The study reasoned that strong hypercapnia would maximally dilate arteries, reducing their ability to influence the hemodynamic response to stimulus. The attenuation of the hemodynamic response observed was remarkably similar to the Δ[HbT] changes that we observed in our study; eradication of the initial peak of the response, replaced by slowly increasing Δ[HbT], peaking at cessation of a 16 second stimulation. However, a number of additional consequences of hypercapnia were also observed that made results difficult to interpret. In particular, globally increased cerebral blood flow led to hyperoxic conditions, such that no stimulus-evoked changes in Δ[HbR] were observed (predicting that the condition would yield no BOLD response at all). Differences in the electrophysiological response of the brain during hypercapnia were also observed, yielding more of a box-car shape throughout stimulus rather than the more usual gradual decrease in current source density (CSD) peaks as stimulation continued. The study concluded that the modified electrophysiological response could just as easily have led to the observed changes in functional hemodynamics as the inability of the arteries to dilate. Our results counter this

argument, since electrophysiological responses were unaffected by LD-treatment. Furthermore, while our very local disruption of pial arteries did cause some pre-dilation, this was not sufficient to cause hyperoxia, as evidenced by the strong Δ[HbR] responses observed in our case (Figure SD. 5). In our controls, we demonstrated that pre-dilation equivalent to the levels seen with LD-treatment was not sufficient to reduce the involvement of pial arteries in the early phase of the functional response. Our high-speed, high-resolution imaging of the pial vasculature allowed direct visualization of arterial diameter changes, and it was these changes that were specifically eradicated by LD-treatment, and which resulted in a reduction in the initial peak of the hemodynamic Δ[HbT] response.

A study by Xu et al sought to demonstrate that astrocytes play a primary role in upstream signaling to and dilation of cortical arteries (Xu et al 2008). Gliotoxin, L-α-aminoadipic acid was found to eradicate *in vivo* pial arterial dilations in response to bicuculine suffusion and sciatic nerve stimulation, whereas LD-treatment failed to significantly attenuate the same dilations. However, a major difference to our study was the intensity and duration of the stimulation used. Bicuculine suffusion induced seizure-level neuronal firing and arterial dilations of over 30% of baseline diameters over the course of up to 20 minutes (compared to around 6% dilations in our study). The strong, direct sciatic nerve stimulation used by Xu et al lasted for 20 seconds, but induced massive arterial dilations exceeding 35% of baseline diameters, peaking around 40 seconds after stimulus onset. We conclude, therefore, that the arterial dilations induced by such strong and

extensive stimulation may be governed by a different mechanism than responses to the more physiological levels of stimulation presented here.

Further, their conclusions are based on data that do not have sufficient temporal resolution (~ 1 frame every 9-10 seconds) to detect fast changes in diameter, and is thus incapable of discerning differences in the early timing of pre and post treatment responses. In addition, they used the maximum diameter change as a summary measure of the entire hemodynamic response to long durations of sciatic nerve stimulation (20 seconds, 0.7mA, 2Hz, and 0.1 ms). At stimulation durations lasting this long, it is entirely possible that later portions of the pre and post-LD responses are capable of reaching the same maximal amplitude, independent of endothelial signaling pathways. Based on previous observations of the response evolution (Chen et al 2011), we know that the spatiotemporal dynamics of these hemodynamic changes have intricate features that cannot be simply summarized by a single measure. Their results do suggest that astrocytes may be involved in the later portion of the sustained blood flow response, which is consistent with our findings.

5.5.4 Conclusions and implications

The finding that endothelial cells are critically involved in mediating blood flow changes also has important implications for pharmacological studies of neurovascular coupling. Endothelial cells possess many of the same signaling pathways as astrocytes and neurons (COX1 and COX2 mediated generation of prostaglandins, EET production etc) (Abbott et al 2006). Due to the lack of specificity of pharmacological agents, it is possible that the same chemical agonists that are used to inhibit or activate astrocytes and neurons are also capable of influencing endothelial cells. Thus, studies that use pharmacological agents to

selectively block astrocyte and neuronal pathways may actually be confounded by the fact that endothelial signaling pathways may also be impaired, leading to incorrect interpretations of results. The endothelium is also the target of a large number of systemic drugs, including common analgesics and anti-inflammatories such as aspirin, which specifically block steps of prostaglandin production and may therefore be inadvertently affecting endothelial function in the cerebral vasculature (Flynn et al 1992, Lida et al 2010, Oyama et al 2011). The prominence of endothelial cells as an active contributor in the neurovascular unit needs to be recognized and future experiments should be designed accordingly.

In summary, our results clearly demonstrate that an intact endothelium is critical for generation of a full hemodynamic response to stimulus. This result provides a new roadmap for understanding neurovascular coupling as well as for interpreting functional imaging signals. Our findings also highlight the arterial endothelium as a possible component in brain pathologies in which neurovascular coupling is impaired, as well as a potential highly accessible target for the development of therapeutics. Finally, our results support the concept that distinct cellular mechanisms or signaling pathways underlie blood flow control in early and late phases of the hemodynamic response. Additional studies designed specifically to investigate mechanisms of blood flow control in the context of a 'multi-phase' framework are required to fully understand the complexity of neurovascular coupling.

Chapter 6

Resolving the hemodynamic response elicited by optogenetic stimulation

6.1 Introduction

Optogenetics is the method of genetically modifying specific neuronal sub-types such that they express a light-sensitive ion channel (Cardin et al 2010). Recent optogenetic studies have used light exposure as a means of direct cortical stimulation to study the neural networks and brain circuitry involved in behavioral studies. These optogenetic techniques have become increasingly common in the past three years and have been applied in neuroscience through the combined use of light stimulation, behavioral monitoring, electrophysiology, and fMRI (Deisseroth 2011, Lee et al 2010). In the field of neurovascular coupling, this technique offers a useful tool for studying the mechanisms underlying

stimulus-evoked changes in blood flow, as it offers the ability to selectively initiate or inhibit neuronal activity. Rapid development of new viral constructs that are specifically expressed in glial cells or other cortical cell types will further enhance our ability to investigate the targeted interactions between cells and vasculature *in vivo*.

The goal of this research is to understand how different stages of neural processing contribute to elicitation of the hemodynamic response. Specifically, this chapter is motivated by the hypothesis that direct innervation of the vasculature from the thalamus, rather than post-synaptic processing, plays a role in the first hemodynamic phase. Optogenetic techniques are well suited to study this question since a variety of viral constructs can be used to stimulate specific neurons or astrocytes, and the subsequent blood flow response can be recorded using wide-field OISI. The work described in this chapter establishes a protocol for performing viral injections and optogenetic stimulation and demonstrates our ability to collect data using this methodology and setup.

In these experiments, we use cortical injections of channelrhodopsin-2 (ChR2) to target excitatory pyramidal neurons in the cortex, causing action potential firing under illumination with 470 nm blue light. This method of cortical stimulation bypasses thalamo-cortical pathways without the use of invasive stimulating electrodes that may cause cortical damage and non-physiological levels of non-specific stimulation. Direct cortical stimulation allows us to isolate a piece of the entire somatosensory signal transduction pathway. We combine the use of optogenetic techniques with high speed, high resolution wide field camera imaging to visualize the response elicited by direct cortical stimulation.

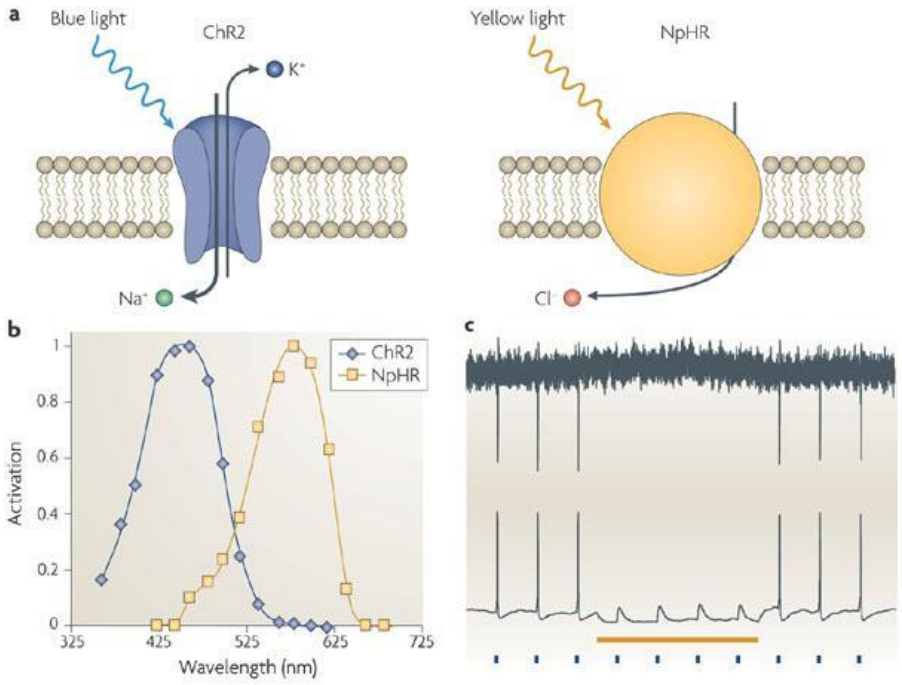

Figure 6.1 Optogenetics invovle light activatable ion channels
(a) Channelrhodpsins are sodium channels that are activated by blue light. Halorhodopsins are light-driven ion pumps that are specific for chloride ions. (b) The excitation spectra of channelrhodopsin and halorodopsin. (c) In a neuron, activating a sodium channel will result in cell depolarization and generation of an action potential. Activation of halorhodopsins results in an influx of chloride ions and cellular hyperpolarization which inhibits the generation of action potentials.

By conducting a detailed comparison between the blood flow responses to stimulation via natural somatosensory pathways and direct cortical activation, we can examine the contributions of distinct processing stages to phases of the hemodynamic response.

A recent study by Scott and Murphy 2012 is the only prior study that has documented OISI of the hemdoynamic response following optogenetic stimulation of excitatory neurons in mice (Scott and Murphy 2012). However, a major limitation of the study was their inability to record the blood flow response during delivery of the blue light stimulus, due to oversaturated light contamination from their stimulus laser (40 – 200 mW/mm^2). This makes it impossible to observe differences in the spatiotemporal patterns of the response

onset during optogenetic stimulation, as compared to normal somatosensory stimulation. We are able to overcome this issue in our setup by minimizing light saturation using a 500 nm long pass emission filter and low exposure times (5ms). Post-processing is then performed to remove any residual signal artifacts caused by the blue light stimulus.

This chapter describes the injections protocol that was established for use in optogenetic stimulation experiments. Preliminary data of the hemodynamic response elicited by optogenetic stimulation is presented and future directions are discussed.

6.2 Methods

6.2.1 Virus injection protocol and animal preparation

Genetic modification of ion channels can be accomplished either through the use of transgenic mouse lines or through the use of viral delivery technology (Arenkiel et al 2007, Cardin et al 2010). We employ the latter, where ChR2 is fused with a fluorescent protein and incorporated into a lentiviral vector (Zhang et al 2006). Lentiviruses are capable of delivering genetic information into the DNA of a host cell and replicating in non-dividing cells, making them an efficient gene delivery vector. Concentrated virus is injected directly into the brain tissue and allowed to spread. An advantage of using viral delivery techniques over transgenic models is that stable gene expression occurs in adult animals within weeks after viral infection. We adopted this method because it can be readily performed in adult rats, allowing us to maintain consistency across our animal models.

To prepare animals for optogenetic stimulation, direct cortical injections of the desired virus is performed at least 3 weeks prior to imaging. The virus that is used in the following

experiments is the AAV-CaMKII ChR2-YFP construct, which causes expression of light-sensitive excitatory sodium ion channels in neurons (University of North Carolina at Chapel Hill Vector core facility). Since the injection procedure is a survival surgery, additional care is taken to ensure that all instruments, tools, and operational surfaces are sterilized prior to use (Figure 6.2).

The cortical injection protocol described here is adapted from (Cardin et al 2010). All injection procedures are conducted with sterilized instruments while wearing sterile gloves in an approved biosafety cabinet within the animal facility. Surgeons wear masks, head covers, clean lab coats, and sterile gloves throughout the procedures. Aliquots of virus are stored in -80C freezer and transported on ice just prior to use.

Female Sprague Dawley rats (250-350 grams, Charles River Labs) are anesthetized with ketamine-xylazine (75-90 mg/kg ketamine, 5-10 mg/kg xylazine) and fixed in a stereotaxic frame with non-rupture ear bars (Kopf Instruments). Once animals are anesthetized, their eyes are lubricated with an application of eye lube or an ophthalmic ointment. Aseptic surgical procedures include: Clipping of hair at the surgical site. Disinfecting the surgical site by swabbing with chlorhexidine or Betadine alternated three times with 70% alcohol followed by a final application of disinfectant solution. Body temperature is maintained at 37°C throughout the procedure with homeothermic heating pad and rectal probe. Prior to procedure, rats are given an injection of Buprenorphine (0.05 mg/kg) as an analgesic. The incision site above the somatosensory cortex is shaved/clipped, cleaned, and subcutaneously injected with 2% lidocaine. Surgical level of anesthesia is ensured by testing animal reflexes via toe pinch throughout the procedure. A single incision is be made using a fresh scalpel blade, and connective tissues pushed back to expose skull. Sites for virus injection are

marked and burr-holes are made using a surgical micro-drill (Fine Science Tools), taking care to stop the drill just before bottom of the skull such that a thin layer of skull remains. A syringe needle is used to carefully remove any remaining skull so the dura can be seen. Overheating and accumulation of bone dust is avoided by flushing the injection site with artificial cerebral spinal fluid (ACSF) during drilling.

A 34 or 35 gauge Hamilton syringe, cleaned with ethanol and phosphate buffered saline (PBS), is then filled with enough virus for approximately 1-2μL per injection site. For initial experiments, three cortical injections of ChR2 virus were made in the left hemisphere at the following coordinates relative to the bregma-midline intersection (ML – medial/lateral, DV – dorsal/ventral, AP – anterior/posterior): 1) 2 μL at -1 mm ML, 3 mm DV, 1.5 mm AP, 2) 2 μL at 1mm ML, 3mm DV, 1.5 mm AP and 3) 2μL at -1mm ML, 3mm DV, 1.5 AP. In subsequent experiments, only a single injection site was made in the hindpaw region of the somatosensory cortex: -2mm ML, 2.5 mm DV, 1.5 mm AP.

The syringe tip is carefully positioned above the injection hole and then lowered to a desired depth in the brain tissue using sterotaxic manipulators (Kopf Instruments), measuring from the surface of the skull being z = 0. The desired volume of virus is injected using a sterotaxic injector system (Stoelting QSI) at a rate of 0.1 uL/min. Following injection, the syringe is left in place for an additional 10 minutes before retraction in two stages, allowing another 5 minutes rest time at the halfway point. Any remaining virus in the syringe is dispensed into a container of bleach prior to disposal. Syringes are then cleaned with bleach and ethanol for storage. When all injections are completed, edges of the skin are be pulled together and sutured closed with 5-0 nylon suture. The sutures are removed 10 – 14 days later.

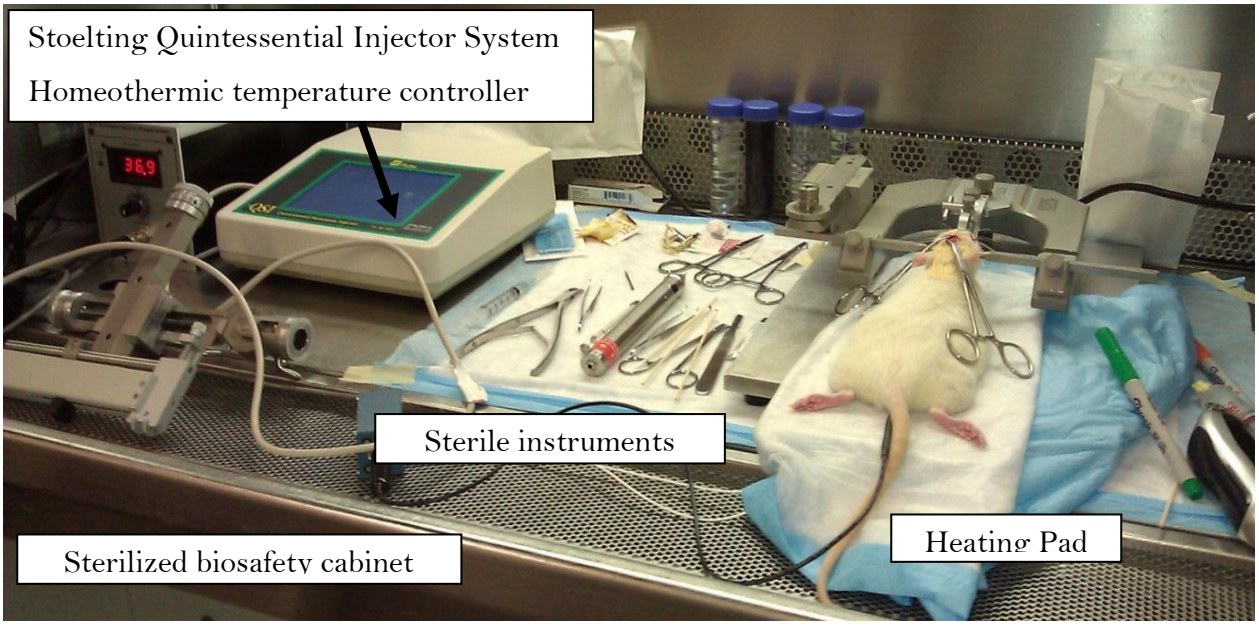

Figure 6.2 Optogenetic virus injection setup
All injection procedures are performed in a clean biosafety cabinet, with sterilized instruments and gloves. Body temperature is maintained using a homeothermic heating pad coupled to a rectal probe. Heart rate is monitored using an external pulse oximeter that can be clipped on the hindpaw.

The animal is allowed to recover from anesthetic and treated with Buprenorphine (0.05 mg/kg) every 8-12 hours for 48 hours following injection. Animals are placed in a clean "recovery cage" on nonparticulate sheet-like material (i.e. sterile gauze, surgical drape) where they are observed until they regain the righting reflex. Animals are then returned to a clean home cage and monitored daily for signs of pain, distress, or infection at the incision site. Signs of poor recovery are indicated by hunched posture, reduced activity, abnormal gait, labored, slow or rapid respiration, poor hydration (sunken eyes or reduced skin elasticity), poor coat condition, reduced eating or drinking, reduced or excessive grooming and weight loss. Any animal exhibiting these symptoms are sacrificed using CO_2 to avoid unnecessary suffering and veterinary staff will be consulted where necessary. At least 3

weeks of incubation is required for effective expression levels of ChR2 in excitatory neurons in the somatosensory cortex (Cardin et al 2010). Beyond potential complications related to the injection procedure, there is no documented effect of ChR2 on the brain that would be expected to cause the animal pain or distress

6.2.2 Imaging protocol and stimulus parameters

When animals are ready for use, the same surgical and experimental protocol as detailed in Chapter 2 is followed. The only change in the experiment is in the stimulation paradigm. A bilateral exposure of the somatosensory cortex is performed so that the right hemisphere (no virus injections) can be used to obtain control hemodynamic responses. Light stimulation is delivered by a 473 nm blue LED (Thorlabs) coupled to an optical fiber with 400um inner core diameter, positioned approximately 1 mm away from the cortical surface. The light stimulation spot is ~500 um in diameter on the cortical surface and is focused on the known injection sites. Light stimulation of ~3mW/mm^2 is strobed for 2-20 seconds at 3-20Hz with a 0.5-20ms pulse width (Cardin et al 2010, Lee et al 2010, Scott & Murphy 2012). The light intensity of the focused blue LED light is well below intensity levels shown to cause tissue damage (>100mW/mm^2)(Cardin et al 2010). Electrical forepaw or hindpaw stimulation is also used in the same rat so that hemodynamic responses to direct optical and electrical somatosensory stimulation can be compared.

Hemodynamic data is obtained using only 630nm red and 530nm green LEDs to prevent imaging light from stimulating the ChR2. A 500nm long pass emission filter is placed in front of the camera to limit the amount of blue stimulation light captured in each image.

This optical setup allows us to image the hemodynamic response throughout the duration of the stimulation, which has previously not been possible (Scott and Murphy 2012). All imaging is done with a 75 fps frame rate, 5ms exposure, and 6 second pre-stim period. Two-photon microscopy of the exposed cortex is conducted following camera imaging to survey the spatial extent of YFP tagged ChR2 expression. In some experiments, both hemispheres are imaged to ensure that the right hemisphere (not injected) can serve as a control. After euthanasia, the rat's brain is removed and stored in 4% paraformaldehyde for further histological examination.

6.3 Results

6.3.1 Methodological results

Optogenetic stimulation evoked hemodynamic responses were obtained in 4 out of 6 rats that were successfully injected with the channelrhodopsin virus. The goal of these studies was to determine the appropriate injection parameters necessary in order to achieve a sufficient level of viral expression that would elicit a hemodynamic response during blue light stimulation. These parameters included: needle gauge, number of injection sites, depth of injection, volume of virus per injection site, and stimulus parameters during imaging. The following section discusses some of these parameters:

Needle gauge We found that the injections performed with a 33 gauge needle and 10 μL gas-tight Hamilton syringe produced the most successful results. Larger needles (32 gauge) caused more significant damage to the dura during injections procedure, which made it

more difficult to remove without excessive bleeding during the craniotomy several weeks later. The smaller needle sizes (34-35 gauge) became easily blocked and were difficult to clean. Special care was needed to ensure that air bubbles did not get drawn up into the Hamilton syringes through the small gauge needles. Although tissue damage was minimized when using the small gauge needles, continuous virus delivery was unreliable due to frequent blockages. The 33 gauge needles did not cause significant damage to the dura or underlying brain tissue and could consistently deliver desired injection volume without becoming blocked.

Injection sites We found that the most robust hemodynamic responses were obtained when positioning the light directly above the injection sites. Multiple injection sites were made in the first 5 rats in order to maximize viral expression. However, the use of multiple injection sites also made data analysis difficult due to the uncertain level of virus expression contributed from each injection site. This is exacerbated by the scattering of the blue light spot through the cranial window, which causes a diffuse region of blue light to reach brain tissue surrounding the focused stimulus spot. Future studies should position injection sites further apart or use only a single injection site to avoid uncertainty over the location of the active region. A range of injection depths up to 2.5 mm seemed to result in adequate levels of virus expression necessary to elicit a hemodynamic response. The two rats that did not respond to blue light stimulation had virus injections at 3 mm below the surface of the skull. We hypothesize that injections at depths greater than 2.8 mm do not produce adequate levels of expression. We injected 1-2 μL of virus per injection site. This injection

volume appeared to be more than sufficient. Additional studies are needed to determine the minimum injection volume necessary to achieve sufficient virus expression.

Stimulus parameters Hemodynamic responses were elicited when the blue light stimulus was pulsed at 20 Hz with a 15-20 ms pulse width. These stimulus parameters were used for all 5 experiments. In three of the four responding rats (OR6, OR7, OR8 see Table 6.1), this stimulus appeared to elicit a hemodynamic response with a much larger amplitude than the sensory-evoked hemodynamic response. This suggests that these stimulus parameters can be adjusted to a lower frequency or shorter pulse width, while still eliciting a hemodynamic response.

Table 6.1 Summary of preliminary optogenetic experiments

Rat ID	Injection sites (#)	Depth (mm)	Volume (µL/site)	Craniotomy	Notes
R159_OR1	2	1) 2.5 2) 3.0	1) 1 2) 1	Unilateral	No responses: injection site was too deep
R188_OR2	3	1) 2.5 2) 2.5 3) 2.5	1) 1 2) 1 3) 1.5	Bilateral	Robust responses: bilateral field of view made it difficult to quantify vessel dynamics
R194_OR5	3	1) 3 2) 3 3) 3.2	1) 1.5 2) 2 3) 2	Unilateral	No responses: injection site was too deep
R197_OR6	3	1) 2.5 2) 3 3) 2/3	1) 2 2) 0.5 3) 1/1	Unilateral	Robust responses: many responses did not fully return to baseline
R201_OR8	2	1) 1.75/2.5 2) 2/2.5	1) 1/1.5 2) 1.3/1.5	Unilateral	Robust responses: several injections sites close together resulted in hemodynamic responses that were not localized
R207_OR7	2	1) 1.75/2.5 2) 2/2.5	1) 1.2/1.5 2) 1.1/1.5	Unilateral	Robust responses: optogenetic responses were much larger than hemodynamic responses elicited by somatosensory stimulation

6.3.2 Hemodynamic response elicited by optogenetic stimulation

We found that the hemodynamic responses elicited by direct cortical optogenetic stimulation exhibited similar properties as the sensory-evoked hemodynamic response. In particular, the hemodynamic response to 12 seconds of blue light stimulation demonstrated the same 'peak' and 'plateau' response as previously observed using 12 seconds of hindpaw stimulation (Figure 4.3), with the later 'plateau' response being more spatially localized than the early 'peak' response. Figure 6.3c shows $\Delta[\mathrm{HbT}]$ timecourses as function of distance from the center of the blue light spot (blue-pink boxes in Figure 6.3a-b). Maps in Figure 6.3d show the $\Delta[\mathrm{HbT}]$ signal averaged between 2 to 4 seconds and 8 – 10 seconds after the stimulus onset for blue light stimulation and hindpaw stimulation. The location of the injection site and the blue light spot are positioned on the posterior side of the cranial window, while the hindpaw region is located on the anterior side. Compared to the sensory-evoked response, the blue light elicited a blood flow response with greater amplitude and larger spatial spread. This suggests that the blue light stimulation elicited neural activity that exceeded physiological levels of neuronal activity, making it difficult to conduct further comparisons of response timing and amplitudes. The lack of simultaneous electrophysiological recordings of neural activity also makes it difficult to quantify how the two methods of stimulation differ.

In general, the blue light stimulation appeared to elicit more consistent spatiotemporal patterns throughout the course of the experiment. This is probably due to the fact that direct cortical stimulation bypasses signaling pathways that may otherwise affect animal physiology or systemic blood pressure during electrical sensory stimulation.

Varying the duration of blue light stimulation also produced patterns of Δ[HbT] responses that were similar to sensory-evoked responses (Figure 6.4, Figure 4.6). Figure 6.4c shows Δ[HbT] responses to 0.75, 2, 4, 8, and 12 seconds of stimulation, with corresponding Δ[HbT] in Figure 6.4d. However, the data from this particular rat revealed that our protocol was imprecisely locating the region of neural activity, which is another consideration that needs to be addressed before extensive data analysis on the response patterns can be performed.

During sensory stimulation, a specific brain region corresponding to the hindpaw exhibits elevated neural activity. However, the localization of the neural activity elicited by blue light stimulation depends on two different parameters: 1) the size and coherence of the blue light spot and 2) the location and spatial spread of ChR2 expression. The data presented in Figure 6.4 displays what can happen if there is a slight mismatch in the location of the virus injection and the location of the blue light spot. In this case, the responses elicited during long stimulus durations reveal a distinct parenchyma response that is anterior to the location of the blue light spot. It is thus difficult to study the spatiotemporal evolution of the response when the neural activity is not localized and the spatial distribution of neural activity is unknown. In the future, stereotaxic coordinates of the injection site should be used to position the blue light spot.

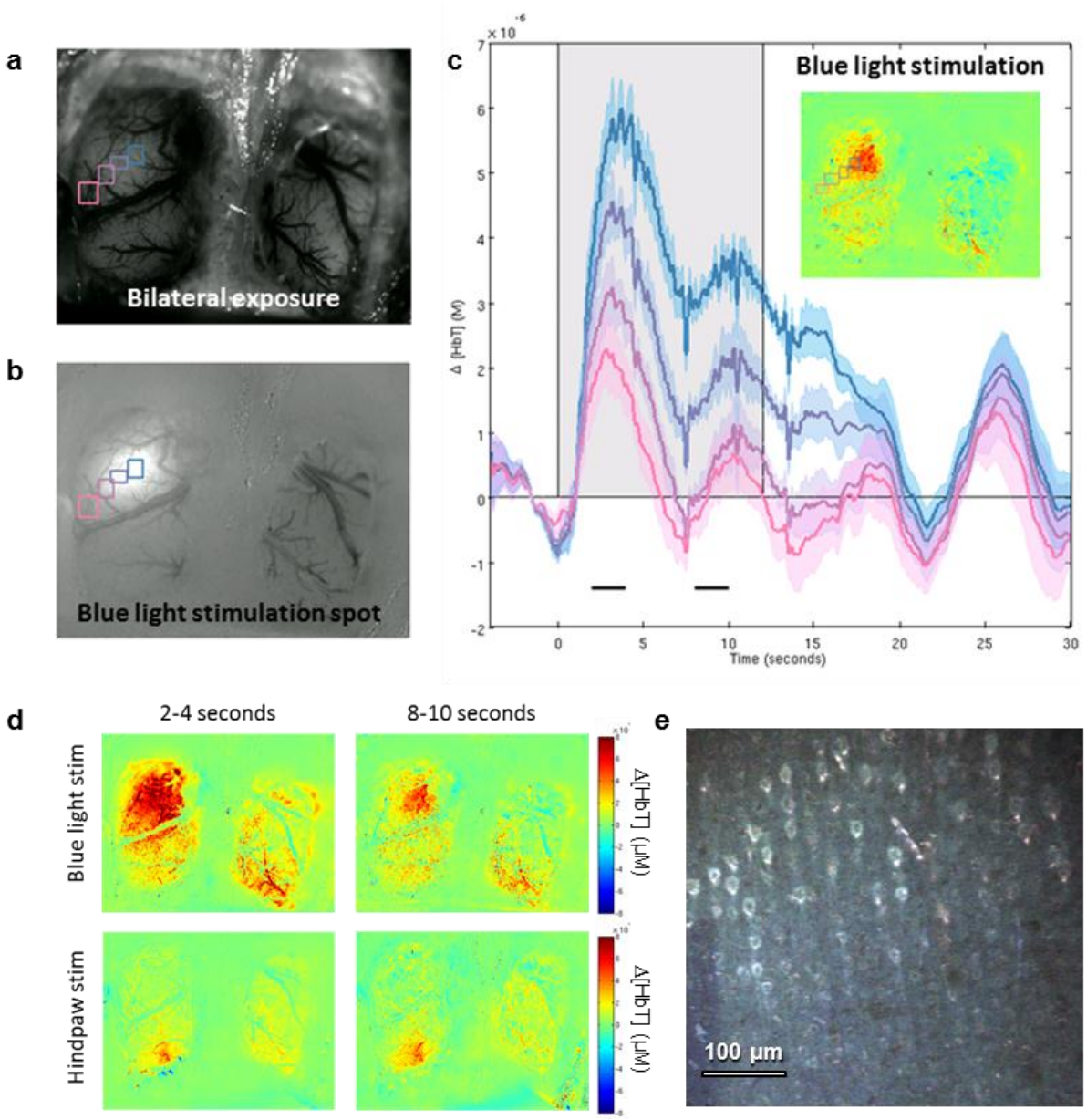

Figure 6.3 Hemodynamic response to optogenetic stimulation
(a) Bilateral craniotomy showing the hemodynamic response elicited during direct cortical optogenetic stimulation (20Hz, 20ms). (b) Location of blue light spot. (c) Δ[HbT] responses to 12 seconds of blue light stimulation is shown for selected regions near the center and peripheral regions of the blue light spot. The map (inset) shows that spatial distribution of Δ[HbT] averaged between 2 and 4 seconds after stimulus onset. (d) Maps showing the early (2-4 seconds) and late (8-10 seconds) Δ[HbT] responses for blue light stimulation and electrical hindpaw stimulation. The location of the virus injection was positioned posterior to the hindpaw region. (e) YFP positive labeled cells that express ChR2.

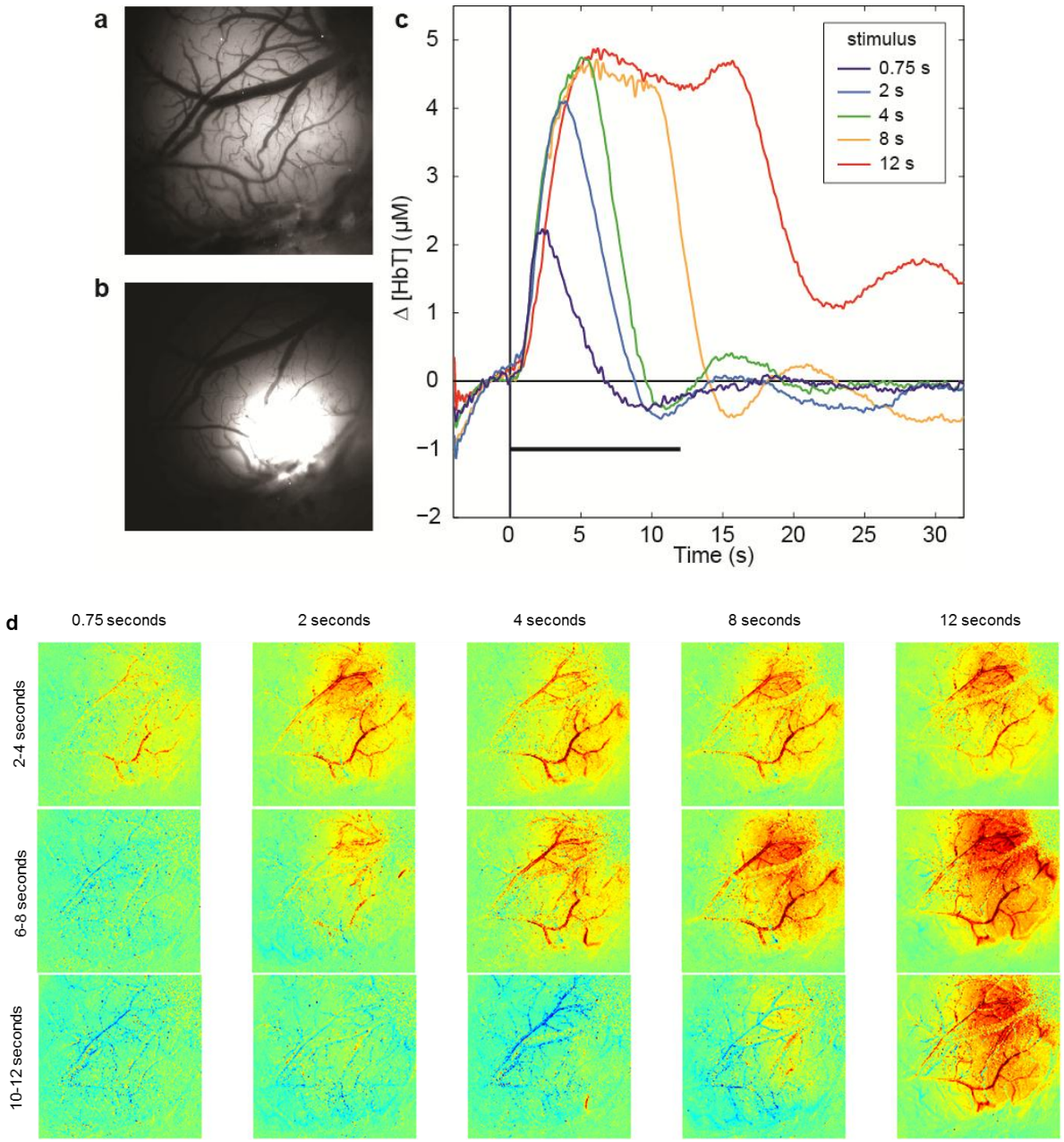

Figure 6.4 Varying durations of optogenetic stimulation
(a) Exposed somatosensory cortex. The location of virus injection is not obvious due to minimal damage from the injection needle. (b) Positioning of the stimulating blue light spot (~1mm in diameter). (c) Time courses showing averaged Δ[HbT] responses for a range of stimulus durations. (d) Functional maps showing the early, middle, and late portions of the hemodynamic responses to varying stimulus durations. A strong Δ[HbT] response is seen in the anterior (top) region of the exposed window, despite the fact that the blue light stimulus is focused on a different arteriole. This mismatch in the responding region and the stimulating light spot produces a hemodynamic response with a larger spatial extent than the sensory-evoked response.

6.4 Discussion & future directions

We have successfully developed and implemented a protocol for integrating optogenetic techniques into our imaging methods, allowing us to use it to study neurovascular coupling *in vivo*. Our optogenetics model is capable of eliciting hemodynamic response via blue light stimulation in adult rats that have been previously injected with a ChR2 viral construct. The incorporation of a more complex assembly of optogenetic techniques, such as halorhodopsin for chloride ions and cell-specific transgenic mouse strains, can significantly improve our ability to selectively excite and inhibit targets of interest.

We report here that direct cortical stimulation via blue light optogenetic stimulation elicits a hemodynamic response that is similar to the response triggered by stimulation of natural somatosensory pathways. These optogenetic responses appear to be more robust and consistent than sensory-evoked responses, perhaps because direct cortical stimulation bypasses several stages of processing through the peripheral and central nervous systems. This is also consistent with the finding that direct cortical stimulation can evoke hemodynamic responses near the end of an experiment, despite degradation of the animal's physiology. It appears that the hemodynamic response is largely associated with post-synaptic processing rather than with presynaptic cortical inputs (Radhakrishnan et al 2011).

Nevertheless, further optimization of injection and stimulus parameters is required before this technique can be used to draw decisive conclusions about neurovascular coupling. Simultaneous electrophysiology recordings collected during stimulation should ensure that the level of neural activity elicited during blue light stimulation is analogous to

physiological levels of neural activity. The use of a single virus injection site, as opposed to several, may minimize confusion over the level of viral expression in a particular area of the cortex. A smaller blue light spot may also be used to increase the specificity of the neural stimulation.

Once these experimental parameters are better understood, the combination of OISI and optogenetic stimulation can provide a very useful technique in the study of neurovascular coupling. In particular, optogenetic stimulation offers a method of direct cortical stimulation that bypasses complications associated with changes in systemic blood pressure changes that occasionally occur during normal somatosensory stimulation. Therefore, the hemodynamic responses elicited by optogenetic stimulation can provide a perspective on neurovascular coupling that is not contaminated by signal artifacts induced by the electrical stimulation. A detailed comparison of all aspects (response timing, spatial evolution, degree of recruitment of vascular compartments) of the responses elicited by blue light stimulation and sensory stimulation can also provide insight into the cellular mechanisms that control blood flow changes.

The variability of the hemodynamic response throughout the experiment can also be used to study properties of its underlying cellular mechanisms. We have previously reported that the 'plateau' response appears to exhibit more variability than the 'peak' response (Chapter 4). In some cases, the amplitude of the 'plateau' response can be equivalent or greater than the amplitude of the 'peak' response. Our preliminary findings of the hemodynamic response to optogenetic stimulation suggests an overall decrease in variability of both 'peak' and 'plateau' portions of the response. A systematic analysis of the response variabilities throughout the experiment may provide additional information about

the qualifying conditions motivating the early and late responses. Alternatively, it may be interesting to use variations in blue light stimulus parameters (intensity, duration or variable parameters throughout a stimulus train) to try to elicit different proportions of 'peak' and plateau' responses.

Chapter 7
Conclusions & implications

7.1 A multi-phase framework of neurovascular coupling

The results presented in this dissertation are consistent with the hypothesis that multiple distinct mechanisms of blood flow control act together to orchestrate the hemodynamic response. Our findings implicate at least two different mechanisms distinguishable by their different spatial and temporal "fingerprints". For exposition, we term these two responses the 'phases' of the hemodynamic response. Integrated with current knowledge of blood flow control, our empirical results provide the basis for a theoretical framework describing how multiple cellular mechanisms act in concert to produce the observed hemodynamic changes. This idea represents a shift in our conceptual understanding of blood flow control during neurovascular coupling and necessitates an analogous shift in experimental paradigms in future studies. This framework is capable of organizing and integrating findings into a

systems-level theory of neurovascular coupling which can direct the design of future experiments.

The key features of the hemodynamic response that serve as evidence for a multi-phase model of neurovascular coupling are:

1) The initial response to stimulation onsets within 200-400 ms and appears to propagate quickly up diving arterioles and along surface pial arterioles (Chapter 2 & 3).
2) Changing stimulus from forepaw to hindpaw in the same rat can recruit the same arterioles during the hemodynamic response but with different directions of propagated vasodilation, irrespective of the direction of blood flow (Chapter 3).
3) Upon increasing stimulus duration to longer than 8 seconds, a second spatiotemporally distinct 'phase' arises. The first phase is characterized by a strong pial arteriole response that extends along the arteriolar tree while the second phase exhibits a spatially localized response in the parenchyma (Chapter 4).
4) The first phase of the response is more consistent, while the later phase of the response exhibits greater variability across trials (Chapter 4).
5) A non-zero hemodynamic response is observed following very short stimulus durations and lasts much longer than the stimulus itself, suggesting that this initial response is not driven by feedback from energetic demands (Chapter 4).
6) Astrocytic calcium responses to prolonged sensory stimulation are inconsistent and exhibit slow onset times relative to the start of stimulus (Chapter 4).

7) Selective disruption of the vascular endothelium of pial arterioles significantly attenuates the blood flow response and essentially eliminates the associated pial arteriolar dilation (Chapter 5).

We have integrated these findings into general statements that form the basis for a multi-phase framework of hemodynamic control that are illustrated in Figure 4.9:

1) The first phase is a "reflexive" blood flow response that occurs regardless of how long the stimulation lasts. This phase requires a signaling mechanism that travels along the vasculature between the capillary bed and the pial arterioles at the cortical surface. Endothelial signaling appears to play a critical role in mediating this first phase.
2) The second phase is not reflexive, and is instead possibly sensitive to neuronal and metabolic conditions of local tissue. It is possible that astrocyte signaling contributes to blood flow control during this phase.
3) Finally, a third mechanism may be responsible for returning the brain tissue to its baseline oxygenation state.

The construction of a solid theoretical framework represents a critical step in bridging knowledge between micro- and macroscopic levels of investigation and in facilitating the translation of basis science observations in healthy rodent models to diseased states and ultimately to human studies (Cauli & Hamel 2010, Lindauer et al 2010, Koch et al 2010). To develop this model further, more experimental evidence is required to define the characteristics of each hemodynamic phase and to identify their associated mechanisms.

Future experiments must be designed specifically to address the open questions associated with a multi-phase framework of neurovascular coupling and results should be interpreted in this context.

7.2 Implications for fMRI

Understanding how the blood flow response to stimulation is controlled at a systems-level can have important consequences for fMRI study designs and interpretations. In particular, fMRI studies rely on models of the relationship between neural activity and blood flow changes to analyze and interpret their data (Lindquist et al 2009). However, there are known limitations in the current models that make interpretation of fMRI results very difficult (Logothetis 2008). Thus, a definitive model for blood flow control could enable the development of biophysical models that can be used to more accurately predict the physiologic nature underlying the BOLD signal (Lindquist et al 2009).

Linear convolution models are commonly used for fMRI data analysis. These models relate experimentally evoked neuronal activity to observed blood oxygen level dependent (BOLD) signals (Stephan et al 2004). This approach depends on knowing the hemodynamic response to a single neural event, known as the hemodynamic response function (HRF). A linear convolution model assumes that successive neural events will produce a hemodynamic response that consists of a linear summation of temporally shifted HRFs (Figure 7.1).

Although the linear convolution model has been shown to be accurate for brief stimuli (Martindale et al 2003), there is evidence for a non-linear relationship between the amplitude of the blood flow response and stimulus duration and amplitude (Ances et al

2000b, Martindale et al 2005b, Martindale et al 2003, Vazquez & Noll 1998, Yeşilyurt et al 2008). Specifically, the linear convolution model cannot predict the 'peak' and 'plateau' response pattern observed during long stimulus durations. As a result, several non-linear convolution models have been formulated in an effort to reproduce the hemodynamic response that is observed during longer stimulus periods (Ances et al 2000b, Gössl et al 2001, Martindale et al 2005b). However, while the mathematical non-linearities introduced in these models may successfully predict the observed hemodynamic response, they have no physiological basis. For example, the second order non-linear model that was used by Martindale et al. was able to produce a good prediction of the hemodynamic response through the addition of a weighting function that took the form of an exponential decay over time. The weighting function was arbitrarily chosen for its mathematical simplicity and was only applied in the case of long stimulus durations, making the model difficult to interpret in the context of physiological mechanisms. Other non-linear models produced a more accurate reconstruction of the hemodynamic response by increasing the order of the terms used in the decomposition (Ances et al 2000b). Thus, building a mathematical model that accurately describes the physiological processes that occur during the hemodynamic response depends on knowing how these processes depart from the simple linear convolution model (Gössl et al 2001).

The multi-phase framework for blood flow control described in this dissertation can be used to prescribe appropriate adjustments to the general linear model that are both mathematically accurate and motivated by actual physiological processes. For example, one could interpret the multi-phase framework as implying that different HRFs should be used in the convolution at different times throughout the stimulus train.

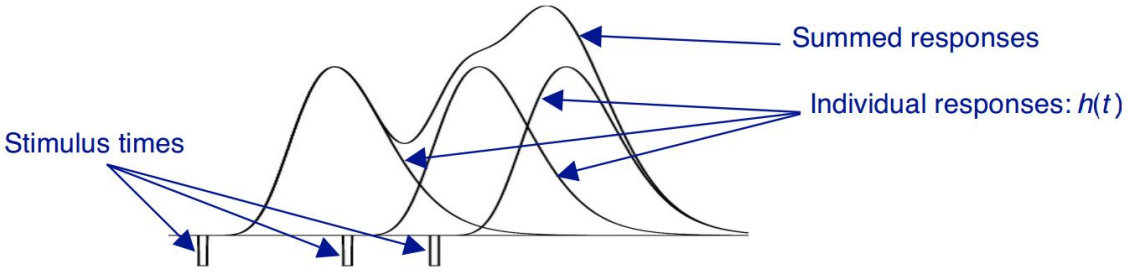

Figure 7.1 Linear convolution model
The predicted hemodynamic response from a linear convolution model is obtained by convolving the hemodynamic response function h(t) with the experimental stimulus train, or experimentally obtained neural activity. The result is shown here as the summed response.

The HRF associated with a second mechanism of blood flow could theoretically be constructed or estimated by comparing the hemodynamic responses to long and short stimulus durations. The relative contributions of each HRF may be described as a function of time in the model, requiring the addition the addition of a temporal threshold (or transition period) defining the time at which the second HRF is recruited. This effect could also be introduced through the use of a weighting function, the parameters of which are based on experimentally obtained time constants (e.g. for describing diffusion, or neurotransmitter accumulation). Alternatively, the second HRF can be convolved with a different stimulus function corresponding to a physiological process (such as glutamate accumulation)[8].

The estimation of the HRF itself has conventionally been done through de-convolution of a hemodynamic response to obtain its 'impulse function'. However, the high spatiotemporal resolution of the imaging systems described in this dissertation makes it

[8] This would result in a slower summation of the second HRF that could feasibly reproduce the later 'plateau' phase of a response to prolonged stimulation.

possible to experimentally obtain a HRF to a single neural event, without the use of mathematical modeling.

Finally, the spatial patterns of the observed blood flow response place new information constraints on hemodynamic response modeling. Moreover, our experimentally determined spatial structure and spatial decay constants can also be incorporated to extend the predictive model to two-dimensions.

In general, the findings presented in this dissertation further our understanding of the relationship between neural activity and the resulting changes in cerebral blood flow. In order for neurovascular research to influence fMRI usability, data analysis methods and HRF models should also be updated and investigated to reflect the physiology underlying neurovascular coupling.

7.3 Implications for neurodegenerative diseases and pathology

Our ability to understand and treat neurodegenerative diseases, such as stroke, Alzheimer's disease (AD), and dementia, is limited by our incomplete knowledge of the cellular mechanisms and signaling pathways that are involved in coupling neural activity to changes in blood flow. These conditions involve the deterioration of brain tissues in response to insufficient delivery of oxygen and nutrients, which arises from compromised neurovascular coupling. Knowing which cellular pathways are involved in this coupling is necessary for the identification of therapeutic targets and the development of pharmacological therapies which might improve blood flow coupling and slow or prevent these diseases.

The work presented in Chapter 5 identifies the vascular endothelium as playing a critical role in mediating the initial oversupply of blood to the active region. This finding can have significant consequences for the study of neuropathology, since the vascular endothelium is already associated with a number of systemic vascular disorders including atherosclerosis, AD, multiple sclerosis (MS), human immunodeficiency virus (HIV) associated neurocognitive disorder, and traumatic brain injury (TBI) (Grammas 2011). The underlying causes of many of these conditions remain an active field of medical research, though growing evidence supports a key role for the brain endothelium in mediating brain diseases (Zlokovic 2008). In general, endothelial dysfunction is thought to contribute to these disorders through the generation of toxic factors that may impair neuronal function or the integrity of the BBB (Grammas et al 2011). Our finding that the endothelium also plays a critical role in efficient coupling of neural activity and blood flow provides an additional mechanism whereby endothelial dysfunction can precipitate into neurodegenerative diseases.

Recent efforts have also focused on using functional neuroimaging as a marker of onset and progression of AD and mild cognitive impairment (Bookheimer et al 2000, Masdeu et al 2005, Petrella et al 2007). Many of these studies find a decrease in blood perfusion to certain regions of the brain during early onset of AD, though exact signatures remain difficult to identify. Comparison of MS-OISI hemodynamics between wild-type mice, transgenic AD mouse models, and mice with disrupted endothelial signaling, could determine whether the hemodynamic signatures due to endothelial disruption match well with those exhibited in AD mouse models. Furthermore, if impaired endothelial signaling does underlie early onset of neurodegenerative disease, a better understanding of how

disrupted endothelial signaling contributes to the fMRI BOLD signal can offer insights into what neuroimaging signatures to look for in patients exhibiting disease symptoms, leading to better detection sensitivity for disease onset.

7.4 Future directions

7.4.1 Energetic dependence of the hemodynamic phases

The experiments conducted in Chapter 4, explored how the hemodynamic response changed following incremental increases in the duration of neuronal activation (Figure 4.6). This subsection describes an experiment which we have not yet conducted, but is designed to further study the qualities of the hemodynamic phases through careful manipulation of stimulus parameters. These studies would vary a combination of stimulus parameters in order to understand the energy dependence of each hemodynamic phase. In particular, we ask – why is the plateau response observed and when it is observed? What conditions will recruit the second phase? Do these conditions rely on summed neural activity or absolute stimulus duration? Understanding the stimulus required to elicit a secondary response will help constrain the characteristics of the underlying mechanism.

Previous studies have characterized how certain stimulus parameters (amplitude, duration, frequency, inter stimulus interval) affect the hemodynamic response, while keeping all other stimulus parameters constant (Martin et al 2006, Nemoto et al 2004, Sheth et al 2004, Sheth et al 2005). We conclude from these studies that there is a roughly linear relationship between stimulus amplitude and the magnitude of hemodynamic change. The hemodynamic response magnitude also appears to scale linearly with stimulus

durations below a certain threshold (Nemoto et al 2004). However, these studies used stimulus durations too short to elicit a plateau response. They also did not examine the spatiotemporal evolution of the response, which represents a key difference between the first and the second phase of the response. In order to investigate these relationships in the context of a multi-phase hemodynamic response, both stimulus amplitude and stimulus duration should be varied.

In addition to acquiring responses for a range of stimulus durations at 1mA (as we did in Chapter 4), responses should also be acquired for 0.5 mA and 1.5 mA stimulus amplitudes. Arterial blood pressure monitoring should be recorded to ensure that stimulus amplitude is not causing increases in systemic blood pressure during stimulation. Electrophysiology should also be used to monitor neural activity in response to stimulus of varying amplitudes and durations.

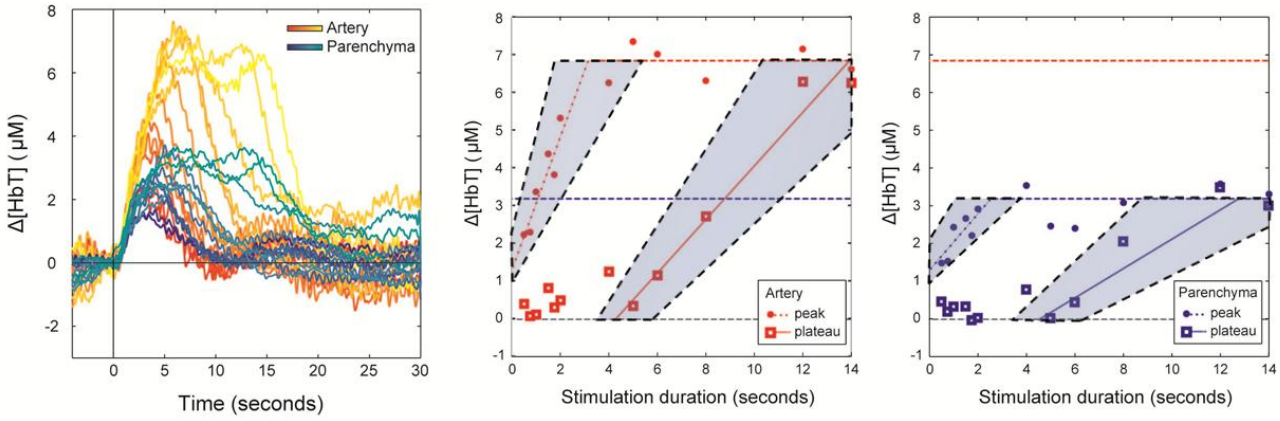

Figure 7.2 Investigating the energy dependence of the hemodynamic phases
Future studies exploring the energy dependence of the hemodynamic phases can use different combinations of stimulus paradigms and simultaneous electrophysiology to modulate the timing and amplitude.

The plots in Figure 4.7 can be replicated for each set of data acquired using 0.5, 1.0, and 1.5 mA stimulus amplitudes. Specifically, it will be useful to compare: 1) the amplitude of the unitary response to very short stimulus, 2) the stimulus duration at which the secondary phase appears to be recruited, and 3) the saturation level of arteriolar and parenchymal compartments. We want to understand whether these threshold levels, and the stimulus duration required to reach these thresholds will change depending on stimulus amplitude.

It will also be informative to compare the responses to similar stimulus durations when different stimulus amplitudes are used. For example, if a 1 mA, 5 second stimulus elicits a peak response, and a 1mA, 7 second stimulus elicits a peak-plateau response – we want to see whether the response to a 1.5 mA, 5 second stimulus exhibits properties that are more similar to the 1 mA, 5 second stimulus or the 1mA, 7 second stimulus.

If higher stimulus shifts the x-intercepts of the plots (Figure 7.2) towards zero (implying that a shorter stimulus is required to elicit a plateau response) then we may conclude that summed neural activity, rather than absolute stimulus duration, drives appearance of the response plateau. On the other hand, if changing stimulus amplitudes does not affect the x- and y- intercepts and the stimulus duration at which saturation is achieved, then there may not be any component of the response that is sensitive to summed neural activity.

7.4.2 Voltage-sensitive dye imaging of endothelial hyperpolarization

A second future study, building off of the work presented in Chapter 5, investigates whether hyperpolarization is the endothelial pathway that is recruited during sensory-evoked hemodynamic response. As discussed in Chapter 5, a number of studies in the

periphery have explored the changes in membrane potential that occur as result of EDHF signaling in the vascular endothelium (Bartlett & Segal 2000, Marrelli et al 2003, Wölfle et al 2011). However, the identity of the endothelium pathway that mediates the sensory-evoked hemodynamic response in the brain has yet to be identified. Several studies have employed the use of VSDs in isolated vessels to demonstrate their ability to propagate changes in membrane potential (Beach et al 1996, Langheinrich & Daut 1997, McNeish et al 2005), but none have been performed *in vivo* during functional stimulation.

To directly test whether or not the endothelium or smooth muscle exhibits hyperpolarization during sensory stimulation, two-photon imaging of VSDs localized to the vascular endothelium and / or smooth muscle cells should be performed through a cranial window during somatosensory stimulation. The challenges associated with this experiment may include difficulties with VSD visualization, precise and sufficient delivery of VSDs into the endothelial wall, and optimization of emission filters to account for the ratiometric nature of VSDs. Nevertheless, this experiment may definitively implicate EDHF-mediated endothelial pathways in the sensory-evoked hemodynamic response.

Appendix A: Surgical procedures

The following surgical procedures are meant to improve our ability to monitor the animal's physiology throughout the imaging experiment via mechanical ventilation, blood pressure monitoring, and delivery of intravenous (IV) fluids. Often times however, the surgical procedures themselves can compromise the quality of the animal's physiology. A number of techniques and guidelines have been developed to minimize surgical complications and to ensure proper physiological monitoring. Various issues including brain swelling, bilateral craniotomies, and ventilator issues are also addressed. These techniques have also helped to streamline the surgical procedures, minimizing the amount of time the animal is kept on anesthesia prior to imaging and improving physiological responsiveness during imaging.

Tracheotomy: The primary reason for a tracheotomy is to counteract the respiration depression caused as a side effect of using alpha-chloralose as a sedative during cortical imaging. The tracheotomy allows mechanical ventilation of the animal and ensures that proper mixture of air, oxygen, and inhalable anesthesia is being delivered. In general, the tracheotomy involves switching the animal from breathing isoflurane (or other inhalable anesthesia) through a nose cone to a tracheal tube. While the animal is on the nose cone, an incision is made along the throat just above the collarbones to expose the trachea. A small incision is made between the tracheal rings, and a premade tracheal tube is inserted and connected to the ventilator through ventilator tubes. It is important to minimize bleeding during exposure of the trachea to avoid unnecessary fluid entry into the lungs. A well-placed suture around the trachea after the tracheal tube is inserted can serve to seal off the

tracheal incision from any excess fluids in the exposed cavity. If fluid build-up is suspected, an empty syringe attached to a flexible piece of tubing can be used to aspirate the tracheal tube. Prior to insertion of the tracheal tube, it is helpful to match the ventilator speed to the animal's natural breathing rhythm. However, most anesthesias cause respiratory depression so it is common to set the ventilation to a slightly lower speed. The animal will only be properly ventilated if the ventilation tubes are securely connected to the tracheal tube, and inspiration and expiration periods do not overlap completely. Inspiration flow should be kept at a minimum to avoid damaging the lungs, although larger animals may require a larger inspiration flow. The mixture of gases supplying the ventilator must be contained in a well-mixed reservoir that is not pressurized. When switching the animal from the anesthesia nose cone to the trachea tube, ensure that ventilator is primed with isoflurane in order to prevent the animal from recovering during a brief period of no anesthesia. Table 2 displays the ventilation settings commonly used as a starting point for a ~250-300 gram rat. Fine adjustment of settings must be established specifically for each animal.

Table A.1 Ventilator settings to start with for a ~250 g rat

Inspiration Flow	0.8-1.1 L/min
Inspiration Pressure	8-10 cmH_2O
Respiration Rate	42-46 bpm

Femoral lines: Insertion of femoral lines is critical for monitoring of blood pressure and heart rate (intra-arterial -IA) and delivery of intravenous anesthesia (intravenous - IV). The lines should be filled with heparinized saline to avoid blood clotting and free of air bubbles. When placing femoral lines, special attention should be paid to the bevel on the end of the

tubing and the size and orientation of the vessel incision. Cutting a bevel on the end of the tube will it easier to insert the lines into the vessels, however it is important not to make the end too sharp or it may puncture the vessel walls during insertion. The vessel incision should be made in the lengthwise along the vessel to avoid cutting the complete circumference of the vessel. The size of the incision should be large enough to fit the tip of the tubing. In the vein, the incision site should be made slightly smaller than in the artery since the venous walls are capable of stretching. This is done to minimize the amount of blood that can leak back out through the incision site. Sutures should be placed tightly around the vessel and the tubing to help minimize excess bleeding and also to maintain pressure seal for arterial blood pressure reading. Before closing the incision site, pull back on the syringes attached to the femoral lines to ensure that blood flows back into the lines. If a significant amount of pressure is needed to draw blood into the line, it is a good idea to reposition the lines within the vessel. It could be that the end of the tubing is blocked or inserted too far in. The femoral lines can be very easily pulled out by mistake unless the lines are securely fixed. One way to minimize movement of lines is to place a suture around both lines before closing the incision site. This way each line is rigidly fixed to the other and parallel to the vessels that are inserted into, making it less likely for them to shift around. When the incision site is sutured closed, carefully tape the lines to the leg and/or tail of the rat. After placement of lines, avoid any unnecessary manipulation of the leg and take extra care when flipping the rat over for the craniotomy. Throughout the experiment, the arterial line may become coagulated which will affect the blood pressure reading. The line can be gently flushed with heparinized saline to clear the any clotting blood.

The blood pressure is an important monitoring parameter that is very indicative of the animal's physiology. Drops in blood pressure should be noted and ventilation and temperature settings should be checked. In some cases, the rhythm of blood pressure becomes synchronized with the ventilator, indicating that the ventilator settings may need to be adjusted. Sharp increases in the animal's blood pressure may also indicate that electrical stimulation amplitude is too high. This should be avoided such that systemic increases in blood pressure do not confound normal hemodynamic responses. The electrical stimulus is not meant to shock the animal. Appropriate amplitudes of stimulus cause a slight twitch in the paw, but should not cause the animal to flinch.

Craniotomy: When the rat is placed in the stereotaxic frame, it is important that the tracheal tube remains aligned with the rat at all times. Securely taping the tubes directly to the stereotaxic frame should help avoid slippage. It may also be helpful to tape the IA and IV lines as well as the temperature probe to the stereotaxic frame itself. This makes it easier to move the stereotax without putting unnecessary strain on any of the lines.

Proper location for ear bars placement can be felt as a slight dimple in the rat skull just in front of the ears. Feeling for the correct location by hand before using the ear bars can help guide ear bars placement. It is not necessary to place the ear bars into the ear canal itself. If the blood pressure drops dramatically when the ear bars are tightened, they should be removed and readjusted. When the rat is securely fixed in the stereotax, the head should not fall out of the ear bars when gently pressed on, and the eyes may bulge slightly. After ear bars are placed, fix tooth bar and nose clamp to secure the head. Adjust the angle of the tooth bar such that the portion of the skull to be exposed will be flat (parallel to the base of

the stereotax). Proper positioning of the ear bars can make a big difference in minimizing motion artifacts due to breathing and brain motion.

Prior to making an incision, the hair on the scalp should be shaved and cleaned. It is important to use iodine and alcohol wipes to clean the incision site and to remove loose hair and debris that may later enter the cranial window by accident. Loose hairs and particles that become entrapped in the cranial window can be troublesome, especially during two-photon imaging.

During the craniotomy, it is important to remove all soft tissue from the bone so that the dental cement can form a secure seal between the glass coverslip and the bone. During drilling, frequent flushing with saline will prevent heat buildup from the drill bit. Layers of the skull contain a lot of blood vessels and will bleed during drilling. The best way to deal with these spots is to continue drilling until the bleeding stops. As the skull gets thinner, it is possible to see the brain vessels through the skull when it is moistened with a drop of saline of ACSF. A small incision in the IVth ventricle just prior to skull removal will minimize brain swelling. This may also help prevent damaging the brain if additional drilling is required. The skull flap should be easily removable. If a significant amount of force is needed to lift the skull flap off, more drilling is required. Pulling on the skull can cause the brain to swell after the skull is removed. Remove the dura as quickly as possible before additional swelling occurs. In some cases, leaving a piece of gel foam soaked in ACSF on top of the dura will allow the dura to separate a little from the cortical surface, making it easier to visualize and remove. When a bilateral craniotomy is required, finish drilling on both sides before removing the skull to minimize the bone dust that enters the craniotomy.

If the brain continues to swell after the dura is removed: 1) Check that the animal is breathing properly with the ventilator. In some cases, improving the animal's respiration has caused brain swelling to decreases almost instantly. 2) Drain more CSF from the IVth ventricle to relieve the pressure. The muscles over the IVth ventricle may sometimes prevent fluid from draining. 3) If the brain is injured, or brain swelling will not go down, place the cranial window as soon as possible to prevent further swelling. In many cases, the stereotaxic frame will need to be positioned at an angle in order to achieve a flat plane for imaging at the cortical surface.

Loading of cell specific fluorescent indicators: Certain dyes such as SR101, which selectively label astrocytes, do not need to be pressure injected into the brain and can be applied topically to the exposed cortical surface. ~15-20 minutes should be allowed for the dye to fully penetrate into the cortical tissue, during which time the exposed region should be protected from light with a piece of foil. Before sealing the cranial window, the exposed surface should be flushed with ACSF to remove any residual dye from the cortical surface. The concentration of SR101 to be used depends on the co-labeling of other fluorophores of interest. For example: when studying intrinsic fluorescence of NADH or FAD, low concentrations of SR101 (1uL stock/10mL ACSF) should be used in order to prevent saturation of the fluorescent signal.

Reactive indicators such as calcium sensitive dye Oregon Green BAPTA-1AM need to be pressure injected directly into the cortex to achieve proper dye loading. In these studies, OGB-1AM was pressure injected using a Picospritzer III (Parker Instrumentation) which delivers millisecond pulses of compressed gas to inject the dye into the brain. Alternatively

an infusion pump may be used with glass pipettes or microliter syringes with 24-26 gauge needles (Quintessential Stereotaxic Injector, Stoelting). There are three main parameters that need to be adjusted together in order to produce optimal dye loading: 1) the tip diameter of glass pipette, 2) the injection pressure, and 3) the pulse duration of each injection. Before inserting the pipette into the brain, proper settings of these parameters should be achieved. The size of the droplet of dye that is expelled per pulse can be used as a measure for adjusting the settings of each parameter. A good size droplet is ~20-30 um in diameter, which corresponds roughly to the width of a 2nd order pial arteriole. Injection pressure and pulse duration will depend on the diameter of the pipette tip. For example: a smaller pipette tip may require higher pressure or longer pulse durations to expel the same amount of dye and vice versa. In addition, each parameter has certain constraints that govern their settings. A small pipette tip may become easily blocked whereas a larger pipette tip has a greater chance of damaging brain tissue during delivery. Tissue damage may also be caused by high injection pressure. If this appears to be the case, the pressure should be lowered and the pulse duration should be increased. If necessary, the tip of the pipette can also be trimmed to create a larger opening for dye delivery that requires less pressure to expel the same amount of dye per pulse.

Inserting the pipette into the brain will cause a slight dent in the cortical surface. Lowering the pipette slowly beyond this point will puncture the surface membrane and allow the brain to "bounce back." If the brain continues to dent, the pipette tip may be too large and will cause bleeding if inserted further. Lower the pipette to the desired cortical depth (~300-400 um for neurons in layer IV). ~10-15 pulses are injected per injection site, waiting ~5-10 seconds in between each pulse. If pulses are delivered too quickly in

succession, the pipette tip is likely to be blocked. It is important to check that the dye is being expelled each time after the pipette is withdrawn from the brain. The dye should be taken up immediately if injection parameters are set properly. Dye loading can be checked by viewing the brain through a 500 um long pass filter while illuminating the loading region with a blue (473nm) LED. If fluorescent spots are visible, then continue to inject dye into the area of interest. Otherwise, adjust injection parameters or change to a new pipette. After injections are finished, the exposed cortex should be protected from light and the dye allowed to incubate for 30-40 minutes prior to imaging. It is important to note that a high level of fluorescent signal recorded at the cortical surfaces does not always mean good dye loading at the neuronal level. Figures show examples of two dye loading preparations, one that produced good labeling of neuron and astrocytic cell bodes in addition to processes in the neuropil, and the other which may have caused tissue damage as evidenced by some loading in neuropil but no delineation of cell bodies.

Alpha-chloralose anesthesia and hemodynamic oscillations: All painful procedures should be completed prior to switching to alpha-chloralose anesthesia for the imaging experiments. This includes placement of stimulation needles in the forepaws and hindpaws. A bolus injection of alpha-chloralose is given to initiate the switch off of isoflurane anesthesia, during which drops in blood pressure should be avoided by injecting at a slow and steady rate. If the blood pressure does drop slightly, wait to start the alpha-chloralose infusion until the blood pressure has mostly recovered. At high dosages, alpha-chloralose can cause severe respiratory depression, which is alleviated through mechanical ventilation. However, in cases where the animal appears to be struggling to breathe against the

ventilator, the ventilator tubes may be removed and the animal can breathe at its own rhythm. This may also help elicit more normal hemodynamic responses. If the animal is breathing off the ventilator, make sure the blood pressure is also remaining at a steady level. If the blood pressure begins to fall steadily, even though the animal appears to be breathing normally, the ventilator tubes should be replaced.

Often times large hemodynamic oscillations are observed to arise near the end of an experiment due to poor physiology or if the level of anesthesia is too light. These vascular oscillations do not appear to be present when normal physiology is maintained. In some cases, adjusting ventilation settings or increasing the rate of alpha-chloralose infusion may eliminate the oscillations. In most cases, oscillations will diminish over time periods of several hours. However the stimulus-evoked hemodynamic responses after a period of oscillations usually appear to be qualitatively different from earlier responses, and should not be included in analyses.

Appendix B : Chapter 3 supplemental figures

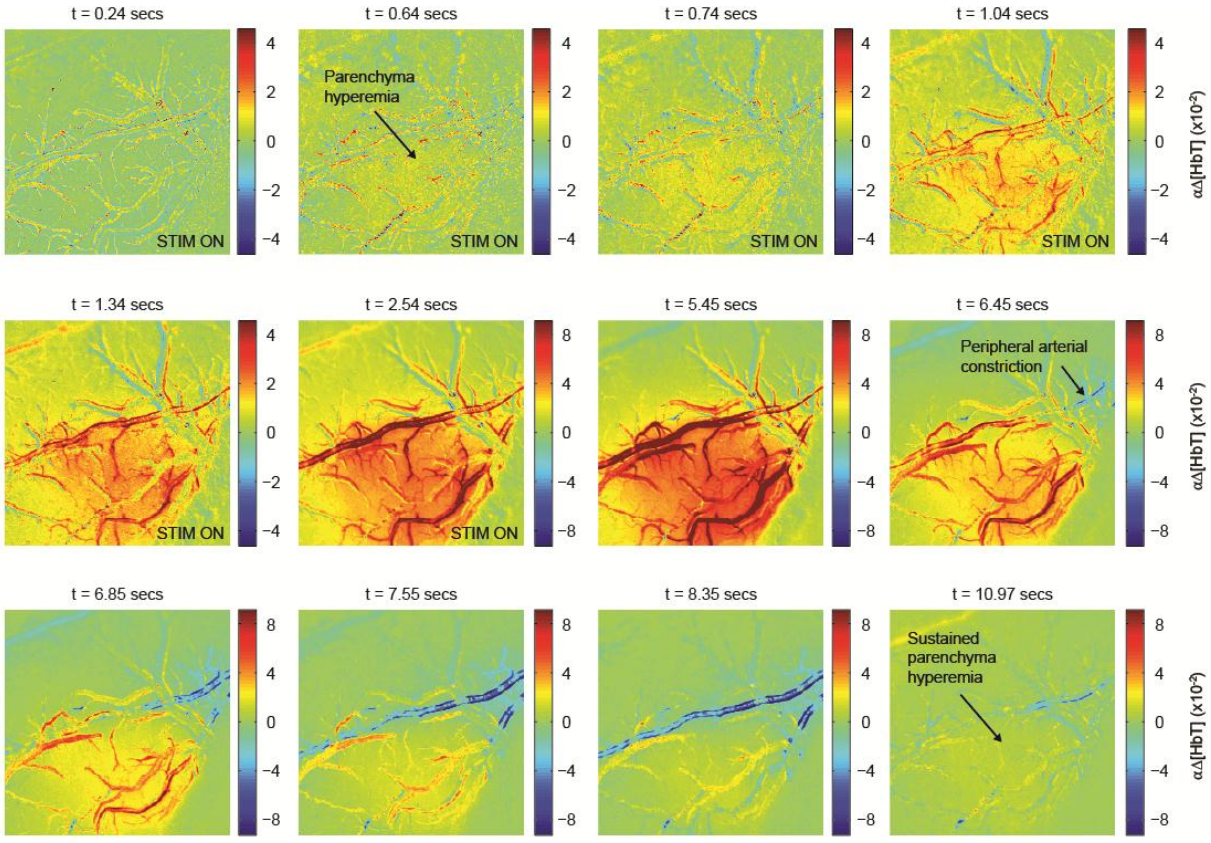

Figure SB.1 Spatiotemporal evolution of the hemodynamic response
Wide field images of the exposed rodent cortex during 4 seconds of electrical hindpaw stimulation beginning at t = 0 seconds. Data shown is the average of 10 runs. Note that the color scale after 5 images is adjusted such that small changes at the beginning of the response can be easily visualized.

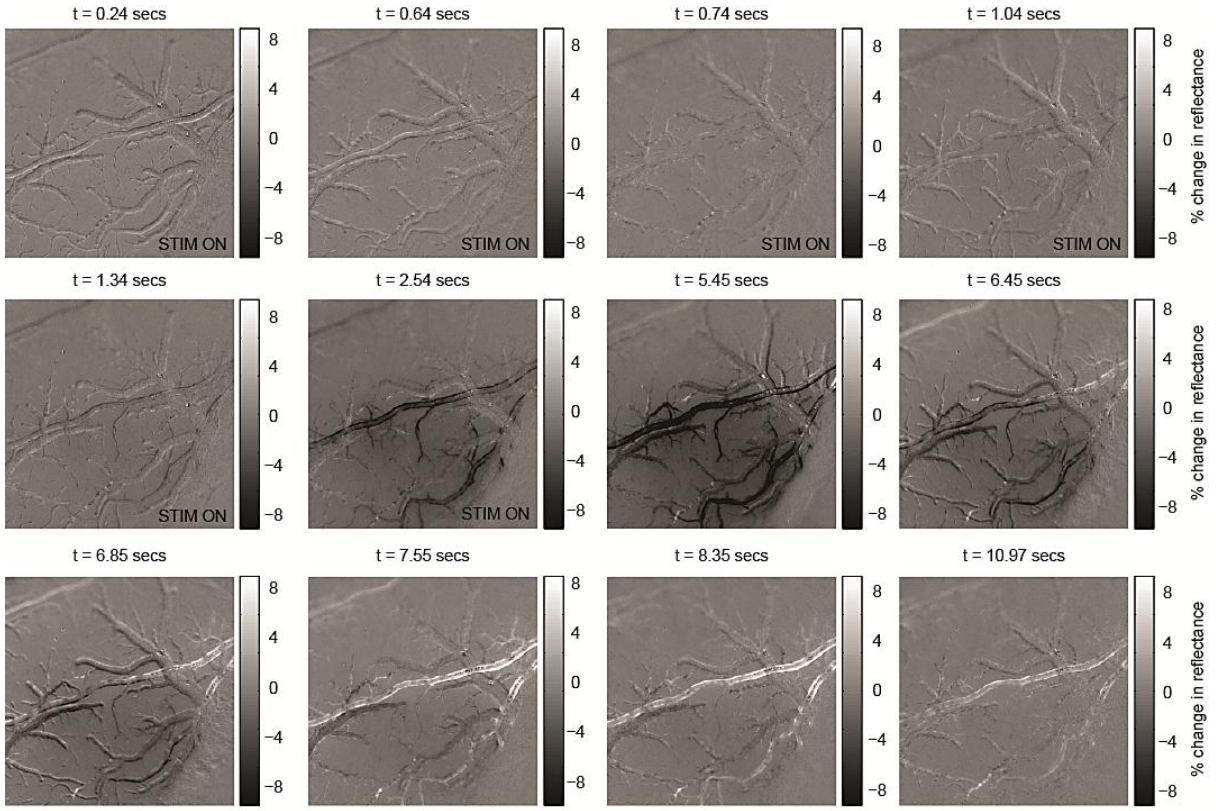

Figure SB.2 Spatiotemporal evolution of the hemodynamic response in grayscale
Grayscale images showing % changes in reflectance during 4 seconds of electrical hindpaw stimulation beginning at t = 0 seconds. Corresponding Δ[HbT] images for the same sequence is shown in Figure SB1.

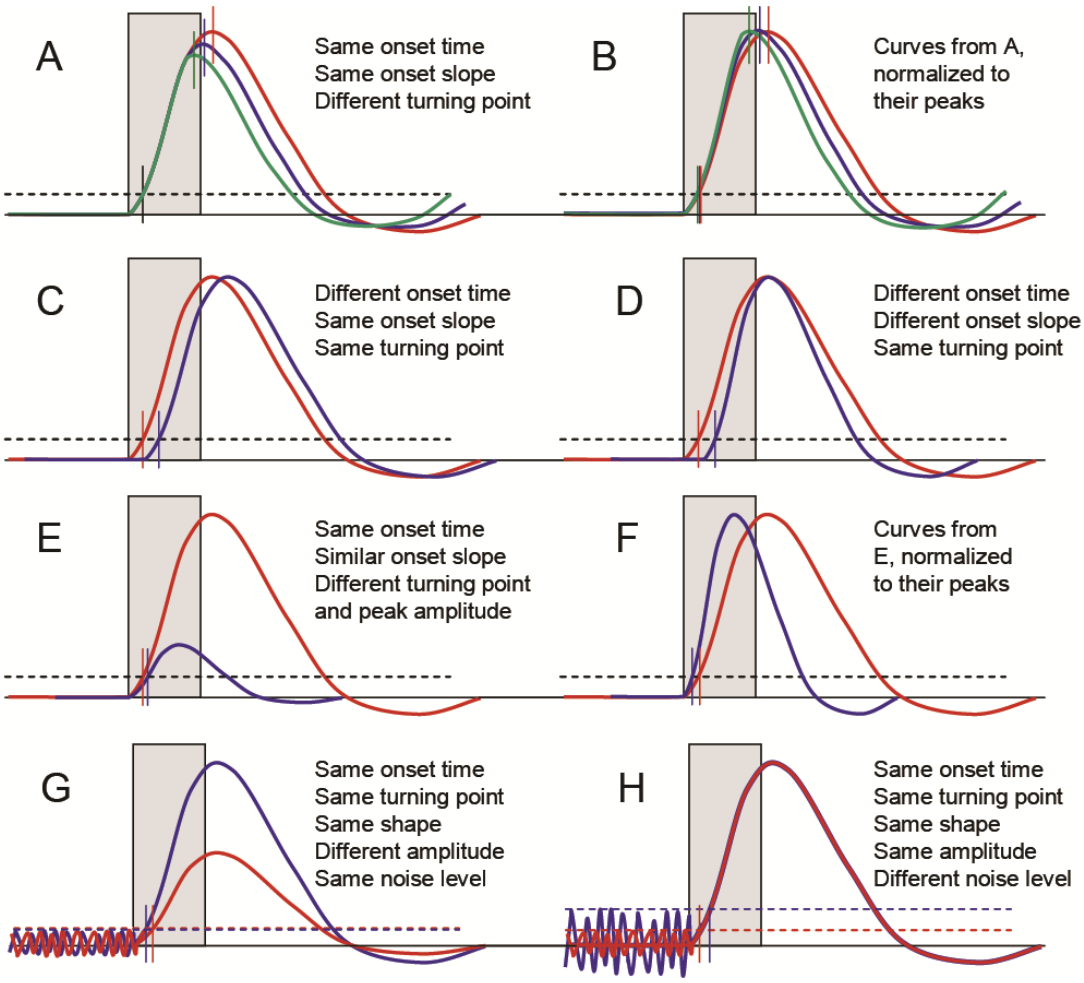

Figure SB.3 Schematics of possible confounds for thresholding and time to peak methods (A) The time to peak (TTP) could purely reflect the inflection point of the peak, corresponding to the initiation of return to baseline. In this case, a static threshold (dotted line) would correctly infer the onset time, whereas TTP would not. (B) If these curves are normalized a measure such as time to 10% (dotted line) would incorrectly infer that the green curve onset first. (C) TTP and thresholds would provide a measure of onset time only if the signals exhibit different onset times but identical shapes, slope and amplitude. (D) Signals could feasibly exhibit different onset times, but the same TTP if their onset slopes grow at different rates. (E) Signals that have identical onset times may exhibit different times to peak depending on rate signal change and time of peak inflection. (F) Normalization of curves such as those in E could lead to completely opposite results for static threshold measures compared to TTP or time to 10% (for example) measures. (G) For noise-based thresholds, two signals with the same noise level, onset time and overall shape, but different peak amplitudes, will cause the signal with a faster rate of increase (higher amplitude) to appear to have a faster onset. (F) Given the same onset time and response shape, a signal with a threshold based on a lower baseline noise level will appear to have a faster onset than a signal with higher baseline noise level.

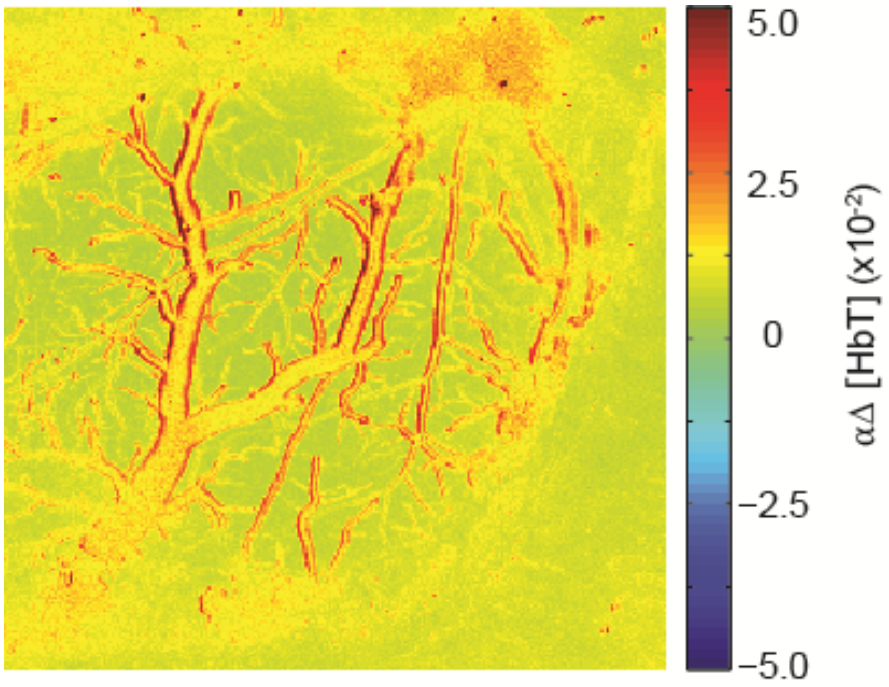

Figure SB.4 Baseline variance map
90% threshold levels computed using the baseline Δ[HbT] PDF for each pixel. Vessels exhibit greater baseline variance than parenchyma regions.

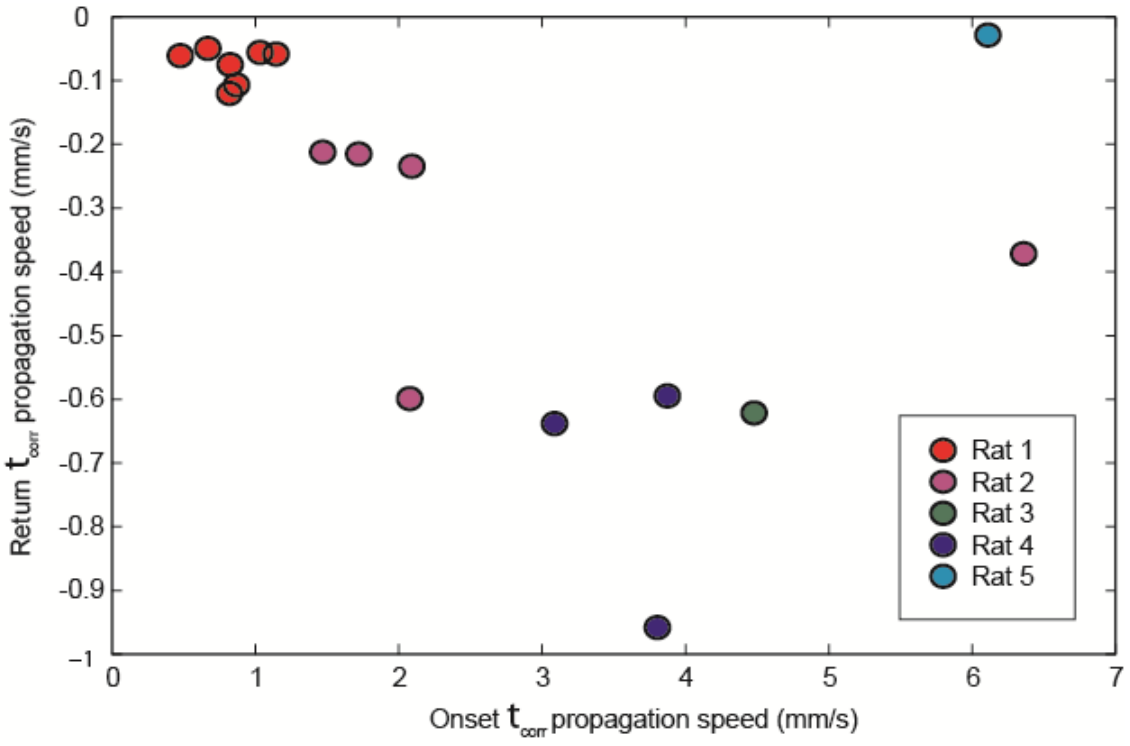

Figure SB.5 Ratio of onset and return propagation speeds
Return propagation speeds plotted against onset propagation speeds for 5 different rats. For all rats, onset (vasodilation) propagation speeds were found to be faster than return (vasoconstriction) propagation speeds. We find that some rats exhibit fast propagation speeds and others exhibit slow propagation speeds for both onset and return.

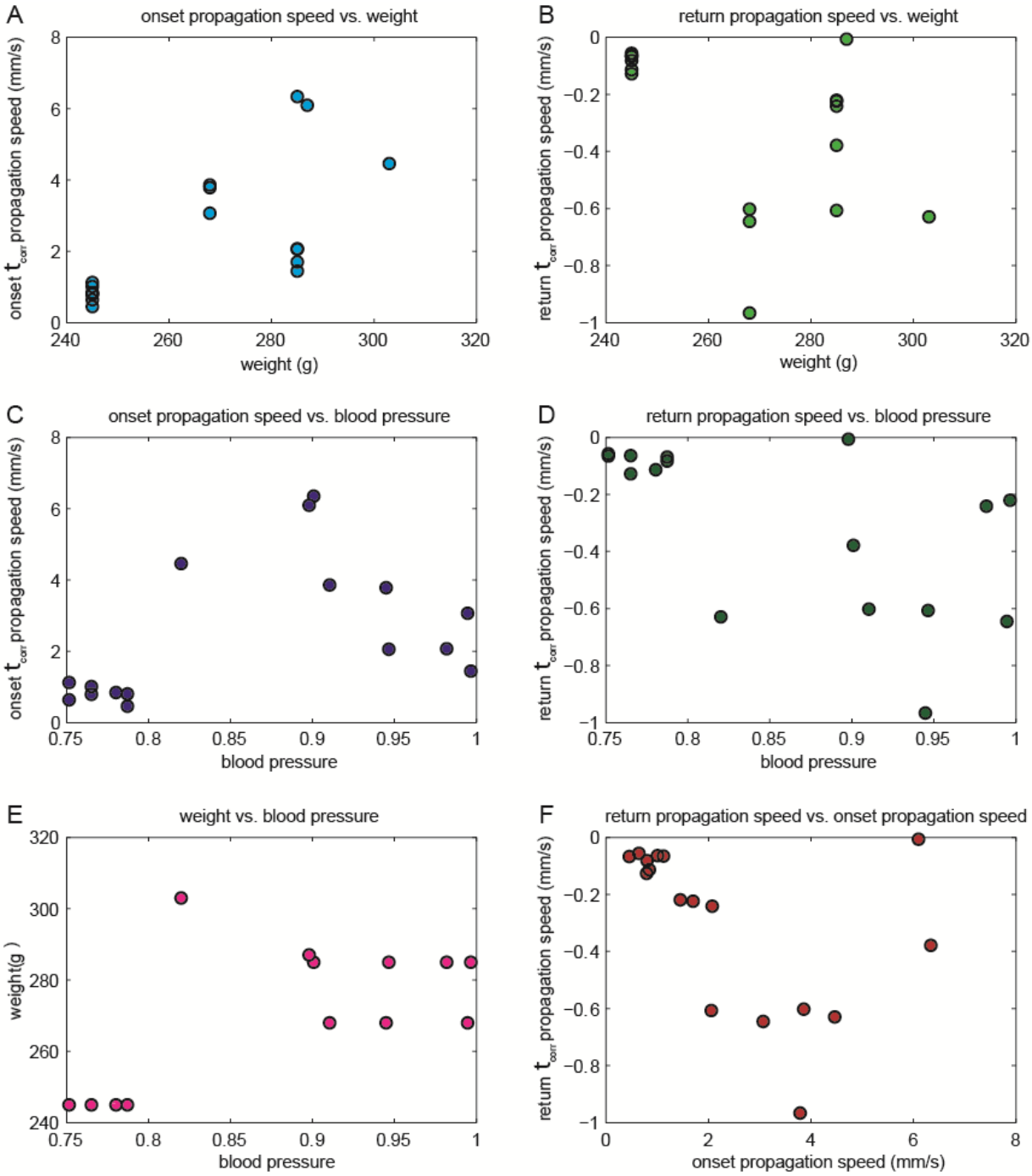

Figure SB.6 Physiology parameters
Onset and return propagation speeds across 5 rats are compared against blood pressure and body weight. (A) Onset propagation speed vs. body weight. (B) Return propagation speed vs. body weight. (C) Onset propagation speed vs. blood pressure. (D) Return propagation speed vs. blood pressure. (E) Body weight vs. blood pressure. (F) Return propagation speed vs. onset propagation speed. Blood pressure is measured from the femoral artery and is averaged over the entire imaging run (pre-stimulus, stimulus, and post-stimulus).

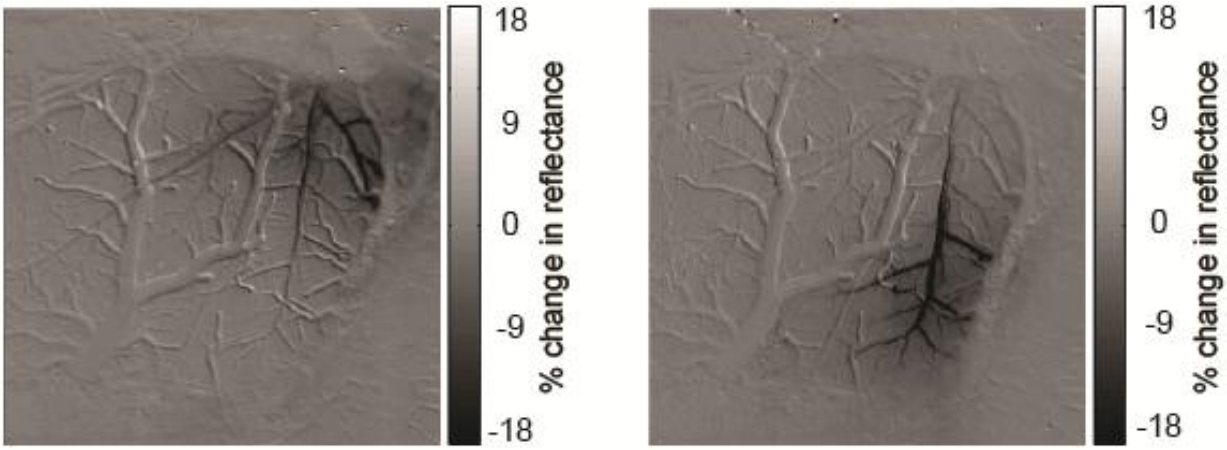

Figure SB.7 Functional maps in grayscale
Grayscale functional maps of % change in reflectance under forepaw (left) and hindpaw (right) stimulation. Corresponding functional maps of Δ[HbT] for this rat are found in figure 4.

Appendix C : Chapter 4 supplemental figures

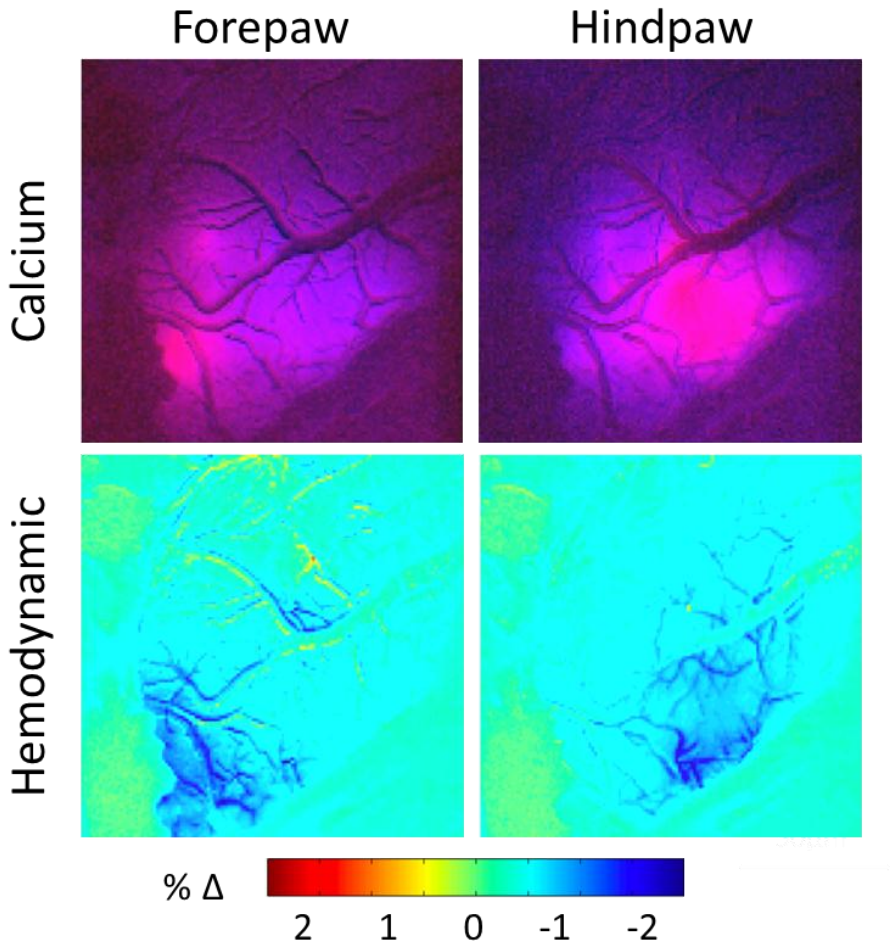

Figure SC.1 Correlation between calcium activity and hemodynamic changes
(Top row) Correlation maps showing regions of greatest calcium activity (pink) during forepaw and hindpaw stimulation. Correlation analysis was done based on a characteristic timecourse of calcium spiking activity (Figure 2.3). (Bottom row) Activation maps showing regions of greatest hemodynamic change during forepaw and hindpaw stimulation. Calcium activity and hemodynamic changes are spatially well correlated.

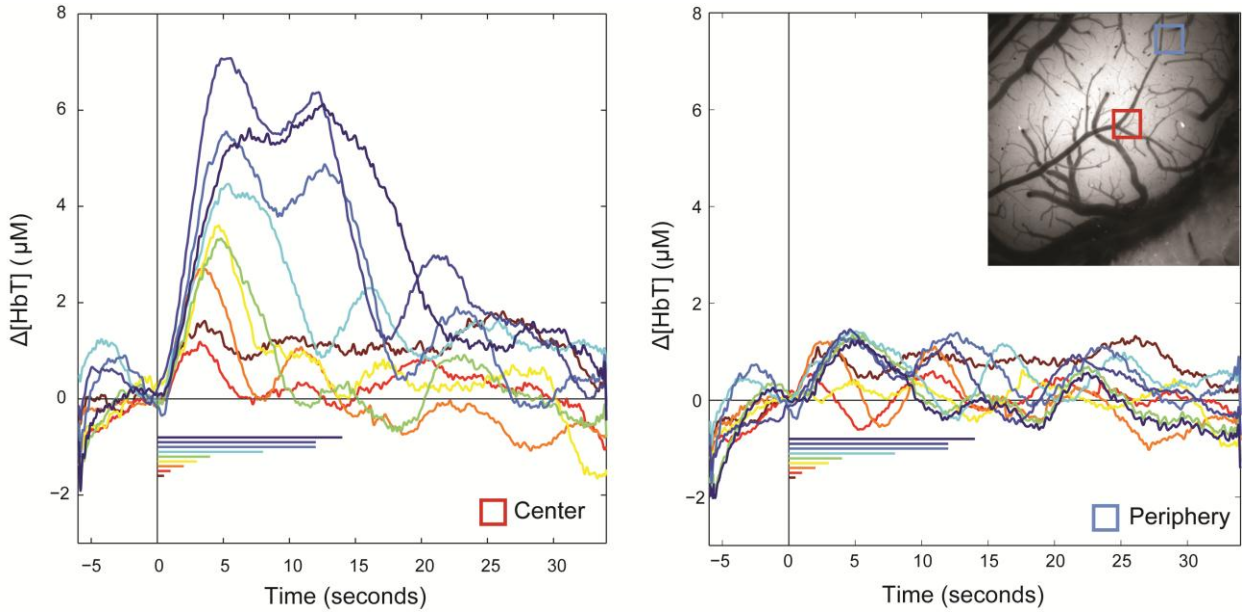

Figure SC. 2 Additional examples of hemodynamic responses to a range of stimulus durations Central and peripheral Δ[HbT] responses to 0.5, 1, 2, 3, 4, 8, 11, 12, and 14 second stimulus durations. Timecourses are averaged over a central region and a peripheral region (inset, red and blue squares).

Appendix D : Chapter 5 supplemental information

Background: The vascular endothelium

The vascular endothelium is the inner lining of all blood vessels in the circulatory system and plays a critical role in maintaining vascular health. In addition to acting as a semi-selective barrier between the vessel lumen and the surrounding tissue, endothelial cells are also involved in immune functions, blood coagulation, angiogenesis, and control of blood pressure through the release of vasodilators, NO and prostacyclin, and vasoconstrictors endothelin and platelet-activating factor (Cines et al 1998). A majority of vascular diseases can be associated with endothelium dysfunction such as atherosclerosis, ischemic stroke, heart attacks, and impaired healing (Cosentino & Luscher 1998, Ross 1993).

Although the endothelium forms a continuous lining throughout the circulatory system, there is considerable amount of heterogeneity in the appearance and function of endothelial cells within different tissue types. For example, the endothelial cells in the brain and retina are tightly connected by tight junctions in order to maintain the blood brain barrier, while endothelial cells in the intestinal villi and kidneys exhibit fenestrations that facilitate selectively permeability for absorption and filtering (Dejana 1996). For this reason, it is important to recognize that certain EC properties may not hold true across all organ systems or tissues.

In this research we are primarily interested in the role of the endothelium in regulating blood flow. Endothelial cells are closely associated with smooth muscle cells and are capable of releasing a number of substances which can actuate changes in vessel tone. One unique feature of the endothelium that has been extensively studied in the peripheral

microcirculation is its ability to mediate conducted vasodilation along blood vessels during coordinated blood flow control in microvascular resistance networks (Bartlett & Segal 2000, Budel et al 2003, Koller et al 1989, Looft-Wilson et al 2004, Wölfle et al 2011). This conducted vasodilation coincides with the propagation of electrical hyperpolarization along the vascular endothelium after local application of chemical vasodilators. The mechanism underlying this phenomenon, which operates independently of nitric oxide or prostacyclin release, has been termed endothelium-derived hyperpolarizaing factor (EDHF) (Bryan et al 2005). EDHF remains a relatively new concept, and the exact signaling pathways and channel complexes that are involved in coupling the endothelial layer to the smooth muscle layer during EDHF-mediated dilations remains uncertain (Figure SD. 1).

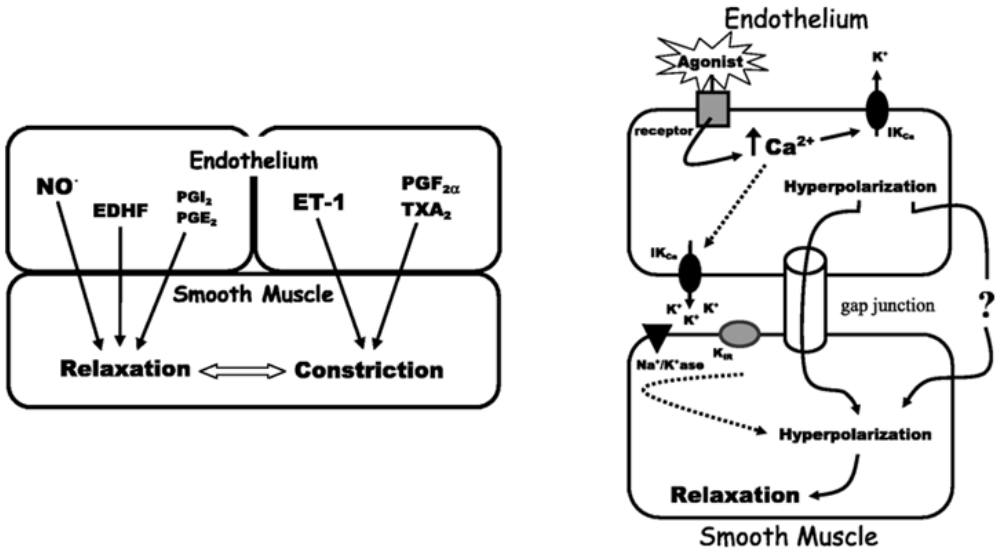

Figure SD. 1 Endothelial signaling pathways influence smooth muscle tone
(Left) Diagram showing several pathways in which the endothelium may induce relaxation or constriction in neighboring smooth muscle cells. (Right) Diagram showing the possible mechanisms underlying endothelial hyperpolarization. EDHF has been proposed to be mediated by gap junctions or potassium sensitive calcium channels of small and intermediate conductances. However the exact mechanism coupling endothelial and subsequent smooth muscle hyperpolarization is unclear, as represented by the question mark pathway. Agonists that are capable of inducing endothelial hyperpolarization include a number of neurotransmitters. Images reproduced from (Andresen et al 2006).

Fewer studies of endothelial hyperpolarization have been done in the brain due to the difficulties associated with studying cortical vessels. In particular, the presence of other potential contributors to blood flow control such as astrocytes, interneruons, and pericytes makes it more difficult to isolate the effect of the endothelium on local hemodynamics *in vivo*. Nevertheless, conducted vasodilations in response to local application of endothelium-dependent vasodilators have been observed in cerebral pial vessels using *in vivo* cranial window preparations (Leffler et al 1994, Rosenblum 1986). In addition, isolated penetrating arterioles and parenchymal arterioles have also been shown to exhibit endothelial dependent vascular changes that can be initiated by ATP and mediated through calcium sensitive potassium channels or purinoceptors (Dietrich et al 1996, Hannah et al 2011). Recent studies are now focusing on the endothelium and its role in neurovascular coupling, hypothesizing that the endothelium may play a more important role in mediating the hemodynamic response than previously thought (Andresen et al 2006, Hannah et al 2011). Indeed, the endothelium-dependent conducted vasodilation is a mechanism that is highly consistent with early upstream vasodilation observed during the hemodynamic response (Berwick et al 2008, Chen et al 2011, Kennerley et al 2011, Tian et al 2010).

Background: Light-dye injury model

The light dye injury method was first introduced as a model for studying thrombogenesis, which is characterized by accumulation of platelet aggregates in the microcirculation (Rosenblum 1986). In this technique, sodium fluorescein (Na-F) or dextran conjugated fluorescein isothiocyanate (FITC-dx) is injected intravenously into the circulation where it acts as a sensitizing agent. Subsequent illumination of a vessel with blue light for a period

of time causes the formation of oxygen free radicals which interact with the endothelium, causing ultrastructural changes, platelet aggregation, and eventual cell death. Figure SD. 2 shows a flow diagram of how excitation of the sensitizing agent leads to endothelial damage. Control studies confirm that intravenous dye or exposure to blue light alone do not produce toxic effects on the blood vessels.

Endothelial damage is either preceded or accompanied by accumulation of fluorescent platelet aggregates within the vessel lumen, which is commonly used as a visual measure indicating extent of endothelial damage (Herrmann 1983, Miller et al 1992). Platelets and leukocytes will adhere to regions of the endothelium or exposed sub-endothelial components during immune response to tissue injury or injection (Cines et al 1998). At the time of platelet aggregation, ultrastructural analysis of the endothelium using scanning electron microscope (SEM) images reveals increased endothelial lucency, swelling of the nuclear envelope, rupture of the luminal membrane, and vacuolization of the endothelium (Miller et al 1992, Povlishock et al 1983). Once the cell membrane is ruptured, damaged endothelial cells can be labeled and identified using propidium iodide, a membrane impermeant nucleic acid stain (Looft-Wilson et al 2004, Sun et al 2009, Wölfle et al 2011). As illumination continues, additional platelet aggregates form and endothelial swelling is increasingly apparent, with all changes occurring first in venules and then later in the arterioles (Herrmann 1983, Povlishock et al 1983). The use of high molecular weight (>70kDa) FITC-dx allows photochemical interactions to be limited to the inner most endothelial layer of the vessel walls, leaving smooth muscle and other perivascular structures unaffected, as large molecules are incapable of diffusing through the blood brain barrier (Herrmann 1983). However, if illumination duration is extended much longer

following obvious endothelial damage, the sensitizing dye may leak into the surrounding smooth muscle cells where it can cause further disruption of smooth muscle integrity. Additional accumulation of platelet aggregates can also become large enough to block the entire vessel lumen, impairing blood flow (Povlishock et al 1983).

Several studies have reported an increase in the resting diameter of arterioles that accompanies platelet aggregation and endothelial damage (Bartlett & Segal 2000, Budel et al 2003, Leffler et al 1994, Povlishock et al 1983, Rosenblum 1986, Rosenblum & El-Sabban 1982). It has been hypothesized that this dilation is caused by the hydroxyl radicals that are chemically generated during light dye disruption. Application of hydroxyl scavengers, dimethyl sufloxide (DMSO) and glycerol, were shown to delay aggregate formation and inhibit the accompanying vasodilation, providing further evidence that the mechanism of endothelial damage is mediated in part by free radicals (Rosenblum & El-Sabban 1982). Aside from this vasodilation, light dye treatment has few other effects on blood cells and vasculature integrity, unlike alternative methods for inducing endothelium damage and platelet aggregation, which include mechanical deformation, electrical, biochemical, or thermal noxious stimuli (Herrmann 1983).

Due to its specificity and innocuous side effects when properly performed, the light-dye injury technique has become a useful *in vivo* model for studying the effect of drugs on platelet aggregation as well as the effects of endothelium disruption on vascular function (Karlheinz S 1983, Leffler et al 1994, Miller et al 1992, Rosenblum & El-Sabban 1982).

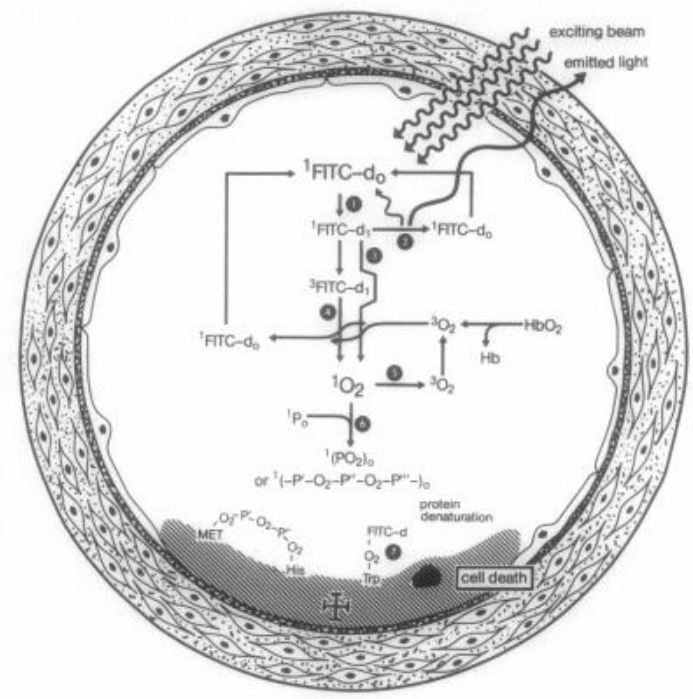

Figure SD. 2 Possible mechanisms of light-dye disruption of endothelium
Possible mechanisms leading to platelet aggregation after excitation of intravascular FITC-dx involves the accumulation of singlet oxygen molecules which subsequently oxygenate neighboring tissue molecules. The affected cells exhibit cell membranes with compromised integrity and function and will eventually swell and die. Image reproduced from (Karlheinz S 1983).

Discussion: Alternative mechanisms

In our current understanding of blood flow control, astrocytes are considered an obvious candidate for having a role in neurovascular coupling (Attwell et al 2010, Cauli & Hamel 2010, Logothetis et al 2001, Schummers et al 2008, Takano et al 2005, Wang et al 2006, Winship et al 2007). Astrocytes have been found to exhibit increases in intracellular calcium in response to stimulation and are able to invoke vasodilation. However, these responses are generally delayed by 2-3 seconds, which is not consistent with rapid onsets of vascular changes occurring within 200-400 ms (Takano et al 2005, Wang et al 2006).

Pharmacological blocking of astrocytic metabotropic glutamate receptors was shown to have little effect on the eary portion of the blood flow response (Calcinaghi JCBFM). Furthermore, astrocytic processes also do not extend beyond the glia limitans and could not directly contact and control rapid dilation of pial arterioles (Giaume et al 2010, Hamel 2006, McCaslin et al 2011).

Nevertheless, astrocytes and endothelial cells possess many of the same biochemical pathways and are capable of producing similar vasoactive substances, making them likely candidates for affecting blood flow (Abbott et al 2006). For example, a recent study demonstrated that the same K_{Ca} channels that are associated with EDHF mediated vasodilations are also expressed in astrocytes (Longden et al 2011). (Longden et al 2011) found a functional role of IK_{Ca} channels, which are associated with increases intracellular calcium of astrocytic endfeet and arteriolar vasodilation. These findings suggest that a portion of the EDHF-mediated signal could be carried through astrocytic pathways. Astrocytes have also been shown to be able to influence smooth muscle tone through the calcium-mediated release of EETs, prostaglandins, and adenosine (Koehler et al 2006, Xu & Pelligrino 2007, Zonta et al 2003), although the timing of their calcium responses have not been consistent with the initial phase of the hemodynamic response (Schummers et al 2008, Wang et al 2006).

Smooth muscle cells may also provide alternative signaling pathways associated with blood flow regulation (Armulik et al 2005, Hamilton et al 2010, Hirschi & D'Amore 1996). A majority of studies on propagated vasodilations in peripheral vascular beds have reported that the endothelium is responsible for conducting the electrical signal along the vasculature, while also inducing hyperpolarization in neighboring smooth muscle cells

(Duza & Sarelius 2003, Koller et al 1989, Rosenblum 1986, Wölfle et al 2011). Nevertheless, studies performed in the hamster cheek pouch have also reported that electrical signaling within the smooth muscle layer can also induce conducted vasodilations along the vasculature (Budel et al 2003). It is therefore feasible that the smooth muscle layer may serve as a 'backup' signaling pathway in the case of endothelial damage.

Pericytes are also closely associated with endothelial cells and are located on blood capillaries, pre-capillary arterioles, and post-capillary venules, where they have been shown to exhibit contractile properties similar to those of smooth muscle cells (Fernández-Klett et al 2010). A single pericyte can contact several endothelial cells through specialized junctions, making it possible for them to play a role in integrating and coordinating endothelial cell responses. However, little empirical evidence documents these functional interactions (Armulik et al 2005).

While multiple cellular mechanisms and signaling pathways are undoubtedly involved in blood flow control, our findings here implicate the vascular endothelium as having a critical role, irrespective of other mechanisms, in mediating the early portion of the hemodynamic response to sensory stimulation. This result does not conflict with prior reports that other mechanisms are capable of effecting blood flow and vessel tone.

Discussion: Endothelial-derived hyperpolarization factor vs. nitric oxide

Although the mechanism of endothelial-mediated dilations is not directly investigated in this study (Chapter 5), we hypothesize that the dilations associated with the initial phase of the hemodynamic response is attributable to EDHF rather than endothelial NO influences.

A key feature in the hemodynamic response is the rapid vasodilation that is observed immediately after stimulus onset, suggesting that the underlying mechanism must involve a fast and consistent signaling pathway. These properties match those of EDHF-mediated pathways which are capable of rapidly propagating signals via gap junctions and influencing smooth muscle tone via MEGJs (Andresen et al 2006). Furthermore, the relationship between electrical hyperpolarization and subsequent vasodilation has recently been shown to be linear up to a threshold amplitude of hyperpolarization, above which associated vasodilations exhibit a constant magnitude. This property of EDHF-mediated vasodilation could explain how precise vessels at the pial surface are recruited in the hemodynamic response, even if responses were initiated in deep arterioles or at the capillary level. In addition, the fact that this propagation is contained within the vascular walls conveniently avoids the dependence of a signaling pathway inherent to the highly varying cellular morphology of perivascular structures outside of the cortical vasculature. The possibility that gap junctions of arteriolar endothelial cells are sufficiently tight that they can propagate long-range signals is consistent with observations made by McCaslin et al of endothelial uptake and gap junction mediated spread of astrocyte-targeted SR101. This uptake was not observed in the more disorganized venous endothelium (McCaslin et al 2011).

Alternatively, the properties of NO are not well matched to these criteria. NO is a highly diffusible and short-lived vasodilator derived from endothelial (eNOS) and neuronal NO synthase (nNOS). It is thought that NO plays a role in several aspects of the cerebral circulation, including autoregulation, resting state blood flow, and responses to hypercapnia, hypoxia, and functional activation (Iadecola et al 1994, Rodrigo et al 1994,

Snyder 1992, Wang et al 1994, Yang et al 1999). Increases in NO concentration have also been found in many pathological states, including stroke, Alzheimer's disease, multiple sclerosis, and head trauma (Toda et al 2009). While the general contribution of NO to blood flow regulation is commonly accepted, there remains conflicting evidence as to whether or not NO plays a critical role in mediating localized dilations in targeted vessels during neuronal activation (Iadecola et al 1994). This uncertainty is compounded by the multiple sources of NO that may be able to compensate for each other, making it difficult to adequately block NO with high levels of specificity (Buxton et al 1993, Peterson et al 1992). The fact that NO is involved in many aspects of cerebral blood flow and circulatory disorders suggests that it may have an obligatory role in maintaining circulatory health (Toda et al 2009). However, the non-specificity of NO influences on vessel tone makes it unlikely that it is responsible or required for mediating such a spatially and temporally precise vasomotor response that is observed immediately following sensory stimulation.

In the context of this study, there are also several specific properties of NO that further weaken the hypothesis that it underlies the observed vascular response. For example, a number of studies have pointed to the greater relative importance of NO over EDHF in modulating tone in larger vessels (>100 μm) than in smaller vessels (<100 μm) (Faraci 1991, You et al 1999). This suggests that EDHF would have a more dominant effect, relative to NO, on the pial and parenchymal arterioles that are recruited during sensory stimulation (Faraci et al 2004). Furthermore, it has been shown that local NO synthesis alone is not sufficient to initiate conducted vasodilation in peripheral vessels (Doyle & Duling 1997), thereby implying that at least one other mechanism is required.

Nevertheless, the potential role of NO cannot be definitively ruled out. A study by (Dirnagl et al 1993) was able to selectively attenuate the early component of the blood flow response to 1 minute of whisker deflection following intravascular application of L-NA, an irreversible inhibitor of endothelial and parenchymal NO-synthase, producing blood flow responses that were much like the post-LD responses presented in this study.

Discussion: EDHF in the brain

Assuming that EDHF is responsible for endothelial signaling pathway underlying the observed vasodilations, we review here the evidence supporting its role in the cerebral microcirculation. The concept of the EDHF playing a role in cerebral blood flow regulation is well supported by a number of studies performed both *ex vivo* and *in vivo*. Although investigations of cerebral endothelium has lagged behind that of endothelium in peripheral vessels and heterogeneity is known to exist among vasodilator pathways in different vascular beds (Hill et al 2001), recent studies performed in isolated cerebral arterioles have identified similar properties underlying endothelial regulation of blood flow in cerebral vessels as in peripheral vessels. The mechanisms that underlie EDHF-mediated vasodilation in small-diameter arterioles (< 100 μm) of peripheral vascular beds are thought to involve the efflux of potassium (K+) ions through calcium-sensitive potassium channels of small (SK_{Ca}) and intermediate conductances (IK_{Ca}) into the myo-endothelial space that ultimately leads to hyperpolarization and relaxation of smooth muscle cells (Andresen et al 2006, Cipolla et al 2009, Marrelli et al 2003). The localization of these K+ channels in the endothelium has recently been identified in isolated cerebral penetrating arterioles and

their role in regulating resting cerebral blood flow has been demonstrated in vivo through the use of pharmacological channel blockers (Hannah et al 2011).

Endothelial hyperpolarization can be initiated by a number of chemical agonists. Naturally occurring agonists (eg. ACh, ATP, and UTP), which are used to experimentally induce endothelial hyperpolarization in peripheral vessels (Duza & Sarelius 2003, Thapaliya et al 1999, Winter & Dora 2007), are also capable of eliciting conducted vasodilations in cerebral arterioles observed through a cranial window preparation *in vivo* (Dietrich et al 2009, Leffler et al 1994, Marrelli et al 2003, Rosenblum 1986, You et al 1997, You et al 1999). Isolated cerebral-penetrating arterioles have been shown to exhibit ATP-induced conducted vasodilations at estimated speeds up to 1 mm/s that are preceded by membrane hyperpolarization (Dietrich et al 1996). At this speed, ATP-mediated conducted vasodilations could allow for extremely rapid adjustment of vessel diameters, which is consistent with the rapid vasomotor changes observed along the arteriolar tree in response to sensory stimulation (Chen et al 2011). Similar observations of EDHF mediated vasodilation of cerebral arteries have also been documented in response to application of K+ ions, adenosine, and ACh (Dietrich et al 1996, Horiuchi et al 2002, Janigro et al 1997, Ko et al 1990, Ngai & Winn 2002, You et al 1999). The fact that the chemical agonists used in these experiments are also known neurotransmitters and/or co-transmitters suggests that physiologically released agonists or neurotransmitters from active neurons may plausibly initiate endothelial hyperpolarization in surrounding capillary beds that subsequently propagate up to surface pial arterioles.

Chapter 5 Supplemental Figures

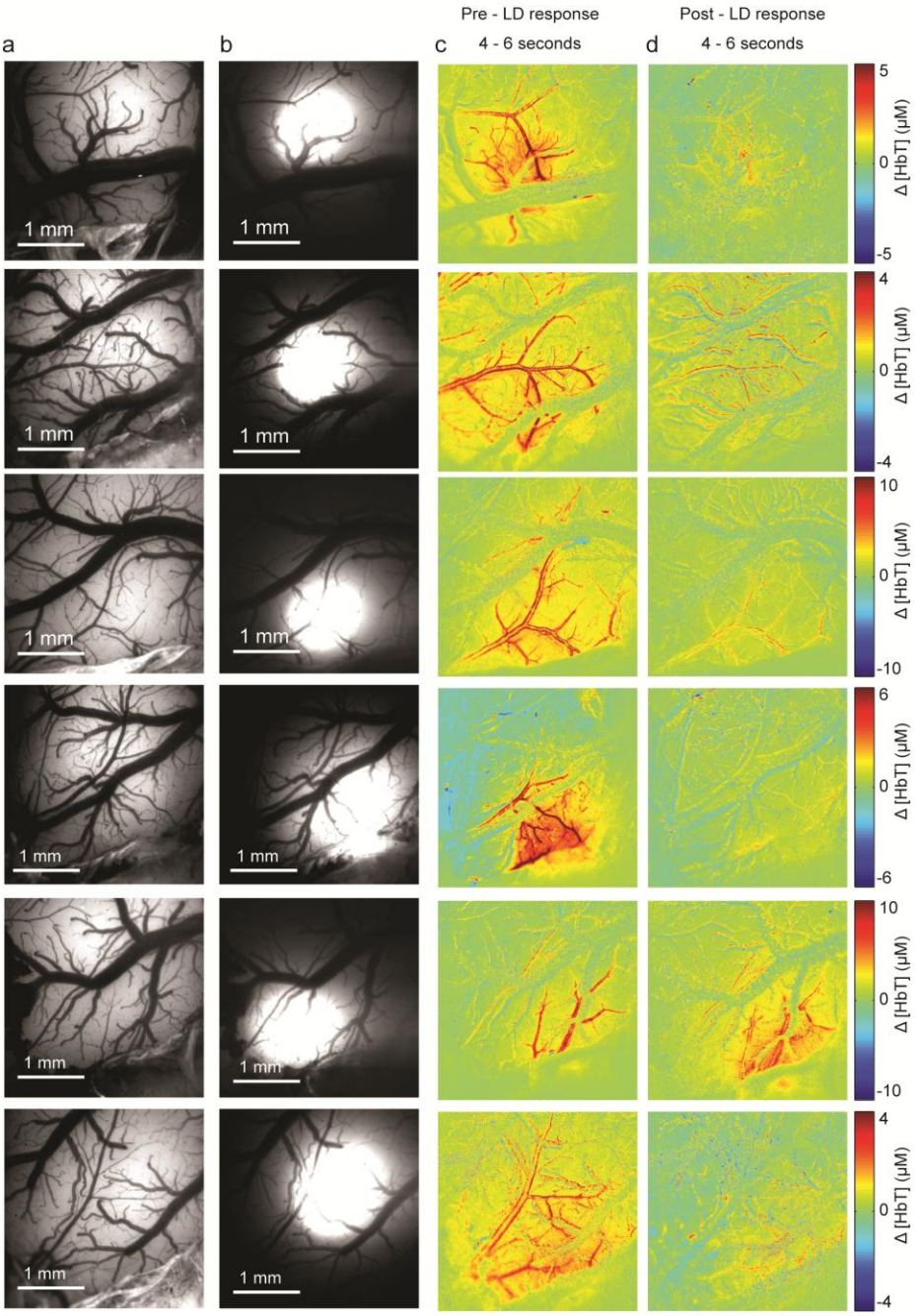

Figure SD. 3 Further examples of responses to 12 second hindpaw stimulation responses pre and post LD treatment. (a) Image of the exposed somatosensory cortex. (b) Image showing the blue light spot (~1-2 mm in diameter after scattering) positioned over a responding pial artery. (c) Pre-LD treatment functional maps showing Δ[HbT] relative to baseline during the "peak" averaged between 4 to 6 s after stimulus onset. (d) Post-LD treatment functional maps showing ΔPHbT] (shown on the same color scale as (c)), relative to baseline. For 6 different rats (rows).

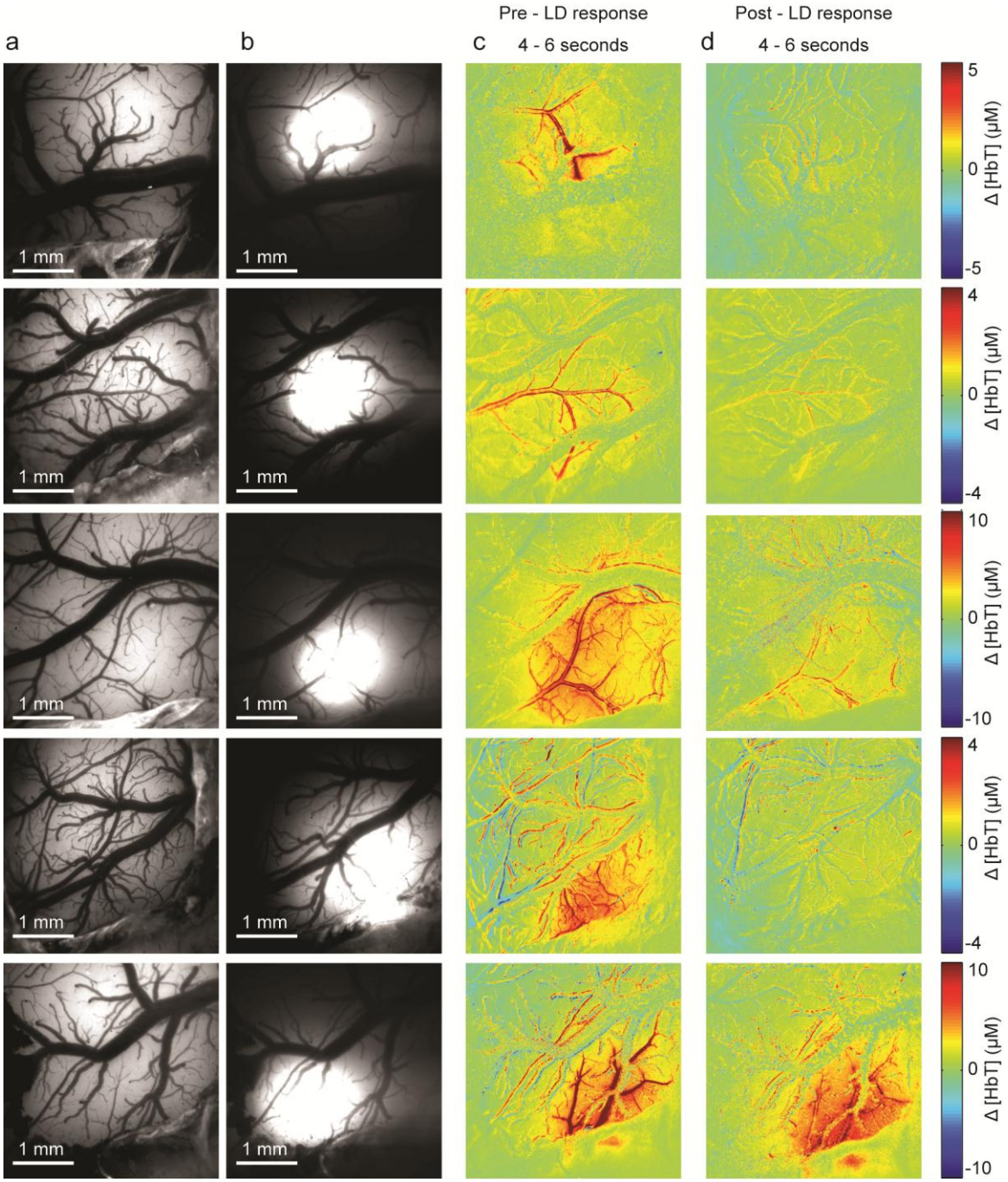

Figure SD. 4 Examples of responses to 2 second hindpaw stimulation responses pre and post LD treatment. (a) Image of the exposed somatosensory cortex. (b) Image showing the blue light spot (~1-2mm in diameter after scattering) positioned over a responding pial artery. (c) Pre-LD treatment functional maps showing Δ[HbT] relative to baseline during the "peak" averaged between 4 to 6 s after stimulus onset. (d) Post-LD treatment functional maps showing Δ[HbT] (shown on the same color scale as (c)), relative to baseline. For 5 different rats (rows).

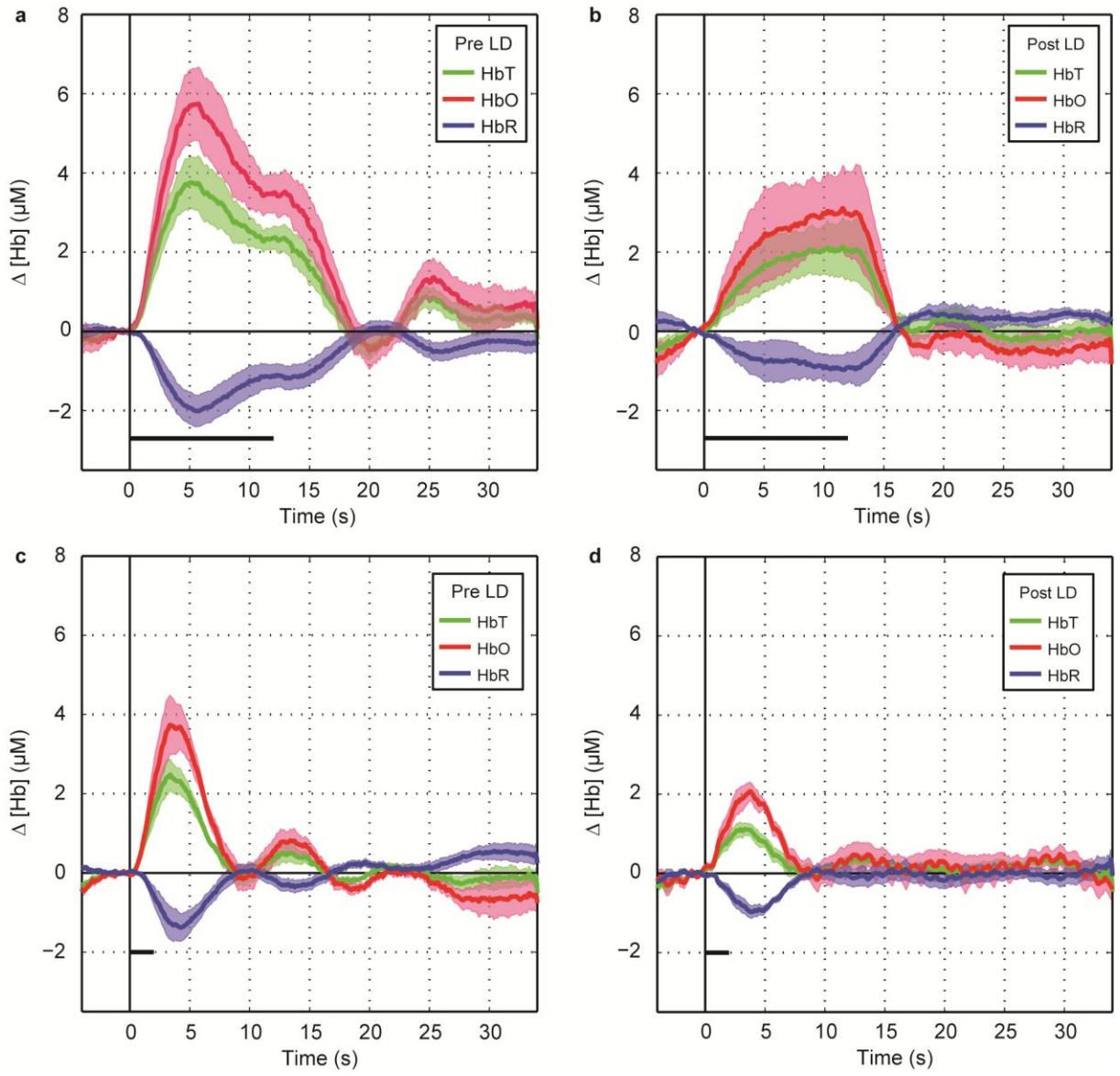

Figure SD. 5 HbO, HbR and HbT responses pre and post LD treatment for 2 and 12 second stimuli (equivalent to HbT responses in Figure 2e). We note that Kennerly et al reported a 25 μM increase in baseline [HbT] under hypercapnia conditions (from 104 μM to 129 μM) (Kennerley et al 2011). The resulting hyperoxia led to functional responses in which no HbR change was observed. In our case, LD treatment caused a 14.4 ± 3.6 μM (measured in 5 rats) increase in baseline [HbT]. As shown above, significant changes in HbR are observed following LD treatment, suggesting that its pre-dilation effects were not sufficient to induce hyperoxia.

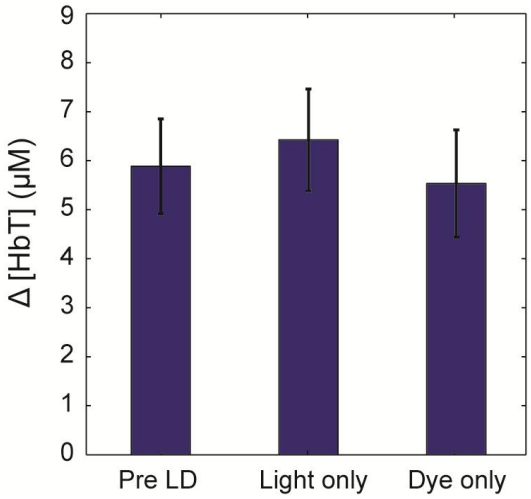

Figure SD. 6 Light-only and dye-only controls. Peak Δ[HbT] responses averaged over the hindpaw response region between 4-6 seconds after stimulus onset for 3 conditions: pre-LD control, after exposure to blue light spot only (no FITC-dx), and after FITC-dx dye intravenous injection only (no blue light) (N = 4 rats, 20 stimulus trials for each condition). Neither exposure to light nor injection of dye alone affected the hemodynamic response.

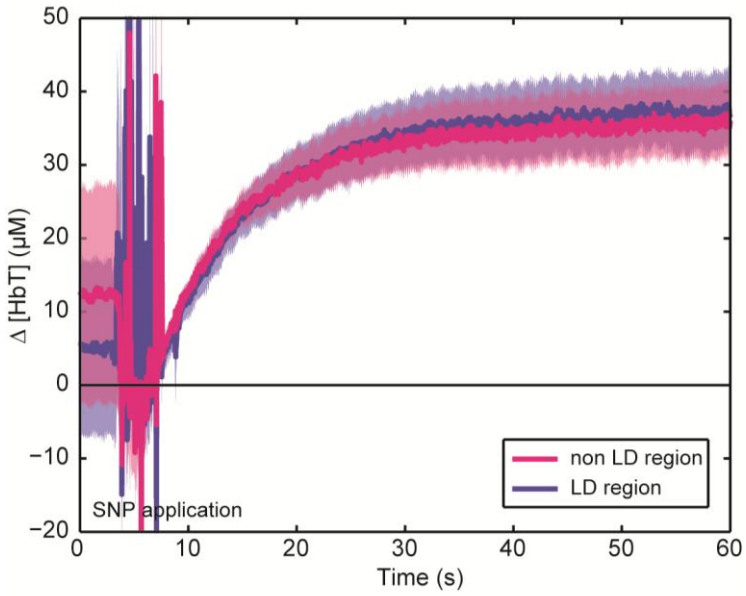

Figure SD. 7 Temporal dynamics of the cortical response to SNP application. In addition to the response amplitude measures shown in Figure 4d, this plot shows that the dynamics of Δ[HbT] responses (as a measure of vasodilation) to topical application of SNP (0.1μM) remain the same in both non LD regions (blue) and LD treated regions (pink). This further confirms that vascular smooth muscle integrity was unaffected by LD treatment. Bold time-courses represent the average response over 5 rats. Shaded regions show SEM.

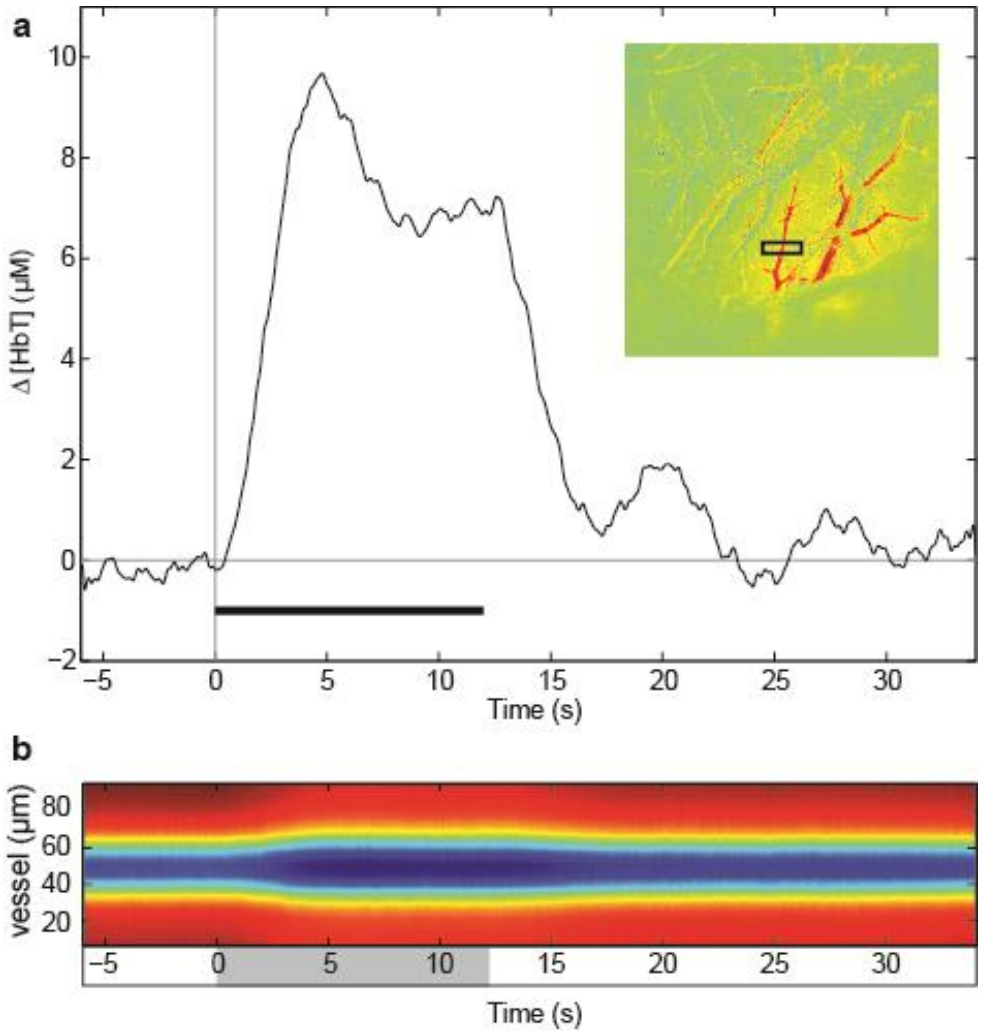

Figure SD. 8 Relationship between Δ[HbT] changes and vessel diameter changes
(a) Timecourse showing the averaged Δ[HbT] response from the selected region shown by the black box (inset) during 12 seconds of electrical hindpaw stimulation. (b) The cross section of the responding arteriole (inset) is plotted over time, displaying vessel diameter changes before, during, and after stimulus period. Changes in vessel diameter are analogous to changes in Δ[HbT].

Bibliography

Abbott NJ, Ronnback L, Hansson E. 2006. Astrocyte-endothelial interactions at the blood-brain barrier. *Nat Rev Neurosci* 7: 41-53

Ances BM, Greenberg JH, Detre JA. 2000a. Effects of variations in interstimulus interval on activation-flow coupling response and somatosensory evoked potentials with forepaw stimulation in the rat. 20: 290-97

Ances BM, Zarahn E, Greenberg JH, Detre JA. 2000b. Coupling of Neural Activation to Blood Flow in the Somatosensory Cortex of Rats Is Time-Intensity Separable, but Not Linear. *J Cereb Blood Flow Metab* 20: 921-30

Anderson CM, Nedergaard M. 2003. Astrocyte-mediated control of cerebral microcirculation. 26: 340-44

Andresen J, Shafi NI, Bryan RM. 2006. Endothelial influences on cerebrovascular tone. *J Appl Physiol* 100: 318-27

Arenkiel BR, Peca J, Davison IG, Feliciano C, Deisseroth K, et al. 2007. In Vivo Light-Induced Activation of Neural Circuitry in Transgenic Mice Expressing Channelrhodopsin-2. *Neuron* 54: 205-18

Armulik A, Abramsson A, Betsholtz C. 2005. Endothelial/Pericyte Interactions. *Circulation Research* 97: 512-23

Attwell D, Buchan AM, Charpak S, Lauritzen M, MacVicar BA, Newman EA. 2010. Glial and neuronal control of brain blood flow. *Nature* 468: 232-43

Attwell D, Iadecola C. 2002. The neural basis of functional brain imaging signals. *Trends in Neurosciences* 25: 621-25

Bartlett IS, Segal SS. 2000. Resolution of smooth muscle and endothelial pathways for conduction along hamster cheek pouch arterioles. *Am J Physiol Heart Circ Physiol* 278: H604-12

Beach JM, McGahren ED, Xia J, Duling BR. 1996. Ratiometric measurement of endothelial depolarization in arterioles with a potential-sensitive dye. *American Journal of Physiology - Heart and Circulatory Physiology* 270: H2216-H27

Bernardinelli Y, Salmon C, Jones EV, Farmer WT, Stellwagen D, Murai KK. 2011. Astrocytes Display Complex and Localized Calcium Responses to Single-Neuron Stimulation in the Hippocampus. *The Journal of Neuroscience* 31: 8905-19

Berwick J, Johnston D, Jones M, Martindale J, Martin C, et al. 2008. Fine Detail of Neurovascular Coupling Revealed by Spatiotemporal Analysis of the Hemodynamic Response to Single Whisker Stimulation in Rat Barrel Cortex. *J Neurophysiol* 99: 787-98

Berwick J, Johnston D, Jones M, Martindale J, Redgrave P, et al. 2005. Neurovascular coupling investigated with two-dimensional optical imaging spectroscopy in rat whisker barrel cortex. *Eur. J. Neurosci.* 22: 1655-66

Birn RM, Saad ZS, Bandettini PA. 2001. Spatial heterogeneity of the nonlinear dynamics in the FMRI BOLD response. *Neuroimage* 14: 817 - 26

Blood AJ, Pouratian N, Toga AW. 2002. Temporally staggered forelimb stimulation modulates barrel cortex optical intrinsic signal responses to whisker stimulation. *J Neurophysiol* 88: 422-37

Bonvento G, Herard AS, Voutsinos-Porche B. 2005. The astrocyte--neuron lactate shuttle: a debated but still valuable hypothesis for brain imaging. *J Cereb Blood Flow Metab* 25: 1394-99

Bookheimer SY, Strojwas MH, Cohen MS, Saunders AM, Pericak-Vance MA, et al. 2000. Patterns of Brain Activation in People at Risk for Alzheimer's Disease. *New England Journal of Medicine* 343: 450-56

Boorman L, Kennerley AJ, Johnston D, Jones M, Zheng Y, et al. 2010. Negative Blood Oxygen Level Dependence in the Rat:A Model for Investigating the Role of Suppression in Neurovascular Coupling. *J. Neurosci.* 30: 4285-94

Borowsky IW, Collins RC. 1989. Metabolic anatomy of brain: a comparison of regional capillary density, glucose metabolism, and enzyme activities. *J Comp Neurol* 288: 401-13

Bouchard MB, Chen BR, Burgess SA, Hillman EMC. 2009. Ultra-fast multispectral optical imaging of cortical oxygenation and blood flow dynamics. *Optics Express in press*

Bryan RMJ, You J, Golding EM, Marrelli SP. 2005. Endothelium-derived Hyperpolarizing Factor: A Cousin to Nitric Oxide and Prostacyclin. *Anesthesiology* 102: 1261-77

Budel S, Bartlett IS, Segal SS. 2003. Homocellular Conduction Along Endothelium and Smooth Muscle of Arterioles in Hamster Cheek Pouch. *Circulation Research* 93: 61-68

Buxton I, Cheek D, Eckman D, Westfall D, Sanders K, Keef K. 1993. NG-nitro L-arginine methyl ester and other alkyl esters of arginine are muscarinic receptor antagonists. *Circulation Research* 72: 387-95

Buxton RB, Wong EC, Frank LR. 1998. Dynamics of Blood Flow and Oxygenation Changes during Brain Activation: The Balloon Model. *Magn Reson Med* 39: 855-64

Calcinaghi N, Jolivet R, Wyss MT, Ametamey SM, Gasparini F, et al. 2011. Metabotropic glutamate receptor mGluR5 is not involved in the early hemodynamic response. *J Cereb Blood Flow Metab* 31: e1-e10

Cardin JA, Carlen M, Meletis K, Knoblich U, Zhang F, et al. 2010. Targeted optogenetic stimulation and recording of neurons in vivo using cell-type-specific expression of Channelrhodopsin-2. *Nat. Protocols* 5: 247-54

Cardoso MMB, Sirotin YB, Lima B, Glushenkova E, Das A. 2012. The neuroimaging signal is a linear sum of neurally distinct stimulus - and task-related components. *Nature Neuroscience* 15: 1298-306

Cauli B, Hamel E. 2010. Revisiting the role of neurons in neurovascular coupling. *Frontiers in Neuroenergetics* 2

Cauli B, Tong X-K, Rancillac A, Serluca N, Lambolez B, et al. 2004. Cortical GABA Interneurons in Neurovascular Coupling: Relays for Subcortical Vasoactive Pathways. *J. Neurosci* 24: 8940-49

Chaigneau E, Oheim M, Audinat E, Charpak S. 2003. Two-photon imaging of capillary blood flow in olfactory bulb glomeruli. *Proceedings of the National Academy of Sciences* 100: 13081?3086

Chen BR, Bouchard MB, McCaslin AFH, Burgess SA, Hillman EMC. 2011. High-speed vascular dynamics of the hemodynamic response. *Neuroimage* 54: 1021-30

Cines DB, Pollak ES, Buck CA, Loscalzo J, Zimmerman GA, et al. 1998. Endothelial Cells in Physiology and in the Pathophysiology of Vascular Disorders. *Blood* 91: 3527-61

Cipolla MJ, Smith J, Kohlmeyer MM, Godfrey JA. 2009. SKCa and IKCa Channels, Myogenic Tone, and Vasodilator Responses in Middle Cerebral Arteries and Parenchymal Arterioles. *Stroke* 40: 1451-57

Cosentino F, Luscher TF. 1998. Endothelial dysfunction in diabetes mellitus. *Journal of cardiovascular pharmacology* 32 Suppl 3: S54-61

Culver JP, Siegel AM, Franceschini MA, Mandeville JB, Boas DA. 2005. Evidence that cerebral blood volume can provide brain activation maps with better spatial resolution than deoxyhemoglobin. *NeuroImage* 27: 947-59

Das A, Gilbert CD. 1999. Topography of Contextual Modulations Resulting from Short-range Interactions in Primary Visual Cortex. *Nature* 399: 655-61

Deisseroth K. 2011. Optogenetics. *Nat Meth* 8: 26-29

Dejana E. 1996. Endothelial adherens junctions: implications in the control of vascular permeability and angiogenesis. *The Journal of Clinical Investigation* 98: 1949-53

Denk W, Strickler JH, Webb WW. 1990. Two-photon laser scanning fluorescence microscopy. *Science* 248: 73-76

Devonshire IM, Papadakis NG, Port M, Berwick J, Kennerley AJ, et al. 2012. Neurovascular coupling is brain region-dependent. *Neuroimage* 59: 1997-2006

Devor A, Dunn AK, Andermann ML, Ulbert I, Boas DA, Dale AM. 2003. Coupling of Total Hemoglobin Concentration, Oxygenation, and Neural Activity in Rat Somatosensory Cortex. *Neuron* 39: 353-59

Devor A, Tian P, Nishimura N, Teng IC, Hillman EMC, et al. 2007. Suppressed neuronal activity and concurrent arteriolar vasoconstriction may explain negative BOLD. *J Neurosci* 27: 4452-59

Dietrich HH, Horiuchi T, Xiang CX, Hongo K, Falck JR, Dacey RG. 2009. Mechanism of ATP-Induced Local and Conducted Vasomotor Responses in Isolated Rat Cerebral Penetrating Arterioles. *J. Vasc. Res.* 46: 253-64

Dietrich HH, Kajita Y, Dacey RG. 1996. Local and conducted vasomotor responses in isolated rat cerebral arterioles. *Am J Physiol Heart Circ Physiol* 271: H1109-16

Dirnagl U, Lindauer U, Villringer A. 1993. Role of nitric oxide in the coupling of cerebral blood flow to neuronal activation in rats. *Neuroscience Letters* 149: 43-46

Doyle MP, Duling BR. 1997. Acetylcholine induces conducted vasodilation by nitric oxide-dependent and -independent mechanisms. *American Journal of Physiology - Heart and Circulatory Physiology* 272: H1364-H71

Duan Q, Angelini E, Herz S, Ingrassia C, Costa K, et al. 2008. Region-Based Endocardium Tracking on Real-Time Three-Dimensional Ultrasound. *Ultrasound in Medicine and Biology* 35: 256-65

Duling BR, Berne RM. 1970. Propagated Vasodilation in the Microcirculation of the Hamster Cheek Pouch. *Circ Res* 26: 163-70

Dunn AK, Bolay H, Moskowitz MA, Boas DA. 2001. Dynamic imaging of cerebral blood flow using laser speckle. *J Cereb Blood Flow Metab* 21: 195-201

Dunn AK, Devor A, Dale AM, Boas DA. 2005. Spatial extent of oxygen metabolism and hemodynamic changes during functional activation of the rat somatosensory cortex. *Neuroimage* 27: 279-90

Dustin LB. 2000. Ratiometric analysis of calcium mobilization. *Clinical and Applied Immunology Reviews* 1: 5-15

Duza T, Sarelius IH. 2003. Conducted dilations initiated by purines in arterioles are endothelium dependent and require endothelial Ca2+. *American Journal of Physiology - Heart and Circulatory Physiology* 285: H26-H37

Emerson GG, Segal SS. 2000. Endothelial Cell Pathway for Conduction of Hyperpolarization and Vasodilation Along Hamster Feed Artery. *Circulation Research* 86: 94-100

Enager P, Piilgaard H, Offenhauser N, Kocharyan A, Fernandes P, et al. 2009. Pathway-specific variations in neurovascular and neurometabolic coupling in rat primary somatosensory cortex. 29: 976-86

Faraci FM. 1991. Role of endothelium-derived relaxing factor in cerebral circulation: large arteries vs. microcirculation. *American Journal of Physiology - Heart and Circulatory Physiology* 261: H1038-H42

Faraci FM, Lynch C, Lamping KG. 2004. Responses of cerebral arterioles to ADP: eNOS-dependent and eNOS-independent mechanisms. *American Journal of Physiology - Heart and Circulatory Physiology* 287: H2871-H76

Feng G, Mellor RH, Bernstein M, Keller-Peck C, Nguyen. QT, et al. 2000. Imaging Neuronal Subsets in Transgenic Mice Expressing Multiple Spectral Variants of GFP. *Neuron* 28: 41-51

Fernández-Klett F, Offenhauser N, Dirnagl U, Priller J, Lindauer U. 2010. Pericytes in capillaries are contractile in vivo, but arterioles mediate functional hyperemia in the mouse brain. *Proceedings of the National Academy of Sciences* 107: 22290-95

Flynn NM, Bulijubasic N, Bosnjak ZJ, Kampine JP. 1992. Isoflurane Produces Endothelium-independent Relaxation in: Canine Middle Cerebral Arteries. *Anesthesiology* 76: 461-67

Foster KA, Beaver CJ, Turner DA. 2005. Interaction between tissue oxygen tension and NADH imaging during synaptic stimulation and hypoxia in rat hippocampal slices. 132: 645-57

Fox MD, Snyder AZ, Vincent JL, Corbetta M, Essen DCV, E.Raichle M. 2005. The human brain is intrinsically organized into dynamic, anticorrelated functional networks. *Proceedings of the National Academy of Sciences of the United States of America* 102: 9673-78

Giaume C, Koulakoff A, Roux L, Holcman D, Rouach N. 2010. Astroglial networks: a step further in neuroglial and gliovascular interactions. *Nat Rev Neurosci* 11: 87-99

Girouard H, Iadecola C. 2006. Neurovascular coupling in the normal brain and in hypertension, stroke, and Alzheimer disease. *J Appl Physiol* 100: 328-35

Gordon GR, Choi HB, Rungta RL, Ellis-Davies GC, MacVicar BA. 2008. Brain metabolism dictates the polarity of astrocyte control over arterioles.

Gössl C, Fahrmeir L, Auer DP. 2001. Bayesian Modeling of the Hemodynamic Response Function in BOLD fMRI. *Neuroimage* 14: 140-48

Grammas P. 2011. Neurovascular dysfunction, inflammation and endothelial activation: Implications for the pathogenesis of Alzheimer's disease. *Journal of Neuroinflammation* 8: 26

Grammas P, Martinez J, Miller B. 2011. Cerebral microvascular endothelium and the pathogenesis of neurodegenerative diseases. *Expert Reviews in Molecular Medicine* 13: null-null

Grinvald A, Lieke E, Frostig RD, Gilbert CD, Wiesel TN. 1986. Functional architecture of cortex revealed by optical imaging of intrinsic signals. *Nature* 324: 361-64

Grosberg LE, Radosevich AJ, Asfaha S, Wang TC, Hillman EMC. 2011. Spectral Characterization and Unmixing of Intrinsic Contrast in Intact Normal and Diseased Gastric Tissues Using Hyperspectral Two-Photon Microscopy. *PLoS ONE* 6: e19925

Hamel E. 2006. Perivascular nerves and the regulation of cerebrovascular tone. *J Appl Physiol* 100: 1059-64

Hamilton NB, Attwell D, Hall CN. 2010. Pericyte-mediated regulation of capillary diameter: a component of neurovascular coupling in health and disease. *Frontiers in Neuroenergetics* 2

Hannah RM, Dunn KM, Bonev AD, Nelson MT. 2011. Endothelial SKCa and IKCa channels regulate brain parenchymal arteriolar diameter and cortical cerebral blood flow. *J Cereb Blood Flow Metab* 31: 1175-86

Harris S, Jones M, Zheng Y, Berwick J. 2010. Does neural input or processing play a greater role in the magnitude of neuroimaging signals? *Frontiers in Neuroenergetics* 2

Haydon PG, Carmignoto G. 2006. Astrocyte control of synaptic transmission and neurovascular coupling. 86: 1009-31

Heim N, Garaschuk O, Friedrich MW, Mank M, Milos RI, et al. 2007. Improved calcium imaging in transgenic mice expressing a troponin C-based biosensor. *Nat Meth* 4: 127-29

Herrmann KS. 1983. Platelet aggregation induced in the hamster cheek pouch by a photochemical process with excited fluorescein isothiocyanate-dextran. *Microvascular Research* 26: 238-49

Higley MJ, Contreras D. 2007. Cellular Mechanisms of Suppressive Interactions Between Somatosensory Responses In Vivo. *Journal of Neurophysiology* 97: 647-58

Hill CE, Phillips JK, Sandow SL. 2001. Heterogeneous control of blood flow amongst different vascular beds. *Medicinal Research Reviews* 21: 1-60

Hillman EM, Devor A, Bouchard MB, Dunn AK, Krauss GW, et al. 2007. Depth-resolved optical imaging and microscopy of vascular compartment dynamics during somatosensory stimulation. 35: 89-104

Hillman EMC. 2007. Optical Brain Imaging In-vivo: Techniques and Applications from Animal to Man. *J Biomed Opt* 12: 051402

Hirano Y, Stefanovic B, Silva AC. 2011. Spatiotemporal Evolution of the Functional Magnetic Resonance Imaging Response to Ultrashort Stimuli. *The Journal of Neuroscience* 31: 1440-47

Hirase H, Creso J, Singleton M, Bartho P, Buzsaki G. 2004a. Two-photon imaging of brain pericytes in vivo using dextran-conjugated dyes. *Glia* 46: 95-100

Hirase H, Qian L, Bartho P, Buzsaki G. 2004b. Calcium dynamics of cortical astrocytic networks in vivo. 2: E96

Hirschi KK, D'Amore PA. 1996. Pericytes in the microvasculature. 32: 687-98

Hoge RD, Atkinson J, Gill B, Crelier GR, Marrett S, Pike GB. 1999. Investigation of BOLD Signal Dependence on Cerebral Blood Flow and Oxygen Consumption: The Deoxyhemoglobin Dilution Model. *Mag. Res. Med* 42: 849?63

Horiuchi T, Dietrich HH, Hongo K, Dacey RG. 2002. Mechanism of extracellular K+-induced local and conducted responses in cerebral penetrating arterioles. *Stroke* 33: 2692-99

Hutchinson EB, Stefanovic B, Koretsky AP, Silva AC. 2006. Spatial Flow-Volume Dissociation of the Cerebral Microcirculatory Response to Mild Hypercapnia. *Neuroimage* 32: 520-30

Iadecola C. 2004. Neurovascular regulation in the normal brain and in Alzheimer's disease. 5: 347-60

Iadecola C, Pelligrino DA, Moskowitz MA, Lassen NA. 1994. Nitric Oxide Synthase Inhibition and Cerebrovascular Regulation. *J Cereb Blood Flow Metab* 14: 175-92

Iadecola C, Yang G, Ebner TJ, Chen G. 1997. Local and Propagated Vascular Responses Evoked by Focal Synaptic Activity in Cerebellar Cortex. *J Neurophysiol* 78: 651-59

Ignarro LJ, Cirino G, Casini A, Napoli C. 1999. Nitric oxide as a signaling molecule in the vascular system: an overview. *34*: 879-86

Janigro D, Nguyen TS, Meno J, West GA, Winn HR. 1997. Endothelium-dependent regulation of cerebrovascular tone by extracellular and intracellular ATP. *Am. J. Physiol.-Heart Circul. Physiol.* 273: H878-H85

Jones M, Berwick J, Johnston D, Mayhew J. 2001. Concurrent Optical Imaging Spectroscopy and Laser-Doppler Flowmetry: The Relationship between Blood Flow, Oxygenation, and Volume in Rodent Barrel Cortex. *NeuroImage* 13: 1002?015

Jones M, Hewson-Stoate N, Martindale J, Redgrave P, Mayhew J. 2004. Nonlinear coupling of neural activity and CBF in rodent barrel cortex. *Neuroimage* 22: 956-65

Karagiannis A, Gallopin T, David C, Battaglia D, Geoffroy H, et al. 2009. Classification of NPY-expressing neocortical interneurons. *29*: 3642-59

Karlheinz S H. 1983. Platelet aggregation induced in the hamster cheek pouch by a photochemical process with excited fluorescein isothiocyanate-dextran. *Microvascular Research* 26: 238-49

Kasischke KA, Vishwasrao HD, Fisher PJ, Zipfel WR, Webb WW. 2004. Neural Activity Triggers Neuronal Oxidative Metabolism Followed by Astrocytic Glycolysis. *Science* 305: 99-103

Kennerley AJ, Harris S, Bruyns-Haylett M, Boorman L, Zheng Y, et al. 2011. Early and late stimulus-evoked cortical hemodynamic responses provide insight into the neurogenic nature of neurovascular coupling. *J Cereb Blood Flow Metab*

Klein B, Kuschinsky W, Schrock H, Vetterlein F. 1986. Interdependency of local capillary density, blood flow, and metabolism in rat brains. *Am J Physiol Heart Circ Physiol* 251: H1333-40

Kleinfeld D, Mitra PP, Helmchen F, Denk W. 1998. Fluctuations and stimulus-induced changes in blood flow observed in individual capillaries in layers 2 through 4 of rat neocortex. *Proceedings of the National Academy of Sciences* 95: 15741-46

Ko KR, Ngai AC, Winn HR. 1990. Role of adenosine in regulation of regional cerebral blood flow in sensory cortex. *American Journal of Physiology - Heart and Circulatory Physiology* 259: H1703-H08

Koch SP, Habermehl C, Mehnert J, Schmitz C, Holtze S, et al. 2010. High-resolution optical functional mapping of the human somatosensory cortex. *Frontiers in Neuroenergetics* 2

Koehler RC, Gebremedhin D, Harder DR. 2006. Role of astrocytes in cerebrovascular regulation. 100: 307-17

Kohl M, Lindauer U, Royl G, Kuhl M, Gold L, et al. 2000. Physical model for the spectroscopic analysis of cortical intrinsic optical signals. *Phys Med Biol* 45: 3749-64

Koller A, Messina EJ, Wolin MS, Kaley G. 1989. Effects of endothelial impairment on arteriolar dilator responses in vivo. *American Journal of Physiology - Heart and Circulatory Physiology* 257: H1485-H89

Kuhn B, Denk W, Bruno RM. 2008. In vivo two-photon voltage-sensitive dye imaging reveals top-down control of cortical layers 1 and 2 during wakefulness. *Proceedings of the National Academy of Sciences* 105: 7588-93

Kwong KK, W.Belliveau J, Chesler DA, Goldberg IE, Weisskoff RM, et al. 1992. Dynamic magnetic resonance imaging of human brain activity during primary sensory stimulation. *Proc Natl Acad Sci U S A.* 89: 5675-79

Langheinrich U, Daut J. 1997. Hyperpolarization of isolated capillaries from guinea-pig heart induced by K+ channel openers and glucose deprivation. *The Journal of Physiology* 502: 397-408

Lecrux C, Toussay X, Kocharyan A, Fernandes P, Neupane S, et al. 2011. Pyramidal Neurons Are "Neurogenic Hubs" in the Neurovascular Coupling Response to Whisker Stimulation. *The Journal of Neuroscience* 31: 9836-47

Lee JH, Durand R, Gradinaru V, Zhang F, Goshen I, et al. 2010. Global and local fMRI signals driven by neurons defined optogenetically by type and wiring. *Nature* 465: 788-92

Leffler CW, Mirro R, Shanklin DR, Armstead WM, Shibata M. 1994. Light/dye microvascular injury selectively eliminates hypercapnia-induced pial arteriolar dilation in newborn pigs. *American Journal of Physiology - Heart and Circulatory Physiology* 266: H623-H30

Leithner C, Royl G, Offenhauser N, Fuchtemeier M, Kohl-Bareis M, et al. 2009. Pharmacological uncoupling of activation induced increases in CBF and CMRO(2).

Lida H, Lida M, Takenaka M, Fukuoka N, Dohi S. 2010. Comparative effects of cilostazol and aspirin on the impairment of endothelium-dependent cerebral vasodialtion caused by acute cigarette smoking in rats. *Journal of Thrombosis and Thrombolysis* 29: 483-88

Lindauer U, Dirnagl U, F?chtemeier M, B?ttiger C, Offenhauser N, et al. 2010. Pathophysiological interference with neurovascular coupling - when imaging based on hemoglobin might go blind. *Frontiers in Neuroenergetics* 2

Lindauer U, Gethmann J, Kühl M, Kohl-Bareis M, Dirnagl U. 2003. Neuronal activity-induced changes of local cerebral microvascular blood oxygenation in the rat: effect of systemic hyperoxia or hypoxia. *Brain Res.* 975: 135-40

Lindauer U, Megow D, Matsuda H, Dirnagl U. 1999. Nitric oxide: a modulator, but not a mediator, of neurovascular coupling in rat somatosensory cortex. 277: H799-H811

Lindquist MA, Meng Loh J, Atlas LY, Wager TD. 2009. Modeling the hemodynamic response function in fMRI: Efficiency, bias and mis-modeling. *Neuroimage* 45: S187-S98

Little TL, Xia J, Duling BR. 1995. Dye Tracers Define Differential Endothelial and Smooth Muscle Coupling Patterns Within the Arteriolar Wall. *Circulation Research* 76: 498-504

Livet J, Weissman TA, Kang H, Draft RW, Lu J, et al. 2007. Transgenic strategies for combinatorial expression of fluorescent proteins in the nervous system. *Nature* 450: 56-62

Logothetis NK. 2008. What we can do and what we cannot do with fMRI. *Nature* 453: 869-78

Logothetis NK, Pauls J, Augath M, Trinath T, Oeltermann A. 2001. Neurophysiological investigation of the basis of the fMRI signal. *Nature* 412: 150 - 57

Longden TA, Dunn KM, Draheim HJ, Nelson MT, Weston AH, Edwards G. 2011. Intermediate-conductance calcium-activated potassium channels participate in neurovascular coupling. *British Journal of Pharmacology* 164: 922-33

Looft-Wilson RC, Payne GW, Segal SS. 2004. Connexin expression and conducted vasodilation along arteriolar endothelium in mouse skeletal muscle. *Journal of Applied Physiology* 97: 1152-58

Lu HD, Chen G, Ts'o DY, Roe AW. 2009. A rapid topographic mapping and eye alignment method using optical imaging in Macaque visual cortex. *Neuroimage* 44: 636-56

Magistretti PJ, Pellerin L. 1996a. Cellular bases of brain energy metabolism and their relevance to functional brain imaging: evidence for a prominent role of astrocytes. 6: 50-61

Magistretti PJ, Pellerin L. 1996b. Cellular mechanisms of brain energy metabolism. Relevance to functional brain imaging and to neurodegenerative disorders. *Ann N Y Acad Sci* 777: 380-7

Malonek D, Grinvald A. 1996. Interactions Between Electrical Activity and Cortical Microcirculation Revealed by Imaging Spectroscopy: Implications for Functional Brain Mapping. *Science* 272: 551-54

Marrelli SP, Eckmann MS, Hunte MS. 2003. Role of endothelial intermediate conductance KCa channels in cerebral EDHF-mediated dilations. *American Journal of Physiology - Heart and Circulatory Physiology* 285: H1590-H99

Martin C, Martindale J, Berwick J, Mayhew J. 2006. Investigating neural-hemodynamic coupling and the hemodynamic response function in the awake rat. *Neuroimage* 32: 33-48

Martindale J, Berwick J, Martin C, Kong Y, Zheng Y, Mayhew J. 2005a. Long duration stimuli and nonlinearities in the neural-haemodynamic coupling. *J Cereb Blood Flow Metab* 25: 651-61

Martindale J, Berwick J, Martin C, Kong Y, Zheng Y, Mayhew J. 2005b. Long duration stimuli and nonlinearities in the neural-haemodynamic coupling. *J Cereb Blood Flow Metab.* 25: 651-61

Martindale J, Mayhew J, Berwick J, Jones M, Martin C, et al. 2003. The Hemodynamic Impulse Response to a Single Neural Event. *J Cereb Blood Flow Metab* 23: 546-55

Masdeu JC, Zubieta JL, Arbizu J. 2005. Neuroimaging as a marker of the onset and progression of Alzheimer's disease. *Journal of the Neurological Sciences* 236: 55-64

Matsuura T, Kanno I. 2001. Quantitative and temporal relationship between local cerebral blood flow and neuronal activation induced by somatosensory stimulation in rats. *Neuroscience Research* 40: 281-90

Mayhew JEW, Askew S, Zheng Y, Porrill J, Westby GWM, et al. 1996. Cerebral Vasomotion: A 0.1-Hz Oscillation in Reflected Light Imaging of Neural Activity. *Neuroimage* 4: 183-93

McCaslin AFH, Chen BR, Radosevich AJ, Cauli B, Hillman EMC. 2010. In-vivo 3D morphology of astrocyte-vasculature interactions in the somatosensory cortex: Implications for neurovascular coupling. *Journal of Cerebral Blood Flow and Metabolism* (submitted)

McCaslin AFH, Chen BR, Radosevich AJ, Cauli B, Hillman EMC. 2011. In vivo 3D morphology of astrocyte-vasculature interactions in the somatosensory cortex: implications for neurovascular coupling. *J Cereb Blood Flow Metab* 31: 795-806

McNeish AJ, Dora KA, Garland CJ. 2005. Possible Role for K+ in Endothelium-Derived Hyperpolarizing Factor–Linked Dilatation in Rat Middle Cerebral Artery. *Stroke* 36: 1526-32

Miller FN, Sims DE, Schuschke DA, Abney DL. 1992. Differentiation of light-dye effects in the microcirculation. *Microvascular Research* 44: 166-84

Misra A, Aliasgar Shahiwala GS, Shah SP. 2003. Drug delivery to the central nervous system: a review. *J Pharm Pharmaceut Sci* 6: 252-73

Moore CI, Cao R. 2008. The Hemo-Neural Hypothesis: On The Role of Blood Flow in Information Processing. *Journal of Neurophysiology* 99: 2035-47

Nemoto M, Sheth S, Guiou M, Pouratian N, Chen JWY, Toga AW. 2004. Functional Signal- and Paradigm-Dependent Linear Relationships between Synaptic Activity and Hemodynamic Responses in Rat Somatosensory Cortex. *J. Neurosci.* 24: 3850-61

Ngai AC, Winn HR. 1995. Modulation of Cerebral Arteriolar Diameter by Intraluminal Flow and Pressure. *Circ Res* 77: 832-40

Ngai AC, Winn HR. 2002. Pial arteriole dilation during somatosensory stimulation is not mediated by an increase in CSF metabolites. *Am. J. Physiol.-Heart Circul. Physiol.* 282: H902-H07

Nimmerjahn A, Kirchhoff F, Kerr JN, Helmchen F. 2004. Sulforhodamine 101 as a specific marker of astroglia in the neocortex in vivo. *Nat Methods* 1: 31-37

Nishimura N, Schaffer CB, Friedman B, Lyden PD, Kleinfeld D. 2007. Penetrating arterioles are a bottleneck in the perfusion of neocortex. *PNAS* 104: 365-70

Ohki K, Chung S, Ch'ng YH, Kara P, Reid RC. 2005. Functional imaging with cellular resolution reveals precise micro-architecture in visual cortex. *Nature* 433: 597 - 603

Orbach HS, Cohen LB, Grinvald A. 1985. Optical mapping of electrical activity in rat somatosensory and visual cortex. *J. Neurosci.* 5: 1886-95

Owen AM, Stern CE, Look RB, Tracey I, Rosen BR, Petrides M. 1998. Functional organization of spatial and nonspatial working memory processing within the human lateral frontal cortex. *Proceedings of the National Academy of Sciences of the United States of America* 95: 7721-26

Oyama N, Yagita Y, Kawamura M, Sugiyama Y, Terasaki Y, et al. 2011. Cilostazol, Not Aspirin, Reduces Ischemic Brain Injury via Endothelial Protection in Spontaneously Hypertensive Rats. *Stroke* 42: 2571-77

Pellerin L, Pellegri G, Bittar PG, Charnay Y, Bouras C, et al. 1998. Evidence Supporting the Existence of an Activity-Dependent Astrocyte-Neuron Lactate Shuttle. *Developmental Neuroscience* 20: 291-99

Peng X, Carhuapoma JR, Bhardwaj A, Alkayed NJ, Falck JR, et al. 2002. Suppression of cortical functional hyperemia to vibrissal stimulation in the rat by epoxygenase inhibitors. 283: H2029-H37

Peppiatt CM, Howarth C, Mobbs P, Attwell D. 2005. Regulation of capillary diameter in rat retina. *J Physiol* 568P: PC32

Peppiatt CM, Howarth C, Mobbs P, Attwell D. 2006. Bidirectional control of CNS capillary diameter by pericytes. *Nature* 443: 700-04

Peterson DA, Peterson DC, Archer S, Weir EK. 1992. The non specificity of specific nitric oxide synthase inhibitors. *Biochemical and Biophysical Research Communications* 187: 797-801

Petrella JR, Wang L, Krishnan S, Slavin MJ, Prince SE, et al. 2007. Cortical Deactivation in Mild Cognitive Impairment: High-Field-Strength Functional MR Imaging1. *Radiology* 245: 224-35

Petzold Gabor C, Murthy Venkatesh N. 2011. Role of Astrocytes in Neurovascular Coupling. *Neuron* 71: 782-97

Pouratian N, Cannestra AF, Martin NA, Toga AW. 2002. Intraoperative optical intrinsic signal imaging: a clinical tool for functional brain mapping. *Neurosurg Focus* 13: 1-9

Povlishock JT, Rosenblum WI, Sholley MM, Wei EP. 1983. An ultrastructural analysis of endothelial change pralleling platelet aggregation in a light/dye model of microvascular insult. *The American Journal of Pathology* 110: 148-60

Prahl SA. 1998. Online resource: http://omlc.ogi.edu/spectra/hemoglobin/summary.html.

Radhakrishnan H, Wu W, Boas D, Franceschini MA. 2011. Study of neurovascular coupling by modulating neuronal activity with GABA. *Brain Res.* 1372: 1-12

Radosevich AJ, Bouchard MB, Burgess SA, Chen B, Hillman EMC. 2008. Hyperspectral in-vivo two-photon microscopy of intrinsic contrast. *Optics Letters* 33: 2164-66

Raichle ME. 2009. A Paradigm Shift in Functional Brain Imaging. *J. Neurosci.* 29: 12729-34

Rodrigo J, Springall DR, Uttenthal O, Bentura ML, badia-Molina F, et al. 1994. Localization of nitric oxide synthase in the adult rat brain. 345: 175-221

Rosenblum W. 1986. Endothelial dependent relaxation demonstrated in vivo in cerebral arterioles. *Stroke* 17: 494-97

Rosenblum W, El-Sabban F. 1982. Dimethyl sulfoxide (DMSO) and glycerol, hydroxyl radical scavengers, impair platelet aggregation within and eliminate the accompanying vasodilation of, injured mouse pial arterioles. *Stroke* 13: 35-39

Ross R. 1993. The pathogenesis of atherosclerosis: a perspective for the 1990s. *Nature* 362: 801-09

Roy CS, Sherrington CS. 1890. On the Regulation of the Blood-supply of the Brain. 11: 85-158

Sarelius I, Pohl U. 2010. Control of muscle blood flow during exercise: local factors and integrative mechanisms. *Acta Physiologica* 199: 349-65

Schummers J, Yu H, Sur M. 2008. Tuned responses of astrocytes and their influence on hemodynamic signals in the visual cortex. *Science* 320: 1638-43

Scott NA, Murphy TH. 2012. Hemodynamic Responses Evoked by Neuronal Stimulation via Channelrhodopsin-2 Can Be Independent of Intracortical Glutamatergic Synaptic Transmission. *PLoS ONE* 7: e29859

Sheth SA, Nemoto M, Guiou M, Walker M, Pouratian N, Toga AW. 2004. Linear and nonlinear relationships between neuronal activity, oxygen metabolism, and hemodynamic responses. *Neuron* 42: 347?55

Sheth SA, Nemoto M, Guiou MW, Walker MA, Toga AW. 2005. Spatiotemporal evolution of functional hemodynamic changes and their relationship to neuronal activity. *J Cereb Blood Flow Metab* Mar 2: 1?2

Shibuki K, Hishida R, Murakami H, Kudoh M, Kawaguchi T, et al. 2003. Dynamic imaging of somatosensory cortical activity in the rat visualized by flavoprotein autofluorescence. *J Physiol* 549: 919?27

Shimamoto K, Sakai R, Takaoka K, Yumoto N, Nakajima T, et al. 2004. Characterization of Novel L-threo-β-Benzyloxyaspartate Derivatives, Potent Blockers of the Glutamate Transporters. *Molecular Pharmacology* 65: 1008-15

Shoham D, Glaser DE, Arieli A, Kenet T, Wijnbergen C, et al. 1999. Imaging Cortical Dynamics at High Spatial and Temporal Resolution with Novel Blue Voltage-Sensitive Dyes. *Neuron* 24: 791?02

Sirotin YB, Hillman EMC, Bordier C, Das A. 2009. Spatiotemporal precision and hemodynamic mechanism of optical point-spreads in alert primates. *PNAS* under review

Skala MC, Riching KM, Gendron-Fitzpatrick A, Eickhoff J, Eliceiri KW, et al. 2007. In vivo multiphoton microscopy of NADH and FAD redox states, fluorescence lifetimes, and cellular morphology in precancerous epithelia. *PNAS* 104: 19494-99

Snyder SH. 1992. Nitric oxide: first in a new class of neurotransmitters. 257: 494-96

Stefanovic B, Hutchinson E, Yakovleva V, Schram V, Russell JT, et al. 2008. Functional reactivity of cerebral capillaries. 28: 961-72

Stephan KE, Harrison LM, Penny WD, Friston KJ. 2004. Biophysical models of fMRI responses. *Current Opinion in Neurobiology* 14: 629-35

Stosiek C, Garaschuk O, Holthoff K, Konnerth A. 2003. In vivo two-photon calcium imaging of neuronal networks. *PNAS* 100: 7319?324

Sun H-S, French RJ, Feng Z-P. 2009. A method for identifying viable and damaged neurons in adult mouse brain slices. *Acta Histochemica* 111: 531-37

Takahashi A, Camacho P, Lechleiter JD, Herman B. 1999. Measurement of Intracellular Calcium. *Physiological Reviews* 79: 1089-125

Takano T, Tian G, Peng W, Lou N, Libionka W, et al. 2005. Astrocyte-mediated control of cerebral blood flow. *Nat. Neurosci* 9: 260 - 67

Takata N, Hirase H. 2008. Cortical Layer 1 and Layer 2/3 Astrocytes Exhibit Distinct Calcium Dynamics <italic>In Vivo</italic>. *PLoS ONE* 3: e2525

Thapaliya S, Matsuyama H, Takewaki T. 1999. ATP released from perivascular nerves hyperpolarizes smooth muscle cells by releasing an endothelium-derived factor in hamster mesenteric arteries. *The Journal of Physiology* 521: 191-99

Tian P, Teng IC, May LD, Kurz R, Lu K, et al. 2010. Cortical depth-specific microvascular dilation underlies laminar differences in blood oxygenation level-dependent functional MRI signal. *Proc Natl Acad Sci U S A* 107: 15246-51

Toda N, Ayajiki K, Okamura T. 2009. Cerebral blood flow regulation by nitric oxide in neurological disorders. *Canadian Journal of Physiology and Pharmacology* 87: 581-94

Ts'o DY, Frostig RD, Lieke EE, Grinvald A. 1990. Functional organization of primate visual cortex revealed by high resolution optical imaging. *Science* 249: 417-20

Vanzetta I, Hildesheim R, Grinvald A. 2005. Compartment-resolved imaging of activity-dependent dynamics of cortical blood volume and oximetry. *J Neurosci* 25: 2233?244

Vaucher E, Tong XK, Cholet N, Lantin S, Hamel E. 2000. GABA neurons provide a rich input to microvessels but not nitric oxide neurons in the rat cerebral cortex: a means for direct regulation of local cerebral blood flow. 421: 161-71

Vazquez AL, Noll DC. 1998. Nonlinear Aspects of the BOLD Response in Functional MRI. *Neuroimage* 7: 108-18

Villringer A, Dirnagl U. 1995. Coupling of brain activity and cerebral blood flow: basis of functional neuroimaging. *Cerebrovascular and brain metabolism reviews* 7: 240-76

Villringer A, Them A, Lindauer U, Einhaupl K, Dirnagl U. 1994. Capillary perfusion of the rat brain cortex. An in vivo confocal microscopy study. *Circ Res* 75: 55-62

Wang Q, Pelligrino DA, Koenig HM, Albrecht RF. 1994. The Role of Endothelium and Nitric Oxide in Rat Pial Arteriolar Dilatory Responses to CO2 In Vivo. *J Cereb Blood Flow Metab* 14: 944-51

Wang X, Lou N, Xu Q, Tian G, Peng WG, et al. 2006. Astrocytic Ca2+ signaling evoked by sensory stimulation in vivo. *Nat Neurosci* 9: 816-23

Welsh DG, Segal SS. 1998. Endothelial and smooth muscle cell conduction in arterioles controlling blood flow. *Am J Physiol Heart Circ Physiol* 274: H178-86

White BR, Snyder AZ, Cohen AL, Petersen SE, Raichle ME, et al. 2009. Resting-state functional connectivity in the human brain revealed with diffuse optical tomography. *Neuroimage* 47: 148-56

Winkler EA, Bell RD, Zlokovic BV. 2011. Central nervous system pericytes in health and disease. *Nat Neurosci* 14: 1398-405

Winship IR, Plaa N, Murphy TH. 2007. Rapid Astrocyte Calcium Signals Correlate with Neuronal Activity and Onset of the Hemodynamic Response In Vivo. *J. Neurosci.* 27: 6268-72

Winter P, Dora KA. 2007. Spreading dilatation to luminal perfusion of ATP and UTP in rat isolated small mesenteric arteries. *The Journal of Physiology* 582: 335-47

Wolf T, Lindauer U, Villringer A, Dirnagl U. 1997. Excessive oxygen or glucose supply does not alter the blood flow response to somatosensory stimulation or spreading depression in rats. *Brain Res.* 761: 290-99

Wolfle SE, Chaston DJ, Goto K, Sandow SL, Edwards FR, Hill CE. 2011. Nonlinear relationship between hyperpolarisation and relaxation enables long distance propagation of vasodilation. *The Journal of Physiology*

Wölfle SE, Chaston DJ, Goto K, Sandow SL, Edwards FR, Hill CE. 2011. Non-linear relationship between hyperpolarisation and relaxation enables long distance propagation of vasodilatation. *The Journal of Physiology* 589: 2607-23

Xu HL, Mao L, Ye S, Paisansathan C, Vetri F, Pelligrino DA. 2008. Astrocytes are a key conduit for upstream signaling of vasodilation during cerebral cortical neuronal activation in vivo. 294: H622-H32

Xu HL, Pelligrino DA. 2007. ATP release and hydrolysis contribute to rat pial arteriolar dilatation elicited by neuronal activation. 92: 647-51

Yang G, Chen G, Ebner TJ, Iadecola C. 1999. Nitric oxide is the predominant mediator of cerebellar hyperemia during somatosensory activation in rats. *Am J Physiol Regul Integr Comp Physiol* 277: R1760-70

Yeşilyurt B, Uğurbil K, Uludağ K. 2008. Dynamics and nonlinearities of the BOLD response at very short stimulus durations. *Magnetic Resonance Imaging* 26: 853-62

You J, Johnson TD, Childres WF, Bryan RM. 1997. Endothelial-mediated dilations of rat middle cerebral arteries by ATP and ADP. *American Journal of Physiology - Heart and Circulatory Physiology* 273: H1472-H77

You JP, Johnson TD, Marrelli SP, Bryan RM. 1999. Functional heterogeneity of endothelial P2 purinoceptors in the cerebrovascular tree of the rat. *Am. J. Physiol.-Heart Circul. Physiol.* 277: H893-H900

Zhang D, Raichle M. 2010. Disease and the brain's dark energy. *Nature Reviews Neurology* 6: 15-28

Zhang F, Wang L-P, Boyden ES, Deisseroth K. 2006. Channelrhodopsin-2 and optical control of excitable cells. *Nat Meth* 3: 785-92

Zlokovic BV. 2008. The blood-brain barrier in health and chronic neurodegenerative disorders. 57: 178-201

Zonta M, Angulo MC, Gobbo S, Rosengarten B, Hossmann KA, et al. 2003. Neuron-to-astrocyte signaling is central to the dynamic control of brain microcirculation. 6: 43-50